2010

Fundamental Studies of Femtosecond Laser Interactions with Solids and Their Applications to Laser Ablation Inductively Coupled Plasma Mass Spectrometry for Environmental Analysis

Mohamed Shaheen
University of Windsor

Fundamental Studies of Femtosecond Laser Interactions with Solids and Their Applications to Laser Ablation Inductively Coupled Plasma Mass Spectrometry for Environmental Analysis

By

Mohamed Shaheen

A Dissertation
Submitted to the Faculty of Graduate Studies
through the Great Lakes Institute for Environmental Research
in Partial Fulfillment of the Requirements for
the Degree of Doctor of Philosophy at the
University of Windsor

Windsor, Ontario, Canada

2010

Fundamental Studies of Femtosecond Laser Interactions with Solids and Their Applications to Laser Ablation Inductively Coupled Plasma Mass Spectrometry for Environmental Analysis

by

Mohamed Shaheen

APPROVED BY:

_____

K. Kyser, external examiner
Department of Geological Sciences and Geological Engineering
Queen's University

_____

K. Drouillard
Great Lakes Institute for Environmental Research

_____

J. Gagnon
Department of Earth Sciences

_____

C. Weisener
Great Lakes Institute for Environmental Research

_____

B. Fryer, Advisor
Great Lakes Institute for Environmental Research

_____

Abdo Alfakih, Chair of Defence
Department of Mathematics and Statistics

January 22, 2010

DECLARATION OF CO-AUTHORSHIP / PREVIOUS PUBLICATIONS

I. Co-Authorship Declaration

I hereby declare that this thesis incorporates material that is result of joint research, as follows:

This thesis incorporates the outcome of joint research undertaken in collaboration with Joel Gagnon and Zhaoping Yang under the supervision of professor Brian Fryer. The collaboration is covered in Chapter 3 of the thesis. In all cases, the key ideas, primary contributions, experimental designs, data analysis and interpretation, were performed by the author, and the contribution of co-authors was primarily through the provision of samples and ideas for the material and methods section.

I am aware of the University of Windsor Senate Policy on Authorship and I certify that I have properly acknowledged the contribution of other researchers to my thesis, and have obtained written permission from each of the co-author(s) to include the above material(s) in my thesis.

I certify that, with the above qualification, this thesis, and the research to which it refers, is the product of my own work.

II. Declaration of Previous Publication

This thesis includes 3 original papers that have been previously published /will be submitted for publication in peer reviewed journals, as follows:

Thesis Chapter	Publication title/full citation	Publication status*
Chapter *3*	M. Shaheen, J. E. Gagnon, Z. Yang and B. J. Fryer, Evaluation of the analytical performance of femtosecond laser ablation inductively coupled plasma mass spectrometry at 785 nm with glass reference materials, J. Anal. At. Spectrom., 2008, 23**,** 1610 – 1621.	Published
Chapter *4*	M. Shaheen and B. J. Fryer, Improving the Analytical Capabilities of Femtosecond Laser Ablation Multicollector Icp-Ms for High Precision Isotopic Analysis: The Role of Hydrogen and Nitrogen. To be submitted to Journal of Analytical Atomic Spectrometry.	To be submitted
Chapter *5*	M. Shaheen and B. J. Fryer, Elemental Analysis of Sediment Reference Materials: A Comparison between Femtosecond Laser Ablation- and solution- Inductively Coupled	To be submitted

	Plasma Mass Spectrometry. To be submitted to Geostandards and Geoanalytical Research.	

I certify that I have obtained a written permission from the copyright owner(s) to include the above published material(s) in my thesis. Chapter 3 is re-printed with the permission of The Royal Society of Chemistry (RSC), Appendix A. I certify that the above material describes work completed during my registration as graduate student at the University of Windsor

I declare that, to the best of my knowledge, my thesis does not infringe upon anyone's copyright nor violate any proprietary rights and that any ideas, techniques, quotations, or any other material from the work of other people included in my thesis, published or otherwise, are fully acknowledged in accordance with standard referencing practices.

I declare that this is a true copy of my thesis, including any final revisions, as approved by my thesis committee and the Graduate Studies office, and that this thesis has not been submitted for a higher degree to any other University or Institution.

ABSTRACT

Laser ablation inductively coupled plasma mass spectrometry (LA-ICP-MS) has been successfully applied in many research areas. Compared to conventional analytical techniques, it has the advantages of minimal sample preparation and high spatial resolution capabilities. Elemental and isotopic fractionation, matrix effects and the lack of matrix-matched standards are problems that limit applications of this technique for routine analysis. The introduction of femtosecond laser (fs) pulses has improved the analytical capabilities of this technique in terms of precision, accuracy and detection limits. However, laser ablation involves complex processes that are not fully understood and requires extensive studies on laser-solid interaction, particle formation, particle transport and ionization of particles in the ICP ion source.

The first main objective of my Ph.D. is to improve the analytical cababilities of LA-ICP-MS. This was covered in chapters 2, 3, and 4. Chapter 2 focused on understanding the mechanisms of laser-solid interactions and the method of generation of femtosecond laser pulses. The differences between nanosecond and femtosecond laser pulses and optimization of the laser beam for better ablation quality were discussed. In Chapter 3, we evaluated the analytic al capabilities of fs-LA-ICP-MS using different standard reference materials (NIST and Basalt glasses). We showed that femtosecond laser pulses ablates materials with different transparency (NIST 612 vs. NIST 610) in a similar way. Matrix effects and fractionations were shown to be greatly reduced in fs-LA-ICP-

MS. In Chapter 4, we investigated the effects of mixed Ar gas plasma by the addition of hydrogen and nitrogen to the central Ar gas before the ablation cell in fs-LA coupled with quadrapole mass spectrometer. Enhancement of sensitivity was observed as a result of increased plasma temperatures due to the high thermal conductivities of these gases. At the same time a slight increase in double charged ions, nitrides and hydrides was observed. Addition of nitrogen to Ar gas before the ablation cell in fs-LA-MC-ICP has improved sensitivity of Tl and Pb and helped to reduce and stabilize the mass bias. This created robust plasma conditions for precise and accurate Pb isotope ratios using Tl as a surrogate to correct for mass bias.

The second objective of my thesis was to validate the application of LA-ICP-MS to the analysis of sediment cores. In Chapter 5, we prepared sediment reference materials using low viscosity epoxy resin to get solid disks suitable for analysis by LA-ICP-MS. The data obtained by fs-LA-ICP-MS agreed well with those obtained by solution based-ICP-MS indicating the applicability of this technique for the analysis of sediment core. The usefulness of core analysis by LA-ICP-MS to interpret variations in element concentrations was demonstrated with a sediment core from Lake Erie.

To my parents, my wife and my children Yousef and Omar

ACKNOWLEDGEMENTS

I would like to thank Arab Republic of Egypt, Ministry of Higher Education, Tanta University, Faculty of Science, Physics department for giving me a 4-year scholarship to study for my Ph. D. at the University of Windsor, Ontario, Canada.

I would like to express my sincere appreciation to my advisor Dr. Brian Fryer for his continuous guidance and support during my Ph. D. program. It is his critical reviews and continuous feedback that enabled me to complete my research work and present it in an acceptable form. Dealing with him was a continuous learning process for me through which I gained experience in my field.

I am sincerely grateful to my committee members: Dr. Ken Drouillard, Dr. Joel Gagnon and Dr. Chris Weisener. I would like to thank Dr. Doug Haffner, Mr. Todd Leadley and Dr. Yasser Abdel-Rahman for their help during sediment sampling.

I would like to express my appreciation to all my colleagues at Great Lakes Institute for Environmental Research (GLIER) who supported and encouraged me in a lot of situations. Many thanks to Pat Murray, Mary Lou Scratch, Arne Sturm, Connie Laquinta, Christina Smeaton, Magda Scarlat, Sonia Melancon, Jill Olin, Jennifer Bronnenhuber, Remi Abisola, Bora Demiri, Mark Cook, Sharon Lackie, Sandra Ellis and Lei Zang. Special thanks are due to Dr. Joel Gagnon, Dr. Zhaoping Yang and Mr. J.C. Barrette for their help during my work.

I would like to extend my gratitude to all my family members for their continuous support and encouragement. My profound appreciation and respect are due to my parents for their endless love. My utmost gratitude and sincere appreciation to my beloved wife who has provided me with every kind of support that I needed while sharing with me this life time experience with unmatched patience. My profound love to my dearest children Yousef and Omar.

I would like to thank all members and staff of the Egyptian Bureau of Cultural and Educational Affairs, Montreal, Canada, and the Mission Department, Ministry of Higher Education, Egypt, for their continuous help. I would like to acknowledge my professors, colleagues and friends at Department of Physics and Department of Chemistry, Tanta University, Egypt. Special thanks are due to Dr. Farouk El-Mekawy, Dr. Riyad Ghazy, Dr. Saleh Abdel Azim, Dr. Bahgat El-Bradiee, Dr. Nabeel El-Seragy, Dr. Mohsen Barakat, Dr. Tarek Elnimr, Dr. Mostafa Elnimr, Dr. Abdel Raoof Tawfeek, Dr. Mohamed Rafat Ismail, Dr. Hussien Badran, Dr. Abdel Latif Mohamed, Dr. Samy El-Daly, Dr. Tarek Fayed. Dr. Hasanain Ellabani, Dr. Mohsen El-khosht, Dr. Abdel-Fattah El-Shora, Dr. Mohamed Ismail, Dr. Mohamed Amer, Dr. Abdel Razek Abdeen, Dr. Abo Alhassan Shafik, Dr. Mahmoud Kamel, Dr. Saad Abo Alenain, Dr. Hassan El-Kashef, Dr. Khaled Abo-El-Maaty, Dr. Salwa Saad, Dr. Fathi El-Husaini, Dr. Usama Hemaida, Dr. Ahmed Abdel Azim, Dr. Mostafa Ellaban, Dr. Talat Maiz, Dr. Samia Saafan, Dr. Dalal Hemaida, Dr. Galal Zedan, Dr. Magda Zaki, Dr.Sami Abdel-Kader, Dr. Gamal abo Kora, Dr. Enas Hassan, Dr. Hassan –El-Gohary and all people at the Faculty of Science, Tanta University, Egypt.

TABLE OF CONTENTS

LIST OF TABLES

LIST OF FIGURES

LIST OF ABBREVIATIONS & SYMBOLS

AAS	Atomic absorption spectroscopy
AES	Atomic emission spectroscopy
c	Speed of light
C	Heat capacity
CANMET	Canada Centre for Mineral and Energy Technology
CCD	Charge coupled device
CPA	Chirped pulse amplification
D	Thermal diffusivity
d	Aperature of the laser device
DUV	Deep ultraviolet
e	Charge of electron
E_g	Energy gap
F	Laser fluence
F_{th}	Threshold laser fluence
f	Focal length
fs	Femtosecond
FWHM	full-width at half-maximum
g_{ff}	Gaunt factor
h	Plank's constant
H_3BO_3	Boric acid
HF	Hydroflouric acid
HNO_3	Nitric acid
I(t)	Intensity of the laser pulse
I_0	Incident laser intensity
IB	Inverse Bremsstrahlung
ICP	Inductively coupled plasma
ICP-MS	Inductively coupled plasma mass spectrometry
IR	Infrared
K	Thermal conductivity

k_B	Boltzmann constant
L	Ablation depth per laser pulse
LA	Laser ablation
LA-ICP-MS	Laser ablation inductively coupled plasma mass spectrometry
LA-MC-ICP-MS	Laser ablation multicollector inductively coupled plasma mass spectrometry
L_c	Grating separation
L_s	Skin penetration depth
L_{sg}	Stretcher grating separation
L_{th}	Thermal diffusion length
L_v	Latent heat of evaporation
MC	Multicollector
m_e	Mass of electron
MS	Mass spectrometry
n(t)	Electron number density
N_e	Number density of electrons
N_i	Number density of ions
NIR	Near infrared
NIST	National Institute of Standards and Technology
ns	nanosecond
P	Power density
PI	Photoionization
PTFE	Polytetrafluoroethylene (Teflon)
r	Radius of spot
R^2	Linear regression coefficient
REE	Rare earth elements
RSD	Relative standard deviation
SEM	Scanning electron microscope
SO-LA-ICP-MS	Solution-based ICP-MS
T_0	Initial temperature

T	Temperature
T_p	Duration of the laser pulse
T_v	Vaporization temperature
t_v	Time required for the sample to reach its vaporization temperature
TIMS	Thermal ionization mass spectrometry
USGS	United States Geological Survey
UV	Ultraviolet
Z	Ionic charge
α	Mass fractionation (mass bias) factor per unit mass
α_a	Avalanche coefficient
α_b	Absorption coefficient
α_{IB}	Inverse Bremsstrahlung absorption coefficient
α_{Pb}	Mass bias coefficient of Pb
α_{PI}	Absorption coefficient of photoionization
α_{Tl}	Mass bias coefficient of Tl
Δm	Mass difference
λ	Wavelength
ρ	Mass density
σ_k	k-photon absorption cross section
υ	Frequency
R_{True}	True isotope ratio
R_{Meas}	Measured isotope ratio
R_{Std}	True isotope ratio of the bracketing standard
r_{Std}^1	Isotope ratios of the bracketing standard measured before the sample
r_{Std}^2	Isotope ratios of the bracketing standard measured after the sample

CHAPTER 1

GENERAL INTRODUCTION

1.1 INTRODUCTION

Since the invention of the ruby laser in 1960, physicists have made extensive investigations of the interaction of laser radiation with all forms of matter [1]. The interaction of a high power laser beam with matter has many applications including chemical analysis, micromachining, pulsed laser deposition for thin film coating, and tissue and bone surgery in laser medicine [2]. The laser-solid interactions involve complex processes (see figure 1.1) of heating, melting, vaporization, ejection of atoms, ions and molecules, shock waves, plasma initiation and plasma expansion [3, 4]. The various species produced during laser-solid interaction include particulates, ground state atoms, excited atoms, and ions, and have all been utilized for elemental analysis via Atomic Absorption Spectroscopy (AAS), Atomic Emission Spectrodcopy (AES), and Mass Spectrometry (MS) [5, 6].

The interaction of a high energy laser beam with solids can result in what is called laser ablation. Laser ablation (LA) is a process in which an intense burst of energy, delivered by a short duration laser pulse, is used to remove a tiny amount of material from the sample [7]. Laser ablation holds the promise of becoming the standard technique for solid sampling. Analytical applications for laser ablation now cover a great range of academic and industrial fields, including geology, environmental science, forensics, medicine, semiconductor manufacturing, and archaeology [7].

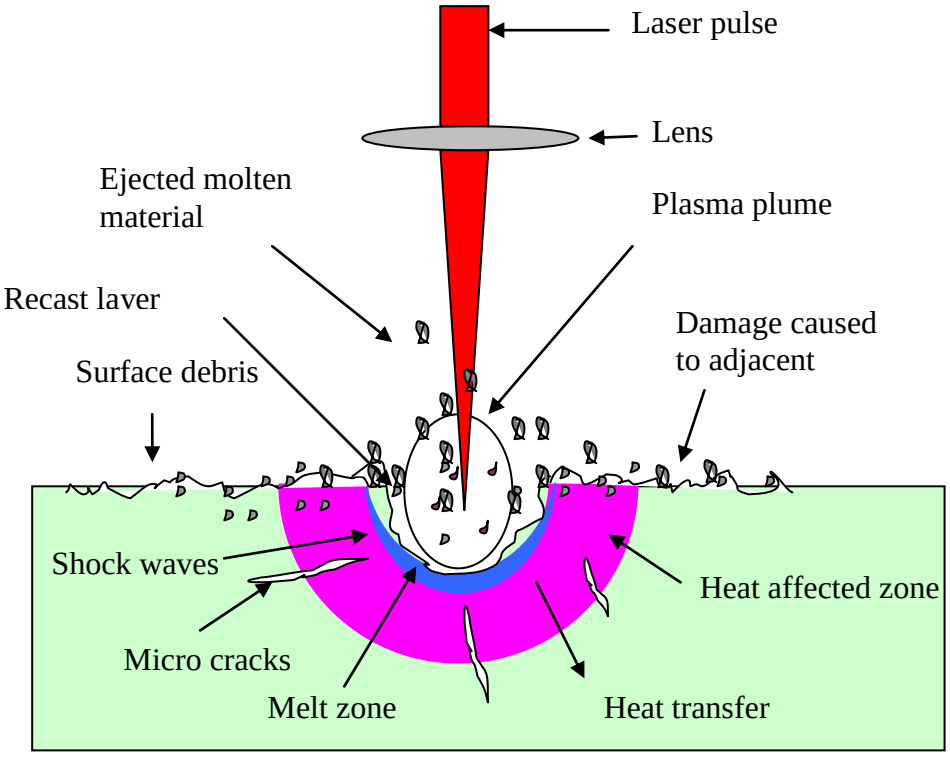

Figure 1.1: Schematic presentation of laser interaction with a solid, modified from reference [4].

The development of techniques to introduce solid samples into analytical instruments and eliminate cumbersome digestion procedures have been a long-term goal of analytical methodology research [8]. Compared with conventional dissolution techniques, laser ablation has many advantages. Most analytical techniques involve removing a portion of the solid sample, which is then dissolved in acid solutions. With this procedure, there is an increased risk of exposure to hazardous materials and there is an increased chance of introducing contaminants or losing volatile components during sample preparation [8]. Chemical analysis using laser ablation typically requires much smaller amounts

of the material (typically less than a microgram) than required for solution nebulization (about a milligram) [7, 9]. For laser ablation, most types of solid sample can be ablated for analysis; there are no sample size requirements and little or no sample preparation procedures [9]. Another advantage of laser ablation is the high spatial resolution of the sampling down to a few micrometers, which makes it superior in some applications such as depth profiling and micromachining. Techniques that separate sample introduction (accomplished by laser ablation) from sample atomization, excitation and ionization sources are of particular interest since each process can be independently optimized [5]. The application of laser ablation sampling in conjunction with inductively coupled plasma mass spectrometry (ICP-MS) has resulted in the development of extremely sensitive microprobes capable of determining most elements of the periodic table [10].

1.2 PROBLEMS

In spite of the many applications, the exact mechanisms of laser ablation are not yet fully understood. Moreover, different kinds of mechanisms can play a role, depending on the type of material, the laser irradiance (energy per unit area per unit time), fluence (energy per unit area), pulse width, wavelength, beam spot size, repetition rate, and the gas environment above the sample. In particular, LA-ICP-MS, which is today's most suitable technique for direct solid analysis, still suffers from a number of drawbacks, which are related to the ablation process, the aerosol transport and the vaporization, atomization and ionization of the laser-induced products within the ICP [11]. Elemental fractionation (selective

vaporization of elements depending on their thermal properties) is one of the drawbacks that may occur during laser ablation, aerosol transport, and in the ICP, and can limit the precision and accuracy of this technique [12 -16]. Matrix effects and the lack of matrix-matched standards are other drawbacks that limit the applications of LA-ICP-MS.

1.3 OBJECTIVES

The work in this thesis can be divided into two parts. The first part concentrates on improving analytical performance of LA-ICP-MS through understanding ablation processes using different types of laser systems (femtosecond and nanosecond lasers) and different gas mixtures (transport and ICP gas). Scanning electron microscopy was used to study surface morphology of ablated materials. By this technique we were able to get invaluable information about the laser beam profile and ablation characteristics which helped us to optimize the operating conditions of the laser beam. In the second part of this work we validated fs-LA-ICP-MS as a technique that can be applied for chemical analysis of sediment cores. This was done by using a simple sample preparation technique and the analysis of sediment reference materials by fs-LA-ICP-MS.

Chapter 2 describes the method commonly used to generate ultra short laser pulses and covers the basics of laser-solid interactions. Differences between femtosecond and nanosecond laser ablation are discussed. The problems encountered during this work regarding the laser beam profile and its optimization are also covered.

In Chapter 3 (published in J. Anal. Atom. Spectrom. 2008, 23, 1610-1621) we evaluate the analytical performance of near infrared (NIR) fs-LA-ICP-MS using femtosecond laser pulses operating at 785 nm and 130 fs with glass reference materials. The analytical results obtained for different reference materials are of great interest to many laboratories working with LA-ICP-MS and other similar techniques. The main questions of whether the pulse width affects the ablation behavior, fractionation and matrix effects were addressed in this chapter.

Chapter 4 investigates the effect of plasma gas mixtures on the sensitivity of fs-LA-ICP-MS. Hydrogen or nitrogen was mixed with the Ar transport gas before the ablation cell. Enhancement of sensitivity is important for determining elements at ultra trace levels or elements with high ionization potential. Mixed gas plasma (N_2+Ar) was also applied to the determination of Pb isotopes in NIST standard reference materials using femtosecond laser coupled to state-of-the art multiple collector inductively coupled plasma mass spectrometry (fs-LA-MC-ICP-MS).

In chapter 5, we applied fs-LA-ICP-MS for chemical analysis of different sediment reference materials (i.e. lake, stream and marine sediments). A simple method of sample preparation using Spurr low viscosity resin was applied to sediment reference materials and sediment cores. The results were compared to those obtained by solution ICP-MS and literature values.

In chapter 6, I summarized my thesis and discussed future work that can be done to improve the cababilities of LA-ICP-MS as a high spatial resolution analytical technique.

1.4 LITERATURE REVIEW

The first paper using laser ablation as a sample introduction technique for ICP-MS was by Alan Gray in 1985 in which limits of detection of less than 1 μg/g were demonstrated using relatively high laser powers to generate large pits [10]. It demonstrated the potential of laser ablation to be a powerful tool in the analytical sciences. In this study, geological samples were prepared in the form of disks and ablated by a low repetition rate (<1Hz) Q-switched ruby laser with λ= 694 nm and energies in the range of 0.3 -3 J. This ablation mode resulted in transient signals with precision limited by the pulse-to-pulse reproducibility of the laser. Laser ablation sample introduction can be broadly divided into two main classes, depending upon the mass of material ablated and the goal of the analysis. The two classes are: (1) bulk sample analysis (spot diameter generally >100 μm); and (2) microprobe analysis (spot diameter generally <100 μm) [12]. While Gray's study produced large pits of 0.5-0.7 mm in diameter (no real microanalyses were done), earlier reports [17-20] of laser ablation had already demonstrated the ability of lasers to make pits that approached the diffraction limit of focus, which is typically a few micrometers. Since Gray's work, there has been a developing trend towards small spot-size, microanalytical developments and applications of laser ablation ICP-MS [17-20].

Arrowsmith reported the first application of high-repetition-rate (10 Hz) Q-switched Nd:YAG (λ=1064 nm) laser ablation to the analysis of solids by ICP-MS [17]. Direct analysis of carbonates, zircon, olivine, and feldspars, and the ability to produce small ablation craters (20-30 μm) using a Nd:YAG laser at its fundamental wavelength (1064 nm) were demonstrated [18]. The use of a laser to

sample geologic materials allowed development of a relatively inexpensive microprobe for trace element and isotopic analysis of minerals. A laser sampling system specifically designed to sample solids at high spatial resolution and coupled to an ICP-MS analyzer for analysis of geological materials was first reported by Jackson et al. in 1992 at the Memorial University of Newfoundland [20].

The basic limitations in infrared (IR) lasers (i.e. coupling efficiency) led researchers to investigate the benefits of shorter wavelengths. A move from the longer wavelength lasers of earlier systems (ruby laser of Gray [10] and fundamental Nd:YAG laser wavelength (1064 nm) of Arrowsmith [17]) to shorter wavelength systems (Nd:YAG frequency quadrupling: 266 nm, and quintupling: 213 nm) improved energy absorption by many minerals and resulted in significantly improved ablation characteristics [12, 21, 22]. Laser wavelengths in the ultraviolet (UV) region are much more strongly absorbed than longer wavelengths resulting in rapid energy deposition over very short depths in most sample matrices. However, some minerals (i.e. quartz, apatite, feldspar, fluorite and calcite) still have relatively low absorption even at wavelengths as short as 266 nm [22]. Consequently, considerable interest has been expressed in shorter wavelength Excimer lasers as the ablation source. Excimer lasers use the primary UV photons emitted by an excited dimer in a gas mixture, such as XeCl (308 nm), KrCl (248 nm), ArF (193 nm), or F_2 (157 nm). The 248 nm wavelength has little wavelength advantage over a frequency quadrupled Nd:YAG laser (266 nm), so most attention has been focused on the ArF option (193 nm) [22]. Owing

to extremely strong absorption at this wavelength, excellent ablation characteristics have been demonstrated in a variety of geological samples [23].

Earlier work by Fryer et al.[12] and Jeffries et al. [24] demonstrated the limitations of LA-ICP-MS analysis because of significant fractionation effects observed during the ablation for some elements, especially Zn, Pb, and U which are of major interest in geological samples. Fractionation effects due to different ablation rates of various elements have prevented quantification without matrix-matched standards with 1064 nm Nd:YAG lasers. These effects have been reduced but not eliminated using shorter UV wavelengths (i.e. quadrupled (266 nm) and quintupled Nd:YAG (213 nm) harmonics) [12, 21].

LA using the 4th and 5th harmonics of Nd:YAG, *i.e.* at 266 and 213 nm, respectively, still represents the most common way of solid sampling [12, 22]. However, the formation of µm-sized particles generated during the initial stage of ablation has been identified to strongly affect precision and accuracy of Nd:YAG-based LA-ICP-MS analysis [13]. These particles are known to insufficiently evaporate within the ICP source resulting in noisy and intensively fractionating elemental signals. In fact, nonaccurate quantification of UV-transparent matrices as a result of particle size-related elemental fractionation has been documented as a limiting factor preventing UV-nanosecond (ns)-LA-ICP-MS at 266 and 213 nm to be considered as a universal tool for the analysis of both opaque and highly transparent materials [13]. In contrast, the introduction of laser systems emitting below 200 nm was found to significantly suppress the formation of µ-sized particles enabling more reliable analyses for a wider range of sample materials. UV-ns-LA at 193 nm using an ArF-type Excimer has been proven to

create well-conditioned aerosols, both in terms of particle size and composition. Recently, UV-ns-LA-ICP-MS at 193 nm applying non-matrix-matched calibration and internal standardization has successfully been applied to analyses of various silicate glasses and minerals [16, 25]. Despite these advantages, excimer laser systems working at deep UV wavelengths are not easy to maintain and require operation in a nitrogen or a vacuum environment, since these wavelengths are easily absorbed by air.

The thermal effects associated with nanosecond (ns) laser ablation lead to material re-distribution during the ablation process. As a consequence, the total composition of aerosols formed can deviate considerably from the bulk value, especially if intensively fractionating matrices such as brass or aluminum alloys, need to be analyzed. Reducing the pulse duration down to the femtosecond range has been suggested to improve the ablation characteristics by reducing thermal effects and to get closer to the concept of matrix-independent, stoichiometric sampling [26-28]. For instance, Russo and co-workers [27] found elemental fractionation during the analysis of various materials by near infrared (NIR)-femtosecond (fs)-LA-ICP-MS to be less pronounced. Furthermore, Gonzalez et al. [28] demonstrated the feasibility of non-matrix-matched calibration for several Zn-based alloy standards applying UV-fs-LA-ICP-MS. Koch et al. [29] explored the analytical figures of merit of ultra-violet femtosecond laser ablation inductively coupled plasma mass spectrometry (UV-fs-LA-ICP-MS) using the 3rd and 4th harmonics of Ti:Sapphire (~265 and ~200 nm, respectively). They demonstrated that signal ratios determined for highly and less fractionating

elemental systems such as $^{66}Zn/^{65}Cu$, $^{208}Pb/^{238}U$, and $^{238}U/^{232}Th$ are hardly affected by the wavelength or laser repetition rate applied.

Successful applicability of laser ablation sampling for chemical analysis depends on several criteria. Among these are: sampling a sufficient and a known amount of mass; spot-to-spot reproducible sampling; absence of matrix effects such as different ablation rates, preferential vaporization, or fractionation, and efficient transfer of the ablated mass to the detection system. However, the ablation rate can be a function of the sample composition and preferential vaporization of low melting point elements can occur [30]. To understand and improve the capability of laser ablation sampling for ICP-MS chemical analysis, fundamental studies on laser-solid interaction, transport of the ablated material, and ionization inside the ICP must be done.

1.5 REFERENCES

[1] S. A. Darke and J. F. Tyson, Interaction of laser radiation with solid materials and its significance to analytical spectrometry, J. Anal. At. Spectrom., 1993, **8**, 145-209.

[2] K. Niemax, Laser ablation-reflections on a very complex technique for solid sampling, Fresenius J. Ana. Chem. 2001, **370**, 332-340

[3] X. Zeng, X. L. Mao, R.Greif, and R.E. Russo, Experimental investigation of ablation efficiency and plasma expansion during femtosecond and nanosecond laser ablation of silicon, Appl. Phys. A 2005, **80**, 237-241.

[4] http://www.devicelink.com/mdt/archive/07/05/002.html

[5] P. Arrowsmith, Laser ablation of solids for elemental analysis by inductively coupled plasma mass spectrometry, Anal. Chem.. 1987, **59**, 1437-1444.

[6] L. Moenke-Blankenburg, Laser Microanalysis, John Wiely and Sons, Inc., New York, 1989.

[7] R. Russo, X. Mao, and S. Mao, The physics of laser ablation in microchemical analysis, Anal. Chem. 2002, **74**, 70 A-77 A.

[8] D. Günther, S. E. Jackson, and H. Longerich, Laser ablation and arc spark solid sample introduction into inductively coupled plasma spectrometers, Spectrochomica Acta Part B 1999, **54**, 381-409.

[9] R. E. Russo X. Mao, H. Liu, J. Gonzalez, and S.S. Mao, Laser ablation in analytical chemistry- a review, Talanta 2002, **57**, 425-451.

[10] Alan. G. Gray, Solid sample introduction by laser ablation for inductively coupled plasma source mass spectrometry, Analyst, 1985, **110**, 551-556.

[11] A. Bogaerts, Z. Chen , R. Gijbels, and A. Vertes, Laser ablation for analytical sampling: what can we learn from modeling?, Spectrochimica Acta Part B, 2003, **58**, 1867-1893.

[12] B.J. Fryer, S.E. Jackson, and H.P. Longerich, The design, operation and role of the laser ablation microprobe coupled with an inductively coupled plasma-mass spectrometer (LAM-ICP-MS) in the earth sciences. Can. Min., 1995, **33**, 303-312.

[13] M. Guillong, H. R. Kuhn, and D. Günther, Application of particle separation device to reduce inductively coupled plasma-enhanced elemental fractionation in laser ablation inductively coupled plasma mass spectrometry, Spectrochemica Acta B, 2003, **58**, 211-220.

[14] H. Kuhn, and D. Günther, Laser ablation-ICP-MS: particle size dependent elemental composition studies of filter-collected and online measured aerosols from glass, J. Anal. At. Spectrom., 2004, **19**, 1158-1164.

[15] J. J. Gonzalez, Scanning vs. single spot laser ablation (λ= 213 nm) inductively coupled plasma mass spectrometry, Spectrochimica Acta B 2004, **59**, 369-374.

[16] D. Günther and B. Hattendorf, Solid sample analysis using laser ablation inductively coupled plasma mass spectrometry, Trends in Anal. Chem., 2005, **24**, 255-265.

[17] P. Arrowsmith, Laser ablation of solids for elemental analysis by inductively coupled plasma mass spectrometry, Anal. Chem. 1987, **59**, 1437

[18] N.G.J. Pearce and W. T. Perkins, Mineral microanalysis by laser ablation inductively coupled plasma mass spectrometry. J. Anal. At. Spectrom. 1992, **7**, 53-57.

[19] H.P. Longerich, S.E. Jackson, B.J. Fryer, and D.F. Strong, The laser ablation microprobe-inductively coupled plasma-mass spectrometer. Geosci. Can. 1993, **20**, 21-27.

[20] S.E. Jackson, H.P. Longerich, G.R. Dunning, and B.J. Fryer, The application of laser-ablation microprobe-inductively coupled plasma-mass spectrometry (LAM-ICP-MS) to in situ trace-element determinations in minerals. Can. Mineral. 1992, **30**, 1049-1064.

[21] T. E. Jeffries, W. T. Perkins and N. J. G. Pearce, Comparisons of Infrared and Ultraviolet Laser Probe Microanalysis Inductively Coupled Plasma Mass Spectrometry in Mineral Analysis, Analyst, 1995, **120**, 1365-1371.

[22] T. E. Jeffries, S. E. Jackson, and H. P. Longerich, Application of a frequency quintupled Nd:YAG source (λ=213 nm) for laser ablation inductively coupled plasma mass spectrometric analysis of minerals, J. Anal. At. Spectrom., 1998, **13**, 935-940.

[23] D. Günther, R. Frischknecht , C. A. Heinrich and H. J. Kahlert, Capabilities of an argon fluoride 193 nm excimer laser for laser ablation inductively coupled plasma mass spectometry microanalysis of geological materials, J. Anal. At. Spectrom., 1997, **12**, 939-944.

[24] T. E. Jeffries, N. J. G. Pearce.a, W. T. Perkins and A. Raith., Chemical fractionation during infrared and ultraviolet laser ablation inductively coupled

plasma mass spectrometry-implications for mineral microanalysis, Anal. Commun., 1996, **33**, 35-39.

[25] M. Guillong, I. Horn and D. Günther , A comparison of 266 nm, 213 nm and 193 nm produced from a single solid state Nd:YAG laser for laser ablation ICP-MS, J. Anal. At. Spectrom., 2003, **18**, 1224-1230.

[26] V. Margetic A. Pakulev1, A. Stockhaus, M. Bolshov, K. Niemax, and R. Hergenroder., A comparison of nanosecond and femtosecond laser-induced plasma spectroscopy of brass samples, Spectrochim. Acta B, 2000, **55**, 1771-1785.

[27] R. E. Russo, Femtosecond laser ablation ICP-MS, J. Anal. At. Spectrom., 2002, **17**, 1072-1075

[28] J. Gonzalez, UV-femtosecond laser ablation-ICP-MS for analysis of alloy samples, J. Anal. At. Spectrom. 2004,**19**, 1165-1168.

[29] J. Koch, M. Walle, J. Pisonero and D. Günther, Performance characteristics of ultra-violet femtosecond laser ablation inductively coupled plasma mass spectrometry at ~265 and ~200 nm, J. Anal. At. Spectrom. 2006, **21**, 932-940.

[30] O. V. Borisov, X.L. Mao, A. Fernandez, M. Caetano, and R.E. Russo, Inductively coupled plasma mass spectrometric study of non-linear calibration behavior during laser ablation of binary Cu-Zn alloys, Spectrochimica Acta B 1999, **54**, 1351-1365.

CHAPTER 2

Fundamental Studies of Laser-Solid Interaction and Generation of Femtosecond Laser Pulses

2.1 INTRODUCTION

The development of femtosecond lasers has already shown an impact on spectroscopic investigations in different areas in physics, chemistry, engineering, medicine, and biology [1, 2]. Time-resolved spectroscopy, multiphoton imaging, micromachining, communications, isotope separation, and generation of intense bursts of x-rays are among the large number of applications of femtosecond laser pulses. The pulse energy obtained directly from a femtosecond laser is in the range of nanojoules, which is not sufficient for many applications. These femtosecond laser pulses have to be amplified to the microjoule and millijoule level to get their full potential. However, the pulses can not be amplified directly since the high pulse intensity would damage the optics in the amplifier. This is because of the non-linear effects induced by the very high intensity of the femtosecond laser pulses. Chirped pulse amplification (CPA) is a technique used for generation of ultrashort laser pulses without damage of the active medium or optics used. The concept of CPA is that a femtosecond pulse train produced by the oscillator (i.e. Ti:sapphire) is stretched (elongated in time by a factor of 1000-10000 times) in a pulse stretcher to reduce the intensity. The stretched pulse is then amplified to increase its energy. Finally, the amplified stretched pulse is compressed to produce energetic femtosecond laser pulses [3, 4]. The CPA is schematically shown in Figure 2.1.

2.2 CHIRPED PULSE AMPLIFICATION

In order to generate a laser pulse within a femtosecond time domain, the active medium should have a broad emission bandwidth. This is because the relationship between the pulse duration and its spectral bandwidth is governed by the Fourier-transform-limited pulse relation: $\Delta\upsilon\ \Delta t \geq K$, where $\Delta\upsilon$ is the frequency bandwidth measured at full-width at half-maximum (FWHM), Δt is the FWHM in time of the pulse and K is a constant depending only on the pulse shape (i.e. it equals 0.441 for Gaussian). The requirement of sufficient bandwidth during the amplification process limits the number of materials (active media) that can be used for the generation and amplification of femtosecond laser pulses to three types of materials: dye lasers (580-900 nm), Excimer lasers (ultraviolet), and solid state media [5]. For solid state media, Ti:sapphire has an emission spectrum that can support pulses down to about 6 femtosecond (fs). Other ultrafast solid state media that have attracted attention include: Nd:glass, Yb:glass, Yb:YAG, Cr:YAG, and chromium-doped forsterite (Cr:forsterite)[3, 6, 7, 8]. A femtosecond laser system consists of four sections [4]: 1- the oscillator, which generates the femtosecond laser pulses. 2- the stretcher, which consists of a pair of optical gratings used to expand the femtosecond pulse width. 3- the amplifier used to amplify the stretched signal, and 4- the compressor, similar to the stretcher, used to compress the amplified pulses.

2.2.1 Ti:SAPPHIRE OSCILLATOR

Titanium-sapphire ($Ti:Al_2O_3$) crystal, the gain medium of the laser oscillator, is most often used for femtosecond pulse generation in the near infrared. Its broad gain bandwidth (~ 200 nm) and its high thermal conductivity and high damage threshold make it suitable for the generation and amplification of ultra short laser pulses of a few femtosecond pulse width at the 800 nm central wavelength [6, 9, 10]. The minimum pulse duration that can be obtained from a spectrum with $\Delta\lambda$ nm at FWHM can be calculated from Fourier transformation: $\Delta t = K\frac{\lambda_0^2}{\Delta\lambda\, c}$, where λ_0 is the central wavelength and c is the velocity of light. This yields an expected minimum pulse duration for Ti:sapphire of about 5 fs [2]. Ultra short laser pulses are generated by mode locking (a technique by which a laser can be made to produce laser pulses of extremely short duration, on the order of picoseconds (10^{-12}s) or femtoseconds (10^{-15}s)). This mode-locked laser typically generates light pulses at high repetition rate (~10^8Hz).

When light propagates through a dispersive medium, different frequency components travel at different speeds (group velocity dispersion) because of the dependence of the refractive index of the medium on the wavelength. These result in stretching out a short pulse made of different frequency components. In case of positive dispersion (i.e. propagation of a pulse in media with normal dispersion), higher frequency components travel slower than lower frequency components and the pulse is said to be positively chirped. The opposite situation, when the pulse travels through a medium of negative dispersion, higher

frequency components travel faster than lower frequency components and the pulse is said to be negatively chirped. In an ultra short laser oscillator, positive dispersion in the gain medium and other optical components must be compensated. This can be done by inserting optical components with negative dispersion (pair of prisms or specially made chirped mirrors) in the oscillator [3]. Figure 2.2 shows a Ti:sapphire oscillator pumped with an argon laser.

2.2.2 THE STRETCHER

The laser pulses obtained from the Ti:sapphire oscillator have energies of the order of a nanojoule and pulse duration of a few femtoseconds. For amplification of these pulses without damage of the optics used, the pulses are first stretched and then amplified. The pulses are stretched in time using the dispersion properties of a pair of gratings arranged to give positive group velocity dispersion, see figure 2.3 [11]. By placing a telescope between the grating pair, the dispersion is controlled by the effective distance between the second grating and the image of the first grating [10]. By making the effective distance between the gratings negative, the sign of dispersion of the grating pair can be changed from negative to positive [12]. The grating disperses different frequency components into different directions. So each frequency component has a different optical path and the one with shorter path length comes out of the stretcher earlier than the one with longer path leading to a stretched or chirped pulse in time (the pulse is stretched to several hundreds of picoseconds). The

amount of pulse stretching is determined from the distance: $L_s = 4f - L_{sg}$ [3] where L_{sg} is the stretcher grating separation and f is the focal length.

2.2.3 AMPLIFICATION

Now the original femtoseconed laser pulses, generated from the oscillator, after being stretched in the optical stretcher can be safely amplified without exceeding the damage threshold of the amplifier materials. Regenerative and multipass amplifiers are most widely used for the amplification of femtosecond laser pulses. Regenerative amplification is a well-established technique for efficient generation of microjoule and millijoule energy ultra short pulses from solid state lasers [13]. In regenerative amplifiers (Figure 2.4) the low energy stretched pulse is injected and trapped in a laser cavity similar to that of the oscillator using a fast-switching Pockels cell and thin film polarizer [10]. This is performed by stepping the voltage in two stages, firstly by a quarter wave, in order to trap the pulse in the amplifier cavity and then up to a half wave for ejection. The pulse makes several roundtrips in the cavity before the gain is saturated. Pulse energies of millijoule levels can be obtained from regenerative amplifiers [3].

For further amplification of the laser pulses, a multipass amplifier is used (Figure 2.5). In the multipass amplifier the laser beam passes through the gain medium multiple times without being trapped in a cavity. Multipass amplifiers have lower efficiency than regenerative amplifiers because the pump-signal

overlap must change on successive passes through the gain medium in order to extract the beam by separating it spatially [10, 11].

2.2.4 PULSE COMPRESSION

Compression of amplified chirped pulses is the last stage in the generation of femtosecond laser pulses. This step is accomplished by using a grating pair similar to that used in the stretcher but arranged in such away to give opposite dispersion, as shown in Figure 2.6. The amount of pulse compression is determined by the grating separation L_c and the shortest pulses can be obtained when the stretcher grating separation L_{sg} equals the grating separation of the compressor. By changing the compressor grating distance L_c, continuous pulse widths can be obtained from the shortest compressed pulse to the uncompressed stretched value [3].

2.3 LASER-SOLID INTERACTIONS

The processes involved in laser-solid interactions are complicated and the mechanisms of interactions are different depending on the type of the material (conductor, semiconductor, or dielectric) and on the laser characteristics (wavelength, pulse duration, and fluence). Thermal and non-thermal mechanisms can be involved. For thermal processes, the laser wavelength plays an important role. For longer wavelengths, interaction of laser radiation with solids starts with the absorption of laser photons by the electrons in the material followed by electron lattice interactions that convert the absorbed laser energy into heat.

Melting and vaporization of the target material occur [14]. At shorter wavelengths(ArF 193 nm , F_2 157 nm), the laser energy may be sufficiently high to break the bonds between the neighboring atoms of the target material and the ablation process takes place largely without heating effects (non-thermal process) [14].

For evaporation to occur, the energy deposited in the laser-irradiated volume must exceed the latent heat of evaporation of the target, L_v, thus the minimum absorbed power density P_{min} below which no evaporation will occur is given by [15]:

$$P_{\min} = \rho L_v (D t_p)^{\frac{1}{2}} \qquad (1)$$

where ρ is the mass density of the solid, D the thermal diffusivity $\frac{K}{\rho C}$, K the thermal conductivity, C the heat capacity, and t_p the duration of the laser pulse.

The time required for the sample to be raised to its vaporization temperature is given by [16]:

$$t_v = \frac{\pi K \rho C (T_v - T_0)^2}{4P^2} \qquad (2)$$

where T_0 is the initial temperature, T_v the vaporization temperature of the sample, and P the laser power density. As K, C, T_v depend on the composition of the sample, t_v varies with composition. Hence, different elements will vaporize at different rates and a strong fractionation is linked to the thermal mechanism. Moreover, at the periphery of the crater, high temperature gradients exist, allowing segregation of elements of high and low boiling-point. Consequently, the ablated materials, in the form of droplets and vapor, may not have a composition wholly representative of the original sample [16].

The laser energy can be absorbed by the electrons of the material through single photon absorption (linear absorption) causing the material to breakdown. The cross section of such linear absorption mechanisms is high for opaque material using long laser pulses. In contrast, non-linear absorption processes (avalanche ionization and multiphoton ionization) become the dominant mechanisms in the interaction of ultra short laser pulses with transparent samples [3, 17].

2.3.1 LASER-INDUCED BREAKDOWN

Laser-induced breakdown is a process where a normally transparent material is transformed into an absorbing plasma by an intense laser pulse [3]. Such breakdown occurs when the density of electrons (known as critical plasma density) reaches approximately 10^{18} cm^{-3} for nanosecond or longer laser pulses and 10^{21} cm^{-3} for femtosecond laser pulses of wavelengths in the visible and near IR [3, 18]. These high electron densities provide a strong optical absorption in the plasma that can cause strong heating and damage to the material [18].

The initiation of laser induced breakdown requires the presence of seed electrons, whose mechanisms of production depend on the material [18]. For metals and semiconductors, free conduction band electrons can directly absorb the incident laser energy and be raised to higher energy levels. The electron energy is then transferred to the lattice via electron-lattice collision. In transparent dielectrics, there are no free conduction band electrons available to absorb the incident laser photons and the valence electrons are so tightly bound to their

nuclei that their ionization potential is greater than the incident laser energy. In fact, at lower laser intensity, the bound electrons do not absorb the laser light. So how can laser-induced breakdown be created in such a transparent dielectric material?

2.3.1.1 AVALANCHE IONIZATION

As mentioned above, to initiate a laser-induced breakdown, seed electrons are required. These electrons are supplied by thermal excitation from impurity (naturally present in any material) states into the conduction band [19]. In the presence of seed electrons, a non-linear process known as avalanche ionization takes place. For nanosecond and long laser pulses, avalanche ionization is the dominant mechanism of laser-induced breakdown. In this process the seed electrons are excited by the high electromagnetic field of the incident laser radiation and gain enough kinetic energy to release bound electrons by colliding with them (impact ionization). The newly freed electrons, then gain enough energy to free more electrons, which can then free more electrons, creating an avalanche effect (Figure 2.7). When enough bound electrons are ionized by this avalanche process, a plasma with critical density is created and the transparent material is brokedown and becomes absorbing [3]. The seed electrons are not uniformly distributed across dielectric materials (i.e. are subject to statistical variation) and their concentration is very low (i.e. about 10^{8}-10^{13} cm^{-3}). The low concentration of seed electrons lowers the probability of the presence of a single seed electron in the interaction volume. The statistical

nature of the distribution of seed electrons and their low concentration explain the stochastic nature of laser ablation with nanosecond laser pulses (i.e. the threshold fluence required to produce laser-induced breakdown will exhibit large fluctuations) [3, 19].

2.3.1.2 MULTIPHOTON IONIZATION

A second non-linear process responsible for the production of laser-induced breakdown is multiphoton ionization. For dielectric materials with wide band gaps, it is not possible to excite a bound electron from the valence band to the conduction band through a single laser photon absorption because the ionization potential of the bound electron is higher than the laser photon energy [17]. For femtosecond lasers where the laser intensity is very high due to the extremely short laser pulse duration, bound electrons can be directly ionized through multiphoton absorption (i.e. simultaneous absorption of multiple photons) [3, 17], Figure 2.8. This process can occur provided that the energy of the absorbed photons exceeds the energy gap E_g of the dielectric material, $kh\upsilon \geq E_g$, where k is the number of absorbed photons, h is Plank's constant, and υ is the frequency of the laser photon. The rate of multiphoton absorption is proportional to the intensity of the laser radiation [3].

The evolution of the free electron density n(t) in a dielectric material under the combined action of multiphoton excitation and avalanche ionization is given by [20]

$$\frac{dn}{dt} = \alpha_a I(t) n(t) + \sigma_k I^k \qquad (3)$$

where I(t) is the intensity of the laser pulse, α_a is the avalanche coefficient, and σ_k is the k-photon absorption cross section with the smallest k satisfying $kh\upsilon \geq E_g$, where υ is the laser frequency. Multiphoton ionization mechanisms dominate for femtosecond laser ablation over nanosecond laser ablation and provide a larger number of seed electrons for the avalanche ionization process [3, 19].

The laser ablation process using a nanosecond laser is different from that using a femtosecond laser. Here the pulsewidth plays an important role in determining the mechanisms of the ablation process. In laser-solid interaction, the vaporization process is often described by the one-dimensional heat flow equation [21]:

$$\rho C \frac{\partial T}{\partial t} = \frac{\partial T}{\partial z}\left(K \frac{\partial T}{\partial z} \right) + \alpha_b A I_0 \exp(-\alpha_b z) \qquad (4)$$

Where $T, \rho, C, K, and\ A$ are the temperature, mass density, specific heat, thermal conductivity and surface absorbance of the target, while I_0, α_b, and z are the intensity of the incident laser pulse, the absorption coefficient, and the z coordinate normal to the target surface. In femtosceond laser pulses the thermal conduction into the target can be neglected. The target temperature at the end of the laser pulse is given by [21]

$$T(z, t_p) = \frac{\alpha_b A F}{\rho C} \exp(-\alpha z) \qquad (5)$$

Where $F = I_0 t_p$ and t_p are the laser fluence and the laser pulse width, respectively. Vaporization occurs when $T\rho C$ exceeds the latent heat of evaporation per unit volume ρL_v, where L_v is the latent heat per unit mass;

$$\alpha_b AF \exp(-\alpha z) \geq \rho L_v \qquad (6)$$

The threshold laser fluence for femtosecond laser ablation is given by $F_{th} = \frac{\rho L_v}{\alpha A}$ and the ablation depth per pulse L is determined by the relation $L = \alpha_b^{-1} \ln \frac{F}{F_{th}}$ [22].

At very short laser pulses, energy is absorbed at a very thin layer at the surface. This layer is the called skin penetration depth $L_s = \alpha_b^{-1}$ and the heat affected volume can be neglected. With increasing pulse width, heat conduction becomes important and heat begins to propagate into a larger volume of the target. The heat penetration depth due to thermal conduction is given by the thermal diffusion length $L_{th} = \sqrt{Dt_p}$, where D is the heat diffusion coefficient [3, 21, 23]. So, with nanosecond pulses, the heat affected volume is determined by the thermal diffusion length which is dependent on the pulse width. A larger volume means a larger amount of laser energy will be required to raise this volume to the vaporization temperature. As a result the material will be heated and melted and ablation and material removal is achieved through liquid splashing.

The minimum spot size (maximum resolution) that can be obtained using a laser beam of wavelength λ in is diffraction limited and is given by the relation: [24, 25]

$$r = \frac{1.22\lambda f}{d}$$

Where r is the radius of the spot, f is the focal length of the objective lens, and d (in cm) is the aperture of the laser device. It is clear from this relation that the spatial resolution increases as the wavelength decreases (i.e. moving from IR to UV). In fact, lens aberrations and thermal effects do not allow ablation pits with theoretical spot sizes to be produced in the case of nanosecond laser ablation. The resultant pit may be larger than theoretical due to heat conduction from the plasma formed at the ablation site. Although the above relation is applied for any light beam passing through a narrow hole, the situation is different when pits are produced by femtosecond laser pulses. The minimum thermal effects, the absence of laser-plasma interaction and the well-defined ablation threshold of femtosecond laser pulses make it possible to produce pits with diameters smaller than the laser focus when the fluence is properly adjusted to be slightly above the ablation threshold. With femtosecond laser pulses the spot size is no longer limited by the smallest focus spot size given by the wavelength [26, 27].

2.3.2 LASER-PLASMA INTERACTION

When an intense laser pulse interacts with a target material, plasma is produced above the target and an interaction (this interaction is negligible in case of femtosecond laser pulses) between the incident laser pulse and the laser-induced plasma exists. The mechanisms of laser-plasma interaction include inverse bremsstrahlung(IB) and photoionization (PI)

In IB, free electrons absorb laser photons and gain enough energy to cause excitation and ionization of the laser-produced vapor through collisions with ground- and excited-state atoms. The IB absorption coefficient α_{IB} of the laser-induced plasma due to electron-ion collisions is given by [21]

$$\alpha_{IB} = \sigma_{IB} N_e = \frac{4}{3}\left(\frac{2\pi}{3k_B T_e}\right)^{\frac{1}{2}} \frac{Z^2 e^6}{hcm_e^{3/2}\upsilon^3} N_i N_e g_{ff}\left(1-\exp\left(-\frac{h\upsilon}{k_B T_e}\right)\right)$$

Where σ_{IB} is the IB cross section, N_i and N_e the number density of ions and electrons, Z the ionic charge, h Plank's constant, k_B Boltzmann constant, υ the laser frequency, T_e the electron temperature, g_{ff} Gaunt factor, m_e and e the electron mass and charge, and c the speed of light. In the IB absorption, a photon can be absorbed only if the electron passes very close to the ion at the instant of absorption, i.e. it must collide with the ion (a free electron is not capable of absorbing a photon, it can only serve as a scattering center). Hence the IB absorption coefficient α_{IB} is proportional to the number of ions as well as to the number of free electrons per unit volume [28]. From the above equation, we can see that the strength of IB absorption is inversely proportional to the cubic frequency of the laser. This means that in laser ablation using IR laser pulses, there is a stronger absorption by the laser-produced plasma to the incident laser pulses (plasma shielding) than ablation using UV laser pulses. Plasma shielding reduces the energy coupling efficiency to the target material and hence the amount of ablated mass.

During photoionization, laser photons are absorbed by atoms, molecules, and ions that compose the plasma and cause ejection of one or more electrons if

the incident photon energy is larger than the binding energy of electrons. These ejected electrons enhance the probability of photon absorption by IB. The absorption coefficient of photoionization α_{PI} is given by [21]:

$$\alpha_{PI} = \sigma_{PI} N_n \approx \sum_n 2.9\times10^{-17} \frac{(\varepsilon_n)^{5/2}}{(h\upsilon)^3} N_n \qquad (7)$$

where σ_{PI} is the photoionization cross section, $h\upsilon$: the photon energy (in eV), ε_n: the ionization energy (in eV), and N_n : the number density of the excited state n (in cm^{-3}). Here the probability of photoionization is dependent on the number of atoms in the excited states per unit volume.

2.4 FEMTOSECOND VERSUS NANOSECOND LASER ABLATION

Figure 2.9 shows in a simple way the difference between femtosecond and nanosecond laser pulses when focused onto a small spot size of micrometer scale. A 10 femtosecond laser pulse with energy of 1 mJ will produce a power density (energy per unit area per unit time) of 3.19×10^{16} $W.cm^{-2}$ when focused on a spot size of diameter 20μm. Production of the same amount of power density on a similar spot size using nanosecond laser pulses requires energy of 1000 Joules which is a huge amount of energy (i.e. 1000000 times the energy required by femtosecond laser pulses). This difference in power density (among other differences) contributes to the superiority of femtosecond lasers over nanosecond lasers in some applications.

Figure 2.10 shows a scanning electron micrograph (SEM) of a crater produced by nanosecond laser pulses (266 nm Nd:YAG laser at pulse width ~ 8

ns) on brass. A considerable portion of large particles (in the form of solidified droplets) are ejected with the formation of high-rim crater. It is clear, from that image that the particles deposited on the sample surface are produced by the ejection of molten material. This is a direct indication of the thermal effects characteristics of nanosecond laser ablation. Large particles are not efficiently transported to the Inductively Coupled Plasma (ICP) and if transported they will not be completely atomized and ionized. Furthermore the elemental composition of laser produced particles from brass [29] and glass [30] samples have been found to be strongly size dependent. This degrades the performance of LA-ICP-MS.

The situation is different when femtosecond laser pulses are used for ablation. Figure 2.11 shows SEM images of femtosecond laser ablation of materials having different properties (i.e. metals (brass, figure 2.11 a-b and gold, Figure 2.11-c) and dielectric (NIST 610 glass, figure 2.11-d)). The ablation craters are clean and the effect of thermal melting is very much reduced. Large fractions of small size particles are produced with a tendency of smaller particles to agglomerate into larger masses (Figure 2.11-b). High reproducibility is associated with femtosecond laser ablation, (Figure 2.11 c and d) even with widely different matrices (glass and metals) indicating the deterministic and less-matrix dependent behavior of femtosecond laser ablation.

2.5 FEMTOSECOND LASER BEAM OPTIMIZATION

During the course of this work, extensive investigations on surface morphology of different ablated materials using the scanning electron microscope

(SEM) have been done. Although the pulse width of a laser plays a very important role in determining the quality of ablation, other parameters (wavelength, fluence, spot size, repetition rate, beam profile and optics used) are also important as controlling factors of the ablation quality. For example, before running different experiments we had to make sure that we were using the right laser conditions. With femtosecond laser pulses, we were concerned about pulse stretching by the optics in the path of the laser beam from the laser source to the sample. We could not measure the pulse width of the raw laser beam at the source and at the sample to estimate the amount of pulse stretching due to problems associated with our autocorrelater (a device used to measure ultra short pulse widths) but we modeled pulse stretching using Lab View that showed insignificant pulse stretching in our optical system. Another problem we met at the beginning of this work was the beam shape. Investigations on surface morphology using SEM indicated the distortion of the femtosecond laser beam and its deviation from a true Gaussian beam. This problem can have serious consequences on the analytical results especially for some applications that require homogeneity of the laser beam such as depth profile analysis and micromachining. Some of SEM images that show this distortion are shown in figure 2.12. Figure 2.12-a. is a crater produced by 20 femtosecond laser pulses of NIST 610. It should be a single crater if the beam has a Gaussian profile (figure 2. 12-e) and has energy above the ablation threshold. But because of beam distortion, different parts across the laser beam have different energies which could be higher or lower than the ablation threshold leading to multiple

craters. The same behavior was confirmed by ablating brass in scanning (figure 2.12-b) and spot (figure 2.12 c-d) ablation modes, respectively. All of this work indicated that the laser beam might have a profile similar to the one shown in figure 2.12 f. There could be many reasons for this; a) the high intensity of femtosecond laser pulses could cause this distortion, b) misalignment of optics in the laser system and c) lens aberration (different rays incident at the lens at different angles are focused at different points). We minimized these problems by careful alignment of optics (both inside the femtosecond laser system and the transfer optics from the laser to the sample) and careful choice of objective lenses that have little aberration.

The work done in this chapter resulted in the significant improvement in the laser beam quality and resulting ablation characteristics that are required for improving the analytical performance of LA-ICP-MS. For example improving the beam profle (Figure 2—11 c,d) is essential for on accurate and precise elemental (Chapter 3 and Chapter 5) and isotopic analyses (Chapter 4).

2.6 REFERENCES

[1] A. Fuerbach, A. Fernandez, A. Apolonski, T. Fuji, and F. Krausz, Chirped-pulse oscillators for the generation of high energy femtosecond laser pulses, Laser and Particle Beams, 2005, **23**,113-116.

[2] D. H. Sutter, I. D. Jung, F. X. Kartner, N. Matuschek, F. Morier-Genoud, V. Scheuer, M. Tilsch, T. Tschudi, and U. Keller, self-starting 6.5-fs pulses from a Ti:sapphire laser using a semiconductor saturable absorber and double-chirped mirrors, IEEE J. Quan. Elec,1998, **4**,169-178.

[3] X. Liu, D. Du, and G. Mourou, Laser ablation and micromachining with ultrashort laser pulses, IEEE J. Quan. Elec., 1997, **33**, 1706.

[4] D. J. Harter, short pulse amplification in tunable solid state material, in Femtosecond to nanosecond high intensity lasers and applications, proceedings SPIE-The International Society for Optical Engineering, vol. 1229 (1990).

[5] F. G. Patterson, M. D. Perry, R. Gonzales and E. M. Campbell, Multiwatt Nd:glass lasers based on chirped pulse amplification, in Femtosecond to nanosecond high intensity lasers and applications, proceedings SPIE-The International Society for Optical Engineering, vol. 1229 (1990).

[6] G. Jonusauskas, J. Oberle, and C. Rulliere, 54-fs, 1-kHz pulse amplification in Cr:forsterite, Opt. Lett., 1998, **23**, 1918-1921.

[7] V. Yanovsky, Y. Pang, F. wise and B. I. Minkov, generation of 25-fs pulses from a self-mode-locked Cr:forsterite laser with optimized group-delay dispersion, Opt. Lett., 1993, **18**, 1541-1545.

[8] A. Sullivan, H. Hamster, H. C. Kapteyn, S. Gordon, W White, H. Nathel, R. J. Blair,'and R. W Falcone, multiterawatt, 100-fs laser, Opt. Lett., 1991, **16**, 1406-1408.

[9] D. E. Spence, P. N. Kean, and W. Sibbett, 60-fs pulse generation from self-mode-locked Ti:sapphire laser, Opt. Lett.,1991, **16**, 42-44.

[10] G. Cheriaux and Jean-paul Chambaret, Ultra-short high-intensity laser pulse generation and amplification, Meas. Sci. Technol., 2001, **12**, 1769-1772.

[11] S. Backus , C. G. Durfee, M. M. Murnane and H. C. Kapteyn, high power ultrafast lasers, Rev. Sci. Instrum., 1998, **69**, 1207-1223.

[12] J. V. Rudd, G. Korn, S. Kane, J. Squier, and G. Mourou, Chirped-pulse amplification of 55-fs at 1-kHz repetition rate in Ti:Al_2O_3 regenerative amplifier, Opt. Lett., 1993, **18**, 2044-2046.

[13] M. Lenzner, C. Spielmann, E. Wintner, F. Krausz, and A. J. Schmidt, sub-20-fs, kilohertz-repetition-rate Ti:sapphire amplifier, Opt. Lett., 1995, **20**, 1397-1399.

[14] R. E. Russo, X. Mao, H. Liu, J. Gonzalez, S.S. Mao, Laser ablation in analytical chemistry- a review, Talanta, 2002, **57**, 425-451.

[15] R. S. Adrian and J. Watson, Laser microspectral analysis: a review of principles and applications, J. Phys. D: Appl. Phys., 1984, **17**,1915-1920.

[16] S. F. Durrant, Laser ablation inductively coupled plasma mass spectrometry: achievements, problems, prospects, J. Anal. At. Spectrom., 1999, **14**, 1385-1403.

[17] S. S. Mao , F. Quéré, S. Guizard, X. Mao, R.E. Russo, G. Petite and P. Martin., Dynamics of femtosecond laser interaction with dielectrics, Appl. Phys. A, 2004, **79**, 1695-1709.

[18] J. D. Winefordner , I. B. Gornushkin, T. Correll, E. Gibb, B. W. Smith and N. Omenetto' Comparing several atomic spectrometric methods to the super stars: special emphasis on laser induced breakdown spectroscopy (LIBS), a future super star, J. Anal. At. Spectro., 2004, **19**, 1061-1083.

[19] M. Lenzner, F. Krausz, J.Kruger, and W. Kantek, Photoablation with sub-10 fs laser pulses, Appl. Sur. Sci., 2000, **154-155**, 11-16.

[20] M. Lenzer, J. Krüger, S. Sartania, Z. Cheng, C.. Spielmann, G. Mourou, W. Kautek, and F. Krausz, Femtosecond optical breakdown in dielectrics, Phys. Rev. Lett., 1998, **80**, 4076-4079.

[21] S. Amoruso, R. Bruzzese, N. Spinelli and R. Velotta, Characterization of laser-ablation plasmas, J. Phys. B: At. Mol. Opt. Phys., 1999, **32**, R131

[22] F. Korte, S.Adams, A. Egbert, C. Fallnich and A. Ostendrof, Sub- diffraction limited structuring of solid targets with femtosecond laser pulses, Opt. Express, 2000, **7**, 41-47.

[23] P. P. Pronko et al., Machining of sub-micron holes using a femtosecond laser at 800 nm, Opt. Communi., 1995, **114**, 106-110.

[24] D. Günther, S. E. Jackson, and H. Longerich, Laser ablation and arc spark solid sample introduction into inductively coupled plasma spectrometers, Spectrochomica Acta Part B 1999, **54**, 381-409.

[25] L. Moenke-Blankenburg, Laser Microanalysis, John Wiely and Sons, Inc., New York, 1989.

[26] D. Ashkenasi M. Lorenz, R. Stoian, and A. Rosenfeld, Surface damage threshold and structuring of dielectrics using femtosecond laser pulses: the role of incubation. Appl. Sur. Sci., 1999, **150**, 101-106.

[27] X. Liu, D. Du, and G. Mourou, Laser ablation and micromachining with ultrashort laser pulses, IEEE J. Quan. Elec., 1997, **33**, 1706-1711.

[28] Ya. B. Zel'dovich and Yu. P. Raizer, Physics of shock waves and high temperature hydrodynamic phenomena, Dover Publications, INC., Mineola, New York, 2002.

[29] J. Koch, A. von Bohlen, R. Hergenröder and K. Niemax., Particle size distributions and compositions of aerosols produced by near-IR femto- and nanosecond laser ablation of brass, J. Anal. At. Spectrom., 2004, **19**, 267-272.

[30] J. Koch H. Lindner, A. von Bohlen, R. Hergenröder and K. Niemax., Elemental fractionation of dielectric aerosols produced by near-infrared femtosecond laser ablation of silicate glasses, J. Anal. At. Spectrom., 2005, **20**, 901-906.

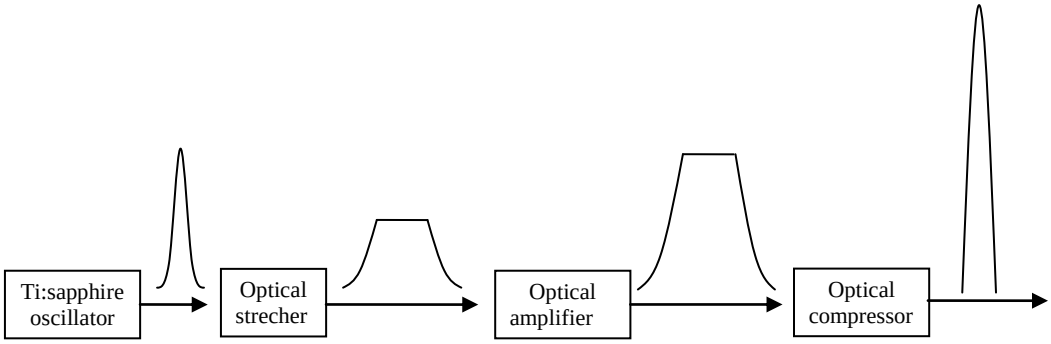

Figure 2.1: Schematic diagram showing the principle of chirped-pulse amplification (CPA). The oscillator output is stretched in the optical stretcher. The peak intensity is reduced in this process. The stretched pulse is then amplified in the amplifier before recompression in a grating-pair compressor.

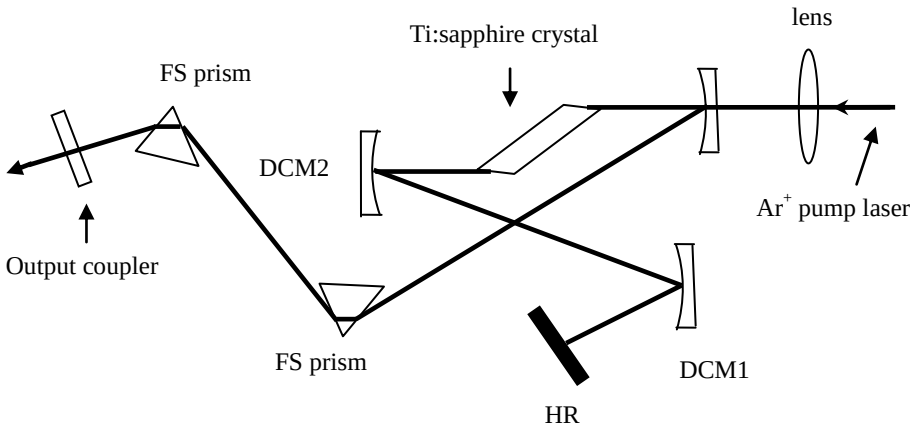

Figure 2.2: Schematic diagram representing Ti:sapphire oscillator which consists of two double chirped mirrors (DCM1, DCM2) and fused silica (FS) prism pair for compensation of dispersion., Modified from Ref. [2].

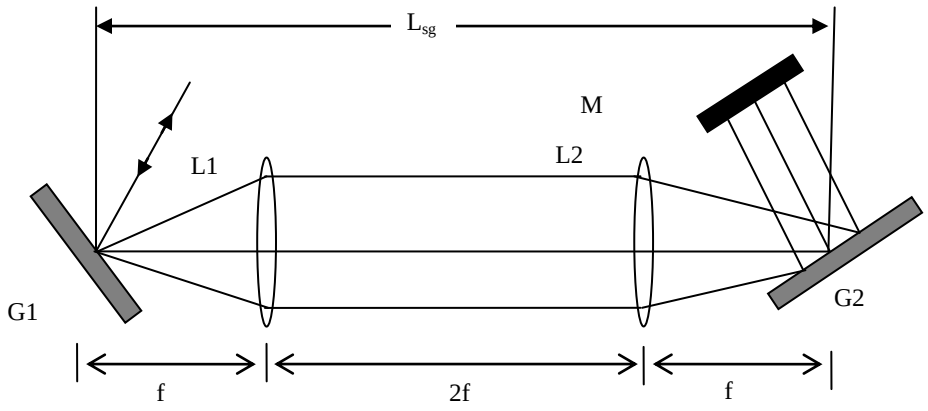

Figure 2.3: Schematic of a grating-pair pulse stretcher showing the arrangement for positive dispersion. G1 and G2 are diffraction gratings, L1 and L2 identical lenses separated by twice their focal length f. M is a mirror acting to double pass the beam through the system, Modified from Ref. [11].

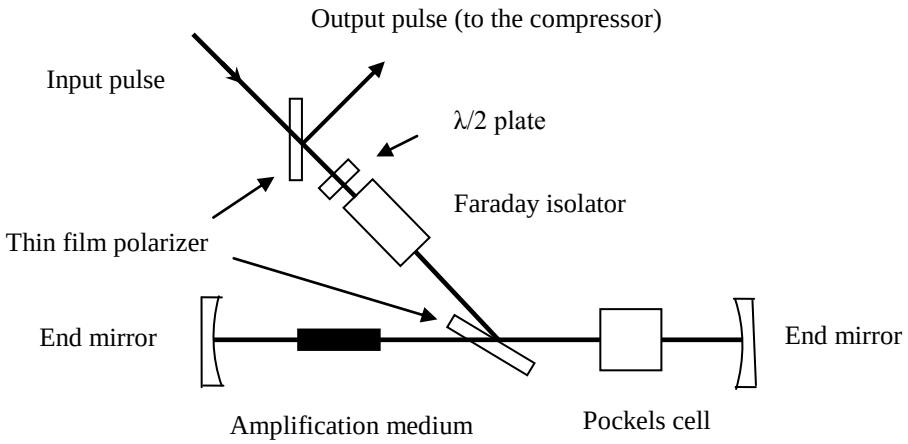

Figure 2.4: Regenerative amplifier, Modified from Ref. [10].

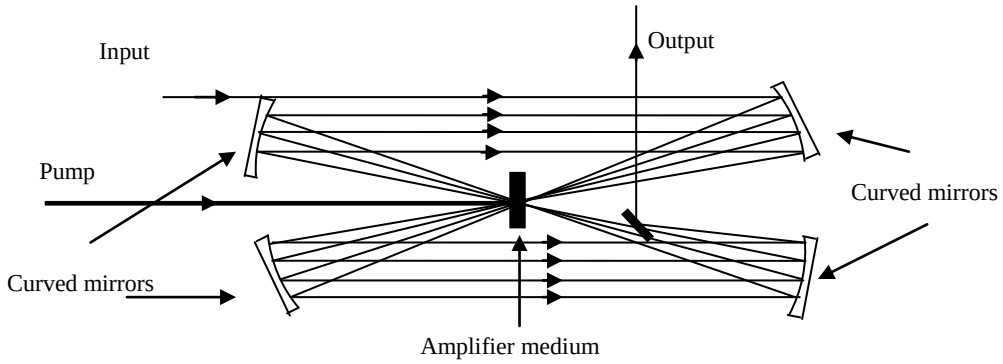

Figure 2.5: Schematic diagram of a multipass amplifier, Modified from Ref. [10].

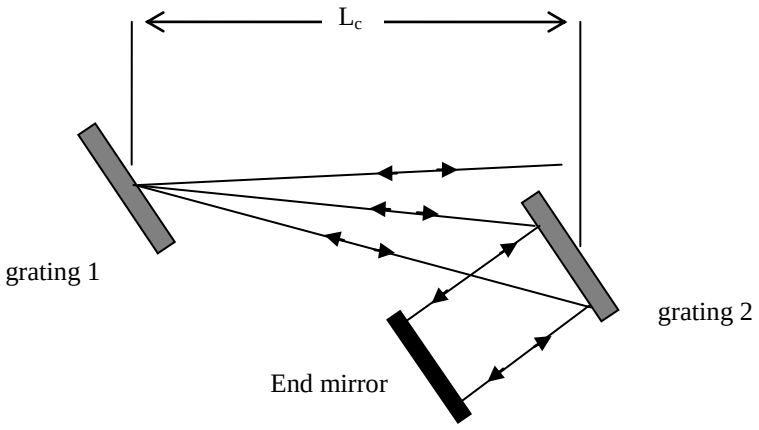

Figure 2.6: Schematic diagram for pulse compressor, Modified from Ref. [11].

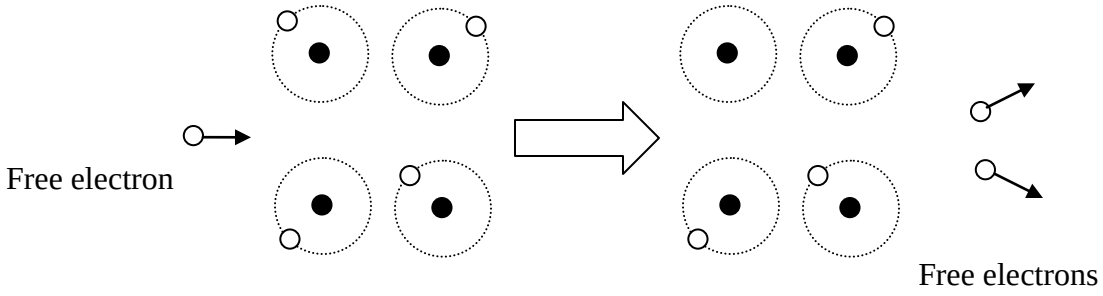

Figure 2.7: Schematic diagram representing avalanche ionization process.

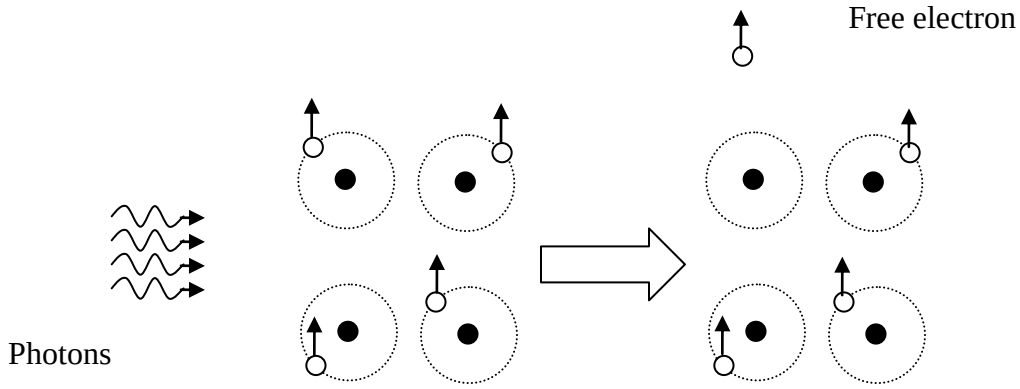

Figure 2.8: Schematic diagram representing multiphoton ionization process.

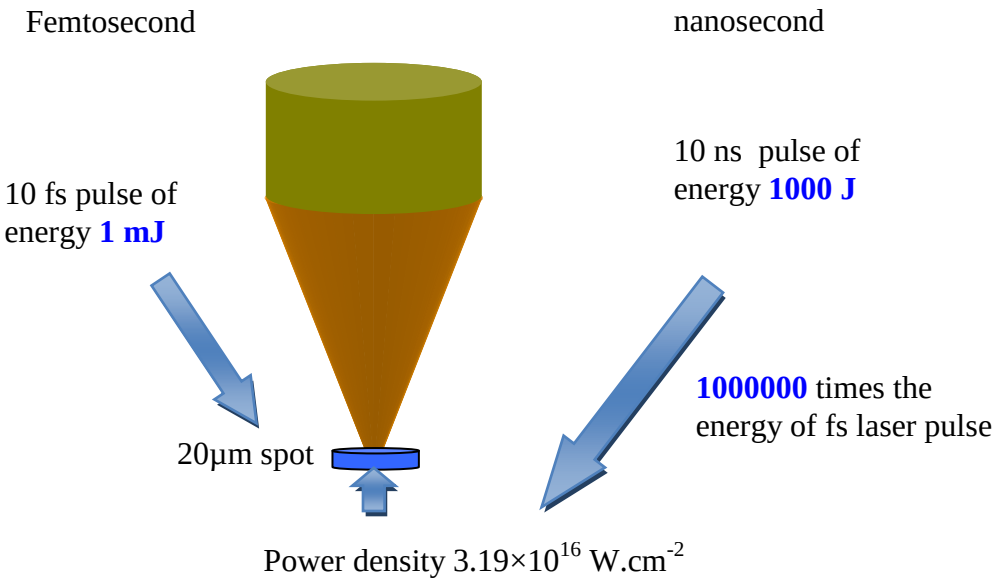

Figure 2.9: Schematic diagram shows a comparison between femtosecond and nanosecond laser pulse.

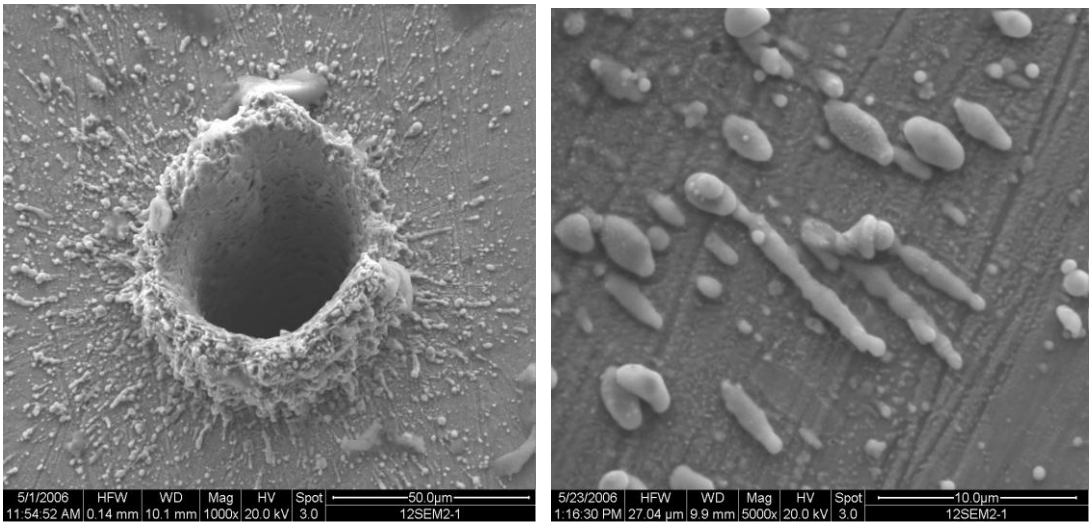

a b

Figure 2.10: Scanning electron micrograph (SEM) of a crater produced by nanosecond laser pulses on brass. The nanosecond laser system used was Nd:YAG laser operating at 266 nm and pulse width of about 8 ns. a: brass b: magnified image of a.

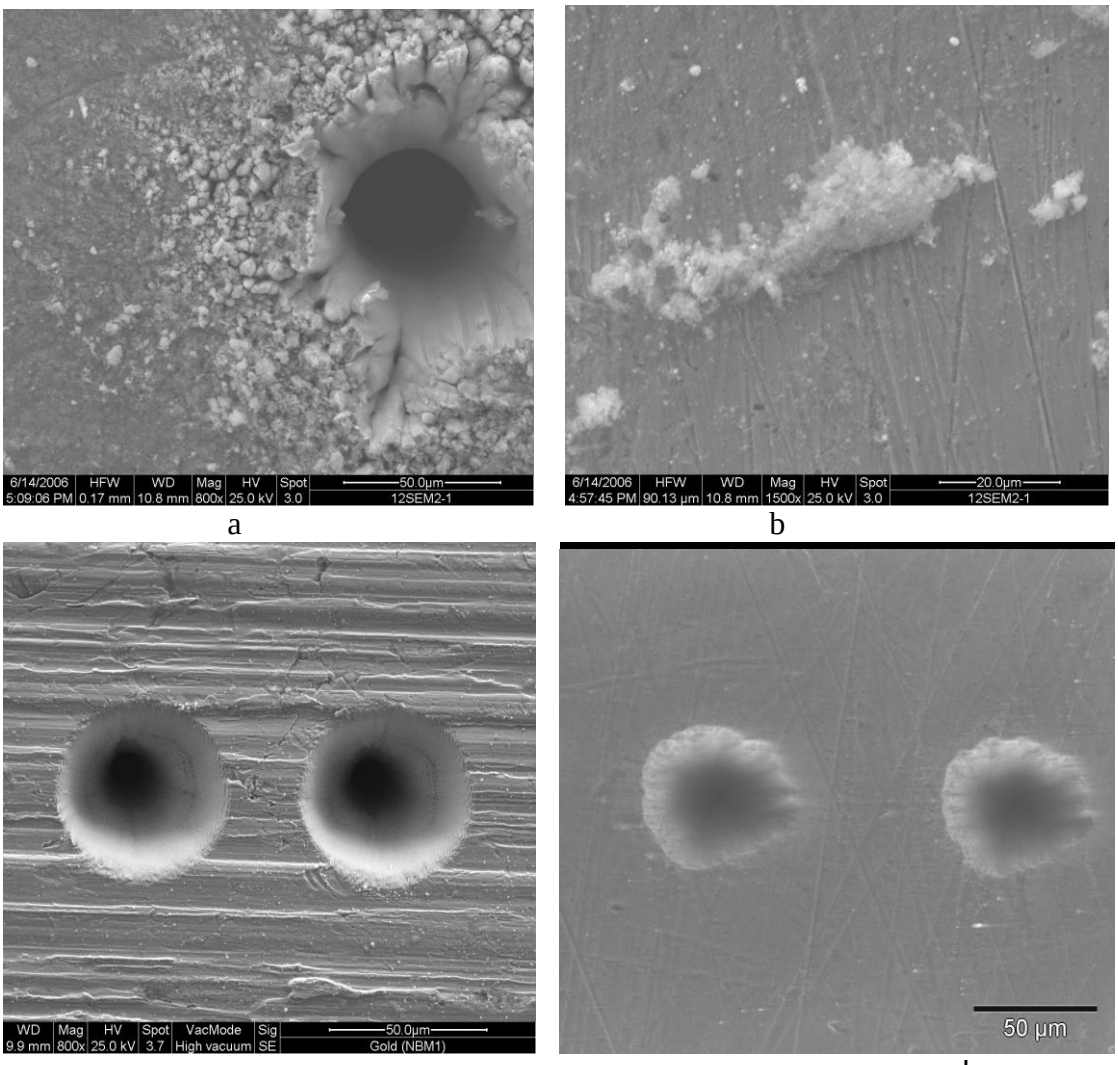

a b

c d

Figure 2.11. Scanning electron micrographs (SEM) of craters produced by femtosecond laser (785 nm) pulses on

a: brass;

b: magnified image of a;

c: gold: the surface is clean, no observed debris or ejecta, and high reproducibility of ablated craters.

d: NIST 610 (glass reference material): similar to c , clean ablation and high reproducibility of the ablated craters.

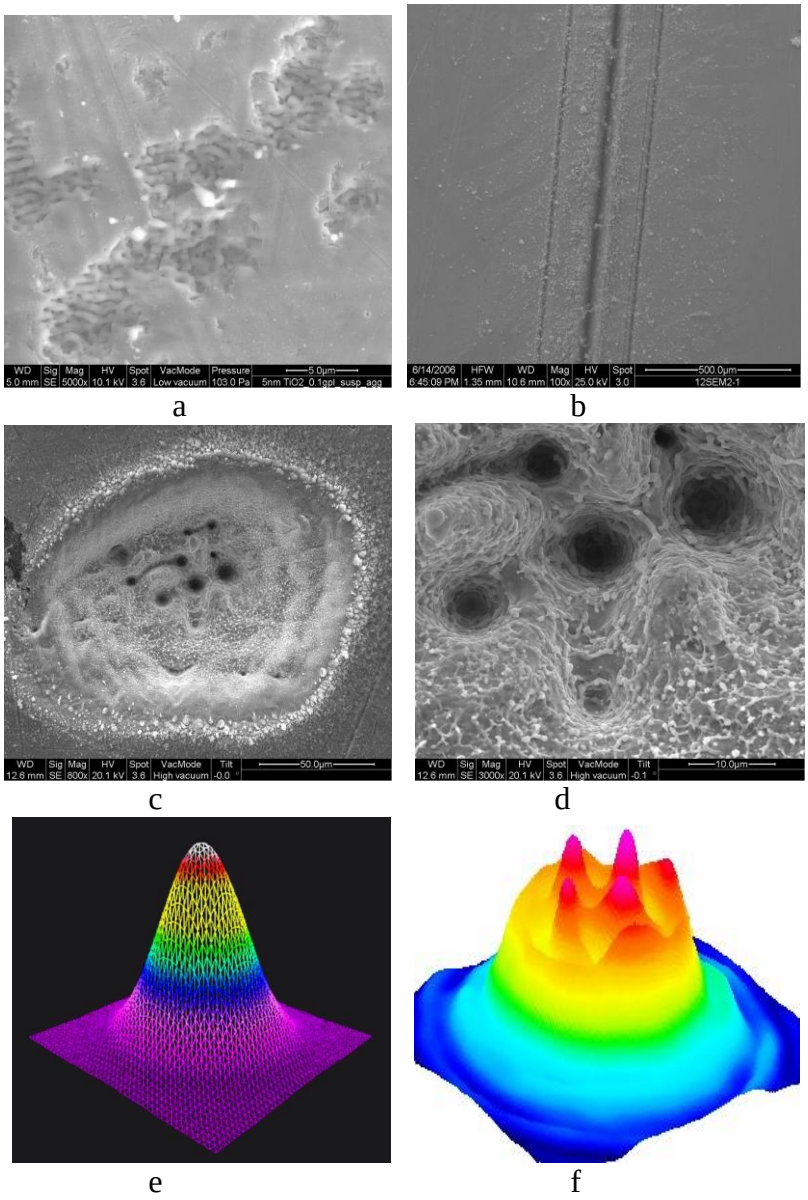

Fig. 2.12 : SEM images of craters produced by femtosecond laser(785 nm) pulses on NIST 610 (a) and brass (b-d), ideal Gaussian beam (e) and distorted Gaussian beam (f).

CHAPTER 3

Evaluation of the Analytical Performance of Femtosecond Laser Ablation Inductively Coupled Plasma Mass Spectrometry at 785 Nm with Glass Reference Materials

3.1 INTRODUCTION

Laser ablation (LA) with inductively coupled plasma mass spectrometry (ICP-MS) is a powerful analytical technique that has been applied to multi-element analysis of trace, minor and major elements of solids in many areas of science including geological [1–3], environmental [4-5], medical [6-7], biological [8-9] and forensic [10] as well as many other applications including semiconductor manufacturing [11-12]. In laser ablation, an intense laser pulse is used to remove a tiny mount of material from the irradiated sample [13–16]. Laser ablation is a complex process that is not fully understood. Many parameters involved in this process can interact in a complex way to make the processes of laser ablation complicated [17–24]. Wavelength, pulse width, fluence and repetition rate of the laser are among these parameters [25–30]. By decreasing the laser pulse width to the femtosecond (fs) range, mechanisms of laser-matter interaction become different. The non-linear mechanisms associated with fs laser ablation (avalanche and multiphoton ionization) are responsible for deterministic ablation behavior (i.e. well defined ablation threshold) and lower threshold fluence [31–33]. Ablation with fs laser pulses is less matrix-dependent and the produced particles have a narrower size distribution, with the maximum shifted toward the smaller size ranges compared to nanosecond (ns) laser ablation [34–36].This improves the transport and ionization efficiencies of the ablated material during LA-ICP-MS analyses.

Over the last few years a number of studies have investigated the application of fs lasers systems to elemental and isotopic analysis of a range of

materials. Quantitative analysis of iron-based samples showed the improved analytical performance of UV-fs-LA-ICP-MS compared to ns laser ablation when non-matrix matched standards were used [36]. More precise elemental (Pb/U, Pb/Th) and Pb isotopic ratios in glass, monazite, and zircon were obtained from UV-fs-LA-ICP-MS compared to UV-ns-LA-ICP-MS [29]. Stable isotope ratios of Si and Fe were also determined using UV-fs-LA coupled to a multicollector inductively coupled plasma mass spectrometer MC-ICP-MS [37-38]. Precisions better than 0.1‰ (2 sigma) were obtained for both raster and spot ablation modes without the need of matrix-matched standards [38]. The use of UV fs laser pulses led to improved accuracy and precision of the analysis of Pb in zinc-based alloys [30].

Elemental and isotopic fractionation have been investigated for a number of elements in different matrices using NIR fs-,UV fs- and deep UV-fs-LA-ICP-MS [40-41]. Russo et al. studied Pb/U ratios and elemental fractionation for most elements in NIST 610 using NIR fs-LA-ICP-MS in the fluence range 1.5–29 J cm^{-2}. The laser fluence has been found to have significant effects on fractionation indices and on Pb/U ratio with fractionation indices of almost unity for fluences between 1.5–3.2 J cm^{-2} [42].

Elemental ratios ($^{66}Zn/^{65}Cu$, $^{208}Pb/^{238}U$ and $^{238}U/^{232}Th$) and fractionation indices of elements from Li to U of aerosols produced by UV (265 nm) and deep UV (200 nm) fs-LA of NIST 610 under varying fluence conditions (2–30 J cm^{-2}) were also studied by Koch et al. [43]. It was found that these elemental ratios are hardly affected by the wavelength or the laser repetition rate. However, Ca-

normalized fractionation indices for elements were found to deviate by more than 20% from unity for fluences close to threshold fluence while at higher fluences less deviation was observed even for the most critical elements like Zn, Cd and Pb. ICP-induced elemental fractionation was observed at higher fluence due to increased mass loading of the plasma source. Horn et al. [40] studied elemental (Pb/U) and isotopic ($^{56}Fe/^{54}Fe$) fractionation using deep UV fs LA coupled to multicollector (MC)-ICP-MS. The results illustrated the absence of elemental and isotopic fractionation when the analyses were carried out without matrix match or when utilizing different ablation protocols between sample and calibration standards for spot ablation. Pecheyran et al. [39] used a high repetition rate (300 Hz) and low energy (0.06 mJ) IR (1030 nm) with fs-LA-ICP-MS to study elemental fractionation of 41 elements in NIST 612. Fractionation indices close to unity have been observed which indicates negligible fractionation effects. Their results indicated that low energy and high repetition rate fs laser ablation behaves similarly to high energy and low repetition rate fs laser ablation in terms of elemental fractionation.

The capabilities of NIR and UV fs LA and the influence of pulse width (from 60 fs to 3000 fs) on the analyses of geomaterials (monazite, zircon and NIST glass reference materials) by ICP-MS have been investigated by Freydier et al. [41]. Better analytical performance and more accurate $^{208}Pb/^{238}U$ ratios were obtained for the shortest pulse width. UV (266 nm) fs-LA did not show any improvement over 800 nm.

In this paper we report the analytical performance for a comprehensive list of elements, in terms of precision and accuracy, of NIR fs LA-ICP-MS replicate spot analyses of NIST and USGS glasses which collectively comprise a wide range of element concentrations in two significantly different matrices. Also the fractionation indices of 63 elements in NIST 610 have been investigated as well as the ability of NIR fs LA-ICP-MS to accurately measure the critical U/Pb ratio in different matrices and at variable concentrations. The purpose of this study is to critically evaluate the robustness of NIR fs LA-ICP-MS as an improved analytical method, for as large an element suite as feasible and at concentrations ranging from many mg g^{-1} to 10's of ng g-1, for a range of silicate glass matrices.

3.2 EXPERIMENTAL

3.2.1 LASER ABLATION SYSTEM

The laser ablation system at the Great Lakes Institute for Environmental Research (GLIER), University of Windsor, Canada, consists of a Quantronix Integra C® fs laser operating at the fundamental wavelength of 785 nm. It is a regenerative and multi-pass Ti:sapphire laser ablation system based on the Chirped Pulse Amplification (CPA) technique. The maximum energy that can be obtained from this laser system is 2 mJ (at 1KHz) in the near infrared (NIR). The operating conditions of the laser are shown in Table 3.1. A raw laser beam of pulse energy 0.58 mJ (prior to focusing) was used without any modifications for the analysis of calibration and reference materials. The pulse width may have been stretched to be greater than the primary output of 130 fs by the objective

lens and the ablation cell window. All work reported here used a repetition rate of 20 Hz to achieve high signal/background ratios. Ablation was conducted in an Ar gas environment in an ablation cell mounted on a 3D computer-controlled translation stage. The sample surface was adjusted to be at the focus of the objective lens by moving the stage up and down and monitoring the clearest image of the sample surface through transmitted light and a CCD camera. The objective lens was simultaneously used for focusing the laser beam and imaging the sample and the focus was assumed to be at the position where the clearest image takes place.

3.2.2 ICP-MS:

The ablated material was transported from the ablation cell to the ICP-MS by Ar carrier gas through a 1.5 m polyethylene transport tube with an internal diameter of 4 mm and analyzed using a ThermoElectron X7-II® ICP-MS. The instrument was optimized prior to analysis for maximum sensitivity and low oxide formation (ThO/Th <0.1%) at constant laser energy (0.58mJ) and constant crater size (75 mm) while NIST 610 was moved at a speed of 5 µm per second under the focus of the laser beam. A summary of ICP-MS specifications and operating conditions is shown in Table 3.2. The experimental setup for laser beam path and optics is shown in Figure 3.1.

3.2.3 MATERIALS:

Trace element doped glass reference materials (NIST 610, NIST 612, and NIST 614) and fused basalt glass reference materials from the United States Geological Survey (BCR-2G, BHVO-2G, and BIR-1G) were used as unknown samples with NIST 612 as an external standard for all experiments. Various studies have verified the homogeneity of these NIST reference materials for most elements with the exception of some volatile or non-lithophile elements, including F, Br, Se, Ag, Cd, Re, Au and Tl, which can be partly lost during glass manufacture and are expected to have heterogeneous distribution within the glass material [44–47]. Analyses of USGS basalt glass reference materials using different analytical techniques have indicated their homogeneity on the µm to mm scale with respect to major and most trace elements [48–50].

All samples were polished and cleaned by immersion in dilute nitric acid (2%) for a minute and then by sonication for 15 minutes in MilliQ® water. Immediately before analysis, the surface of each sample was cleaned with ultrapure ethanol. For each measurement, a fresh area on the sample surface was ablated at a fixed position at the focus of the laser beam. To determine the precision and accuracy of the analysis, 10 replicate analyses of each sample were conducted. The experiments were carried out in the following cycle sequences (2 NIST 612, 10 unknown, 2 NIST 612). The unknown can be NIST 610, NIST 612, NIST 614, BCR-2G, BHVO-2, or BIR-1. Sixty three elements have been quantified using the internal standard method, with Ca as an internal standard.

3.3 DATA ACQUISITION AND REDUCTION

All LA-ICP-MS measurements were carried out using time- resolved analysis operating in a fast peak jumping mode (one point per peak, 10 ms dwell time and 1.78 ms average settling time). Each spot analysis consists of 60 s gas background followed by 150 s ablation for signal collection. The ablation cell was flushed for 1 minute (no ablation) between analyses to reduce memory effects. Background-corrected signals were obtained by subtracting the acquired analyte intensity (counts s^{-1}) of a gas blank (60 sec without laser firing) from the gross analyte signal intensity (counts s^{-1}) obtained during lasering the sample (150 s of ablation). Data manipulation was performed off-line using commercial spreadsheet software by manual operation and in-house written software based on Longerich et al. [51]. The element concentrations used for calibration (NIST 612) and analytical comparisons were obtained from the preferred values of GeoRem (Jochum, Nehring and Stoll, Max Plank Institute for Chemistry, 2006) published online [52].

3.4 RESULTS AND DISCUSSION

3.4.1 ABLATION CHARACTERISTICS

Figure 3.2 shows CCD camera images of NIR-fs laser ablation of 3 different transparent materials (NIST 610, 612, and 614). The images show that the ablation behavior of fs laser pulses at the fundamental wavelength (785 nm) is similar for materials with significantly different transparencies (lowest NIST 610 to highest NIST 614. More information on the ablation behavior of fs laser pulses

can be obtained by going down to the microscopic scale, through the study of the ablated materials using a Scanning Electron Microscope (SEM). The Quanta FEG SEM at the Great Lakes Institute for Environmental Research (GLIER), University of Windsor, Canada, was used to image ablated surfaces to investigate the morphology of ablation structures on NIST 610. Figure 3.3a presents a traverse ablation (speed 5µm s^{-1}) of NIST 610 in air produced by NIR-fs laser pulses at an energy of 0.12 mJ (measured before the focusing lens) and a repetition rate of 10 Hz. Figure 3.3b and 3.3c are magnified images of figure 3.3a. The SEM images show minimal thermal effects. Most of material deposited on the surface around the ablation line consists of fine condensate particles of fluffy material with only a few spherical particles of melt droplets having diameters smaller than ~500 nm. Figure 3.3e shows an individual NIR-fs laser pit on NIST 610. The crater walls are clean and do not show the high rim or solidified droplets of melt ejecta characteristic of ns laser ablation. The irregularities in the edge structure are likely related to inhomogeneities in the raw laser beam that was used for ablation. Cracks on the bottom of the craters were observed and signs of some thermal effects can be seen through the worm-like structure at the bottom of the craters. Figure 3.3f shows the reproducibility of two craters produced by 300 laser pulses on NIST 610. In general, SEM images indicate that the dominant mechanism responsible for fs laser ablation is vaporization and subsequent condensation (as can be seen from the produced fine particles) in contrast to ns laser ablation where melt expulsion is the dominant mechanism of ablation.

The abundance-normalized sensitivities for elements in NIST 612, 612, 614, BCR-2G, BIR-1G, and BHVO-2G ablated under conditions listed in Tables 3.1, and 3.2 while moving the samples at a speed of 5 µm per second are shown in Figure 3. 4. For ablation using NIR fs laser pulses, all the glasses have very similar values and patterns of abundance-normalized sensitivity indicating little relative matrix dependency. The average abundance-normalized sensitivity for most elements higher than mass 89 (Y) was greater than 25000 cps /ppm for NIST 612 for scanning mode.

3.4.2 ELEMENTAL FRACTIONATION

Figure 3.5 shows the fractionation indices calculated in this study. The results are compared to those calculated by Fryer et al. [53] using a ns laser (266 nm). Fractionation indices were determined for two different ablation times (80 and 140 s) to test the influence of the increased depth of the ablation craters on elemental fractionation. We used a 20 Hz repetition rate in our experiment (Fryer et al. used 10 Hz) which means that the sample in our experiment was ablated by almost the same number of pulses as in the Fryer experiment. However the ablation rates in both cases are not the same which makes it difficult to get the same aspect ratios for a fair comparison.

Elements (P, Cu, Zn, Ga, Ge, As, Se, Mo, Ag, Cd, In, Sn, Sb, W, Re, Au, Ti, Pb, and Bi) which tend to have high fractionation indices (i.e. >1.5) in nanosecond laser ablation (266 nm, Fryer et al.[53]) have fractionation indices close to unity when using NIR fs laser pulses for ablation. The calculated

fractionation indices for 140 s ablation do not show significant differences from those calculated for 80 s ablation and are similar to those calculated for 193 nm nanosecond laser pulses [54].

3.4.3 QUANTIFICATION OF REFERENCE MATERIALS

In a test primarily of precision, all measured concentrations of NIST 612, treated as an unknown, agreed very well with the GeoReM values, although it is perfectly matrix matched, being calibrated against itself. Most of the elements (52 of 59) are within ±1% of the GeoReM values. The seven other elements (Sc, Rh, Cd, Pt, Au, Tl, and Bi) have deviations greater than ± 1%, but all lie within ± 1 SD (standard deviation) of the GeoReM values. RSDs are better than 3% for the majority of elements.

Concentration data for NIST 614 (Table 3.3, most elements at < 2 ppm) are within ±4 % of the GeoReM data for the majority (43 of 54) of elements detected. Only 6 elements lie outside ± 10% (Li, Be, B, Ti, Cr, and Au). Of these Li, Be, and Ti have concentrations very close to the detection limit (less than twice the detection limit). The detection limit was calculated as 3 times the standard deviation of the background according to Longerich et al. [51] (the list of detection limits is provided in Appendix B). The B concentration measured in this study (10.75 ppm) was much higher than the GeoReM value (1.44). Gagnon et al. [55] determined the concentration of B in NIST 614 as 19.7 ppm while Kurosawa et al [56] determined it to be 4.83 ppm. This variation in the measured B concentration might be an indication of contamination of the samples by B. RSDs for NIST 614 are less than 10 %, except for Li, Be, Ti, V, Cr, Co, Zn, Ga, Ge, Mo,

and W. The high RSDs of Be, V, and Co are related to the low concentration of these elements in NIST 614. Five elements (P, Sc, Fe, Ni, and Se) had concentrations lower than the detection limits and could not be quantified.

The measured NIST 610 concentrations (Table 3.4) for most elements lie within ±4 % of the GeoReM published values (44 of 59). Deviation greater than 10 % are observed for a few elements: B, Mg, P, K, Pd, and Bi. Deviation of Pd can be attributed to its lower concentration in NIST 610 (1.1 ppm). Most elements have external reproducibility of less than 10 %.

Table 3.5 lists the measured element concentrations in the basalt glass BHVO-2G. The majority of elements (40 out of 52) are within ± 15 % of the GeoReM values while six elements have concentrations lower than the detection limits (As, Rh, Pd, Cd, Re and Bi). Of the 7 elements that deviate more than 15% from the GeoReM values (P, Fe, Zn, Ge, Y, Sb and W) Ge, Y, Sb and W are either within the range of other reported values (Y) or within 1 ppm of the GeoReM values. The major deviation is Zn, which also has a fractionation factor slightly lower than unity in our fractionation experiment (figure 3.5) as well as in that of Koch et al.[43] , and this might be the reason for its deviation from GeoReM values. RSDs for the majority of elements are better than 10 % with the exception of Be, Ge, In, Sb, Cs, Pt, and Ti.

Analytical errors of elements in BIR-1G (Table 3.6) were less than ± 15 % for the majority of elements (30 of 51 detected). Deviations of more than ± 15 % were observed for K, Ti, Ge, Y, Ag, Gd, Tb, Ho, Er, Tm, Lu, Hf, Pt, Au and U. Beryllium, B, As, Mo, Rh, Pd, Cd, Cs, W, Re, Tl and Bi are found in BIR-1 at

concentrations lower than the detection limits. RSDs for the majority of most elements are better than 10 % with the exception of Ge, Ag, Pt, Au, Pb, and U.

Concentrations of most elements in BCR-2G (Table 3.7) agree within ± 15 % of the GeoReM values. Deviations greater than ± 15 % were observed for 5 elements; B, Ga, Ge, Cd, and Pt. Pt had the greatest deviation but it agreed with the value of Gagnon et al. [55]. Ge has a low concentration in BCR-2G (1.5 ppm) while Cd has a concentration (0.2 ppm) close to the detection limit (0.1 ppm). Precisions (RSDs) were better than 10 % except for B, Na, Cr, Ni, Ag, Cd, In, Pt, Au, Tl and Bi. The lower precisions for Cd, In, Pt, and Bi are related to counting statistics since these elements are present at low concentrations in BCR-2G. The chondrite-normalized concentrations of BCR-2G (Figure 3.6) indicate the utility of NIR fs LA under typical analytical conditions for accurate multielement analyses across the broad spectrum of elements and concentrations (Li-U) used in geological research investigations.

3.4.4 ANALYTICAL PERFORMANCE OF NIR (785 NM) FS LA-ICP-MS

The combined analytical data for the 6 glass reference materials studied demonstrate reduced (virtually eliminated except for Zn and Cd?) elemental fractionation by NIR femtosecond laser ablation under typical analytical conditions. The measured ^{206}Pb /^{238}U ratios of all the NIST and the USGS reference materials (Table 3.8) are identical to those calculated from elemental concentrations of Pb and U listed in reference [52], taking into account their natural isotopic abundances. This lack of measurable fractionation is achieved

while using laser fluence required for very low detection limits during LA-ICP-MS analysis.

The excellent agreement of our analytical data with reference values even at very low concentrations (e.g. at 100 ppb in BHVO-2G, for such diverse elements as Sb, Cs, and W; Table 3.4) during multielement (63) analyses demonstrates that NIR (785 nm) fs LA is a robust front end for ICP-MS analysis. UV fs LA systems appear to provide equivalent quality data to NIR systems [41, 43], when fluences significantly above ablation thresholds are used. However, typically, fs laser systems have primary pulse energies in the few (1-3) mJ range and the loss of pulse energy moving to the UV and deep UV range will compromise their performance when low detection limits are required or when large ion beams are required for isotopic analyses of elements at moderate concentrations, e.g. Sr at a few 100 ppm.

3.5 CONCLUSIONS

The concentrations determined for NIST glasses and basalt glasses using fs-LA-ICP-MS agree well with the certified, reference, and information values within a mean relative difference of ± 1 % (NIST 612, calibrated against itself), ± 4 % (NIST 610) and ± 4 % (NIST 614), and ± 15 % (BIR-1, BHVO-2, BCR-2G). NIR fs laser ablation showed little evidence of matrix effects. Elemental fractionation of elements that tend to have higher fractionation indices in ns laser ablation has been greatly reduced or eliminated when an NIR fs laser was used. This is related to the minimal thermal effects and the fine particles produced by

the NIR fs laser. Accurate single spot analyses (assuming the sample is homogenous) can be obtained by NIR-fs-LA-ICP-MS, which can avoid the problems associated with surface contamination, surface roughness, and sample size (in case of samples of limited sizes) encountered during raster analysis. More investigations are needed to establish the benefits of NIR vs UV and deep UV fs laser pulses, i.e. wavelength, for different applied analytical applications, as studies to date have not addressed this fundamental question. Based on studies [41, 43] to date there do not appear to be any obvious advantages to the added complexities of working in the UV and the loss of available laser energy may be a distinct disadvantage for studies requiring low detection limits or high precision in-situ isotopic measurements of elements at trace levels.

3.6 ACKNOWLEDGEMENTS

Support for this research was provided by National Sciences and Engineering Research Council Discovery Grants to B. Fryer and J. Gagnon. Infrastructure support was provided by CFI/OIT grants to B. Fryer and by the University of Windsor. M. Shaheen was supported, in part, by Cultural Affairs and Missions Sector, Ministry of Higher Education, Egypt.

3.7 REFERENCES

[1] D. Gunther, R. Frischknecht , C. A. Heinrich and H-J Kahlert, Capabilities of an Argon Fluoride 193 nm Excimer Laser for Laser Ablation Inductively Coupled Plasma Mass Spectometry Microanalysis of Geological Materials, J. Anal. At. Spectrom., 1997, **12**, 939-944.

[2] C. Geerstein., A. Briand, F. Chartier, J.-L. Lacour, P. Mauchient and S. Sjöström, Comparison between infrared and ultraviolet laser ablation at atmospheric pressure—implications for solid sampling inductively coupled plasma spectrometry**,** J. Anal. At. Spectrom., 1994, **9**, 17-22.

[3] E. V. Putten, F. Dehairs,E. Keppens and W. Baeyens, High resolution distribution of trace elements in the calcite shell layer of modern *Mytilus edulis*: Environmental and biological controls, Geochim. Cosmochim. Acta, 2000, **64,** 997–1011.

[4] W. R. Berti and L. W. Jacobs, Distribution of Trace Elements in Soil from Repeated Sewage Sludge Applications, J. Environ. Qual. 1998, **27,**1280-1286.

[5] S. F. Durrant, Multi-elemental Analysis of Environmental Matrices by Laser Ablation Inductively Coupled Plasma Mass Spectrometry, Analyst, 1992, **117,** 1585-1592.

[6] E. Hoffmann, H. Stephanowitz, E. Ullrich, J. Skole, C. Ludke and B. Hoffmann, Investigation of mercury migration in human teeth using spatially resolved analysis by laser ablation-ICP-MS , J. Anal. At. Spectrom., 2000, **15,** 663-667.

[7] F. Lochner, J. Appleton, F. Keenan and M. Cooke, : Multi-element profiling of human deciduous teeth by laser ablation-inductively coupled plasma-mass spectrometry, Anal. Chem. Acta, 1999, **401,** 299-309.

[8] J. Feldmann, A. Kindness and P. Ek, Laser ablation of soft tissue using a cryogenically cooled ablation cell, J. Anal. At. Spectrom., 2002, **17**, 813-818.

[9] S. Wang, R. Brown and D. J. Gray, Application of laser ablation_ICP-MS to the spatially resolved microanalysis of biological tissue, Appl. Spectrosc., 1994, **48,** 1321-1325.

[10] R. J. Watling, Novel applications of laser ablation inductively coupled plasma mass spectrometry in forensic sciene and forsenic archeology, , Spectroscopy, 1999, **14**, 16-34.

[11] L. Fuhe, M.K. Balazs and R. Pong, Total dose measurement for ion implantation using laser ablation ICP-MS , J. Anal. At. Spectrom., 2000, **15**, 1139-1141.

[12] V. Kanicky, V. Otruba and J. M. Mermet, Depth profiling of tin-coated glass by laser ablation inductively coupled plasma emission spectrometry with acoustic signal measurement, Fres. J. Anal. Chem., 2000, **366,** 228-233.

[13] A. L. Gray, Solid Sample Introduction by Laser Ablation for Inductively Coupled Plasma Source Mass Spectrometry, , Analyst, 1985, **110,** 551-556.

[14] B. J. Fryer, S. Jackson and H. P. Longerich, The application of laser ablation microprobe-inductively coupled plasma-mass spectrometry (LAM-ICP-MS) to the in situ (U)-Pb geochronology, , Chem. Geol., 1993, **109**, 1-8.

[15] C. A. Heinrich, T. Pettke, W. E. Halter, M. Aigner-Torres, A. Aud'etat, D. Günther, B. Hattendorf, D. Bleiner, M. Guillong and I. Horn, Quantitative multi-element analysis of minerals, fluid and melt inclusions by laser-ablation inductively-coupled-plasma mass-spectrometry, Geochim. Cosmochim. Acta, 2003, **67,** 3473-3497.

[16] J. E. Gagnon , I. M. Samson, B. J. Fryer and A. E. Williams-Jones, Compositional heterogeneity in fluorite and the genesis of fluorite deposits: Insights from LA-ICP-MS analysis, Can. Min., 2003, **41,** 365-382.

[17] D. Günther and B. Hattendorf, Solid sample analysis using laser ablation inductively coupled plasma mass spectrometry, Trends in Anal. Chem., 2005, **24,** 255-265.

[18] R. Russo, Laser ablation, Appl. Spectrosc., 1995, **49**, 14A-A28.

[19] A. Bogaerts , Z. Chen , R. Gijbels and A. Vertes, Laser ablation for analytical sampling: what can we learn from modeling?, Spectrochim. Acta, Part B, 2003, **58,** 1867-1893.

[20] S. Amoruso, Modeling of UV pulsed-laser ablation of metallic targets**.** Appl. Phys. A, 1999, **69**, 323-332.

[21] N. Bityurin and A. Malyshev, UV-laser ablation of absorbing dielectrics by ultra-short laser pulses, , Appl. Surf. Sci ., 1998, **127–129,** 199-205.

[22] A. Bogaerts, Z. Chen, Nanosecond laser ablation of Cu: modeling of the expansion in He background gas, and comparison with expansion in vacuum, J. Anal. At. Spectrom., 2004, **19**, 1169-1176.

[23] N.M. Bulgakova and A.V. Bulgakov, Pulsed laser ablation of solids: transition from normal vaporization to phase explosion, , Appl. Phys. A, 2001, **73,** 199-208.

[24] B.N. Chickov, C. Momma, S. Nolte, F. yon Alvensleben and A. Tiinnermann, Femtosecond, picosecond and nanosecond laser ablation of solids**,** Appl. Phys. A, 1996, **63**, 109-115.

[25] R. E. Russo, X. L. Mao, O. V. Borisov and H. Liu, Infuence of wavelength on fractionation in laser ablation ICP-MS, J. Anal. At. Spectrom., 2000, **15**, 1115-1120.

[26] J. S. Becker and D. Tenzler, Studies of LA-ICP-MS on quartz glasses at different wavelengths of a Nd:YAG laser, Fres. J Anal. Chem., 2001, **370,** 637-640.

[27] T.V. Kononenko S.V. Garnov , S.M. Klimentov, V.I. Konov, E.N. Loubnin, F. Dausinger, A. Raiber and C. Taut, Laser ablation of metals and ceramics in picosecond–nanosecond pulsewidth in the presence of different ambient atmospheres, , Appl. Surf. Sci., 1997, **109-110**, 48-51.

[28] J. Koch, H. Lindner, A. von Bohlen, R. Hergenroder and K. Niemax, Elemental fractionation of dielectric aerosols produced by near-infrared femtosecond laser ablation of silicate glasses, J. Anal. At. Spectrom., 2005, **20**, 901-906.

[29] F. Poitrasson,, X.i Mao, S. S. Mao,. Freydier and R. Russo, Comparison of Ultraviolet Femtosecond and Nanosecond Laser Ablation Inductively Coupled

Plasma Mass Spectrometry Analysis in Glass, Monazite, and Zircon, Anal. Chem., 2003, **75,** 6184-6190.

[30] J. Gonzalez, C. Liu, X. Mao and R. E. Russo, UV-femtosecond laser ablation-ICP-MS for analysis of alloy samples, J. Anal. At. Spectrom., 2004, **19**, 1165-1168.

[31] X. Liu and D. Du, G. Mourou, Laser Ablation and Micromachining with Ultrashort Laser Pulses, IEEE J. Quan. Elec., 1997, **33,** 1706-1716.

[32] J. D. Winefordner, I.B. Gornushkin, T.Correll, E. Gibb, B. W. Smith and N. Omenetto, Comparing several atomic spectrometric methods to the super stars: special emphasis on laser induced breakdown spectrometry, LIBS, a future super star, J. Anal. At. Spectrom. 2004, **19,** 1061-1083.

[33] M. Lenzner, F. Krausz, J.Kruger and W. Kantek, Photoablation with sub-10 fs laser pulses, Appl. Surf. Sci., 2000, **154-155,** 11-16.

[34] C. Liu, X. L. Mao, S. S. Mao, X. Zeng, R. Greif, and R. E. Russo, Nanosecond and Femtosecond Laser Ablation of Brass: Particulate and ICPMS Measurements, Anal. Chem., 2004, **76**,379-383.

[35] C. C. Garcia, H. Lindner, A. von Bohlen, C. Vadla and K. Niemax, Elemental fractionation and stoichiometric sampling in femtosecond laser ablation, J. Anal. At. Spectrom., 2008, **23**, 470-478.

[36] V. Mozna, J. Pisonero, M. Hola, V. Kanicky, and D. Günther, Quantitative analysis of Fe-based samples using ultraviolet nanosecond and femtosecond laser ablation-ICP-MS, J. Anal. At. Spectrom., 2006, **21**, 1194-1201.

[37] J. Chmeleff, I. Horn, G. Steinhoefel, F. Von Blackenburg, In situ determination of precise stable Si isotope ratios by UV-femtosecond laser ablation high-resolution multi-collector ICP-MS, Chem. Geology. 2008, **249**, 155-166.

[38] I. Horn , F. von Blanckenburg, R. Schoenberg, G. Steinhoefel and G. Markl, In situ iron isotope ratio determination using UV-femtosecond laser ablation with application to hydrothermal ore formation processes, Geochimica et Cosmochimica Acta, 2006, **70**, 3677–3688.

[39] C. Pecheyran, S. Cany, P. Chabassier, E. Mottay and O. F. X. Donard, High repetition rate and low energy femtosecond laser ablation coupled to ICPMS detection: a new analytical approach for trace element determination in solid samples, J. Physics: Conference Series 2007, **59**, 112-117.

[40] I. Horn, F. von Blanckenburg, Investigation on elemental and isotopic fractionation during 196 nm femtosecond laser ablation multiple collector inductively coupled plasma mass spectrometry, Spectrochimica Acta Part B, 2007, **62**, 410–422.

[41] R.Freydier, F. Candaudap, F. Poitrasson, A. Arbouet and B. Dupre, Evaluation of infrared femtosecond laser ablation for the analysis of geomaterials by ICP-MS, J. Anal. At. Spectrom., 2008, **23**, 702-710.

[42] R. E. Russo, X. Mao, J. J. Gonzalez and S.S. Mao, Femtosecond laser ablation ICP-MS, J. Anal. At. Spectrom., 2002, **17**, 1072-1075.

[43] J. Koch, M. Walle, J. Pisonero and D. Günther, Performance characteristics of ultra-violet femtosecond laser ablation inductively coupled plasma mass spectrometry at 256 and 200 nm, Anal. At. Spectrom., 2006, **21,** 932-940.

[44] A. Rocholl , P. Dulski and I. Raczek, New ID-TIMS, ICP-MS and SIMS Data on theTrace Element Composition and Homogeneity of NIST Certified Reference Material SRM 610-611, Geostand. Newsl. ,2000, **24**(2), 261-274.

[45] R. W. Hinton and B. Harte, : Ion probe measurements of national-institute-of-standards-and-technology standard reference material srm-610 glass, trace-elements, Analyst, 1995, **120**, 1315-1319.

[46] A. B.E. Rocholl, K. Simon, K. P. Jochum , F. Bruhn, R. Gehann, U. Kramar, W. Luecke, M. Molzahn, E. Pernicka, M. Seufert, B. Spettel and J. Stummeier, Chemical characterisation of NIST silicate glass certified reference material SRM 610 by ICP-MS, TIMS, LIMS, SSMS, INAA, AAS and PIXE , Geostand. Newsl, 1997, **21**, 101-114.

[47] N. J.G. Pearce, W. T. Perkins, J. A. Westgate, M. P. Gorton,S. E. Jackson, C. R. Neal and S. P. Chenery, A compilation of new and published major and trace element data for NIST SRM 610 and NIST SRM 612 glass reference materials , Geostand. Newsl, 1997, **21**, 115-144.

[48] K. Jochum, M. Willbold, I. Raczek, B. Stoll and K. Herwig, Chemical characterisation of the USGS reference glasses GSA-1G, GSC-1G, GSD-1G, GSE-1G, BCR-2G, BHVO-2G and BIR-1G using EPMA, ID-TIMS, ID-ICP-MS and LA-ICP-MS, Geostand. Newsl, 2005, **29**, 285-302

[49] A. Rocholl, Major and trace element composition and homogeneity of microbeam reference material: Basalt glass USGS BCR-2G, Geostand. Newsl, 1998, **22**, 33-45.

[50] L. Kempenaers, K. Janssens, K.P. Jochum, L. Vincze, B. Vekemans, A. Somogyi, M. Drakopoulas and F. Adams, Micro-heterogeneity study of trace elements in USGS, MPI-DING and NIST glass reference materials by means of synchrotron micro-XRF , J. Anal. At. Spectrom. 2003, 18, 350-357.

[51] H. P . Longerich, S. E. Jackson and D. Günther, Laser Ablation Inductively Coupled Plasma Mass Spectrometric Transient Signal Data Acquisition and Analyte Concentration Calculation, J. Anal. At. Spectrom., 1996, **11**, 899-904.

[52] http://georem.mpch-mainz.gwdg.de/sample_query_pref.asp.

[53] B.J. Fryer, S.E. Jackson and H.P. Longerich, The design, Operation and role of the laser-ablation microprobe coupled with an inductively coupled plasma-mass spectrometer (LAM-ICP-MS) in the earth sciences, Can. Min., 1995, **33**, 303-312.

[54] D. Günther and C. A. Heinrich, Comparison of the ablation behavior of 266 nm Nd5YAG and 193 nm ArF excimer lasers for LA-ICP-MS analysis, J. Anal. At. Spectrom., 1999, **14**, 1369-1374.

[55] J. E. Gagnon, B. J. Fryer, I. M. Samson and A.E. Williams-jones, Quantitative analysis of silicate certified reference materials by LA-ICPMS with and without an internal standard, J. Anal. At. Spectrom., 2008, 23, 1529-1537.

[56] M. Kurosawa, SE. Jackson, and S. Sueno, Trace Element Analysis of NIST SRM 614 and 616 Glass Reference Materials by Laser Ablation Microprobe-Inductively Coupled Plasma-Mass Spectrometr**y,** Geostandard. Newsl., 2002, **26** (1), 75-84.

[57] D. Jacob, High Sensitivity Analysis of Trace Element-Poor Geological Reference Glasses by Laser Ablation-Inductively Coupled Plasma-Mass Spectrometry (LA-ICP-MS), Geostandards and Geoanalytical Research, 2006, **30**(3), 221-235.

[58] S. Gao, X. Liu, H. Yuan, B. Hattendorf, D. Gunther, L. Chen and S. Hu, Determination of Forty Two Major and Trace Elements in USGS and NIST SRM Glasses by Laser Ablation-Inductively Coupled Plasma-Mass Spectrometry, Geostandard. Newsl., 2002, **26**(2), 181-196.

[59] P. Dulski, New ID-TIMS, ICP-MS and SIMS Data on the Trace Element Composition and Homogeneity of NIST Certified Reference Material SRM 610-611 Geostandard. Newsl., 2001, **25**(1), 87-125.

[60] http://minerals.cr.usgs.gov/geo_chem_stand/powdered_RM.html

[61] S. M. Eggins, J. D. Woodhead, L. P. Kinsley, G. E. Mortimer, P. Sylvester, M. T. McCulloch, J. M. Hergt and M. R. Handler, A simple method for the precise determination of >=40 trace elements in geological samples by ICPMS using enriched isotope internal standardisation , Chem. Geol. 1997, **134**, 311-326.

Table 3.1: LA system specifications and operating conditions

Manufacture:	Quantronix
Model:	Integra C®
Type:	Ti:sapphire based on the Chirped Pulse Amplification (CPA) technique
Wavelength:	Fundamental: 785 nm
Repetition rate:	Up to 1kHz, experiment: 20 Hz
Pulse energy:	Maximum: 2mJ/pulse, experiment: 0.58 mJ
Pulse width:	<130 fs
Fluence:	13 Jcm^{-2}
Objective lens:	10X

Table 3.2: ICP-MS instrumentation and operating conditions

Manufacture:	ThermoElectron®
Model:	X7-II®
Detector type:	ETP® dual mode (pulse and analogue counting)
Dynamic range:	~1.3 x 10^9 ICPS
Sensitivity (sol.):	~350× 10^6 ICPS/ppm
Cone type:	High Performance Interface (HPI)
Plasma conditions:	Standard
Resolution:	Standard (125), High (140)
RF power:	1400 W
Plasma gas:	13 L min^{-1}
Auxiliary gas:	0.98 L min^{-1}
Nebulizer gas:	1.04 L min^{-1}
Sampling depth:	140 mm
Data acquisition parameters	
Data acquisition protocol	Time-resolved analysis
Scanning mode	Peak-jumping mode
Masses analyzed	76
Elements quantified	63
Dwell time:	10 ms
Average settling time	1.78 ms
Time / scan	895 ms
Number of scans	233

Table 3.3: Analyses of NIST 614 and comparison to published values, the relative error (%) were calculated relative to Jochum et al. [52]. Concentrations are in ppm, DL=detection limit.

Element	Isotope	This study	RSD (%)	Relative error (%)	Jochum et al. [52]	Gagnon et al. [55]	Jacob [57]	Gao et al. [58]	Kurosawa et al. [56]	Dulski [59]
Li	7	2.46	11.23	53.88	1.60	1.80	1.65	1.70	1.69	--
Be	9	0.82	22.25	22.14	0.67	--	0.69	0.74	0.66	--
B	11	10.75	9.10	668	1.40	19.80	1.66	--	4.83	--
Na	23	103005	1.81	--	--	103000	86622	93469	--	--
Mg	25	35.85	3.08	2.44	35.00	35.00	34.33	32.00	34.90	--
Al	27	11001	1.30	--	--	10600	--	--	--	--
Si	29	335528	1.91	--	--	343000	--	--	--	--
P	31	<DL	--	--	13.00	13.00	--	--	--	--
K	39	29.97	3.05	-0.11	30.00	--	--	--	--	--
Ca	43	85764	0.00	--	--	73300	--	--	--	--
Sc	45	<DL	--	--	1.60	--	--	--	1.53	--
Ti	47	4.21	10.59	23.94	3.40	--	--	--	3.37	--
V	51	1.02	20.95	1.85	1.00	1.00	0.97	1.09	1.00	--
Cr	52	1.28	15.10	-28.88	1.80	--	--		1.23	--
Mn	55	1.41	5.44	0.54	1.40	1.30	1.37	2.20	1.35	--
Fe	57	<DL	--	--	19.00	--	--		15.60	--
Co	59	0.84	21.74	-0.84	0.85	0.88	0.69	0.71	0.68	--
Ni	60	<DL	--	--	1.00	--	--	--	1.04	--
Cu	65	1.37	3.38	0.12	1.37	--	--	--	1.19	--
Zn	66	2.52	15.36	0.80	2.50	--	1.76	1.90	2.16	--
Ga	69	1.48	17.44	-1.02	1.50	1.40	1.10	1.12	1.19	--
Ge	72	0.88	10.30	-0.87	0.89	1.11	0.81	--	0.88	--
As	75	<DL	--	--	0.66	--	0.59	--	--	--
Rb	85	0.85	5.44	-0.22	0.86	1.157	0.95	0.87	0.87	0.98
Sr	86	45.97	1.65	0.37	45.80	42.6	42.62	44.30	45.00	46.00
Y	89	0.80	3.79	0.47	0.80	0.70	0.75	0.77	0.79	0.81
Zr	90	0.83	4.02	-0.74	0.84	0.85	0.78	0.80	0.77	0.93
Nb	93	0.84	1.99	3.30	0.81	0.80	0.79	0.78	0.78	--
Mo	95	0.80	11.91	0.38	0.80	0.80	0.76	0.70	0.80	--
Rh	103	1.65	2.45	2.83	1.60	1.60	--	--	--	--
Pd	105	2.10	1.92	5.21	2.00	2.00	--	--	--	--
Ag	107	0.43	5.91	3.42	0.42	0.43	0.36	--	--	--
Cd	110	0.54	7.16	-7.36	0.58	--	0.57	--	--	--
In	115	0.88	6.57	-0.06	0.88	0.82	--	--	0.73	--
Sn	118	1.59	3.01	-0.74	1.60	--	1.57	--	1.56	--
Sb	121	0.79	6.05	0.79	0.78	0.82	0.78	--	0.69	--
Cs	133	0.66	2.70	6.98	0.62	0.62	0.60	--	0.59	0.66
Ba	137	3.22	7.39	0.56	3.20	3.0	2.90	--	3.15	3.30
La	139	0.71	2.90	-1.88	0.72	0.67	0.69	--	0.75	0.72
Ce	140	0.80	1.69	-1.32	0.81	0.85	0.74	--	0.78	0.79
Pr	141	0.76	2.17	-0.30	0.76	0.80	0.72	--	0.76	0.80
Nd	146	0.76	3.01	3.22	0.74	0.74	0.70	--	0.77	0.73
Sm	147	0.75	5.27	-0.06	0.75	0.73	0.73	--	0.79	0.75
Eu	153	0.76	4.62	-0.38	0.76	0.73	0.73	--	0.78	0.78

Gd	155	0.75	6.19	0.11	0.75	0.78	0.74	--	0.80	0.79
Tb	159	0.73	3.04	0.16	0.73	0.74	0.71	--	0.76	0.77
Dy	163	0.74	7.91	-0.01	0.74	0.74	0.76	--	0.83	0.74
Ho	165	0.74	3.83	0.51	0.74	0.76	0.75	--	0.81	0.74
Er	166	0.74	4.86	0.21	0.74	0.68	0.75	--	0.81	0.75
Tm	169	0.74	3.73	0.97	0.73	0.68	0.74	--	0.80	0.75
Yb	172	0.77	4.16	-0.62	0.77	0.74	0.78	--	0.84	0.74
Lu	175	0.72	3.44	-0.99	0.73	0.70	0.75	--	0.80	0.74
Hf	178	0.70	5.60	-0.19	0.70	0.70	0.77	--	0.74	0.74
Ta	181	0.80	4.31	0.88	0.79	0.81	--	--	0.83	---
W	182	0.88	11.53	-0.56	0.88	0.92	0.74	--	0.74	--
Re	185	0.17	5.21	2.25	0.17	0.17	--	--	--	--
Pt	195	2.40	1.82	4.55	2.30	2.43	--	--	--	--
Au	197	0.63	6.55	40.25	0.45	2.50	0.42	--	0.41	--
Tl	205	0.31	8.91	9.83	0.28	0.28	--	--	0.24	--
Pb	206	2.35	3.50	1.10	2.32	2.63	2.22	2.40	2.07	2.50
Bi	209	0.57	3.18	-2.44	0.58	0.59	0.55	--	0.50	0.78
Th	232	0.75	3.88	-0.13	0.75	0.79	0.77	0.74	0.83	0.83
U	238	0.83	2.73	1.36	0.82	0.79	--	--	0.80	--

Table 3.4: Analyses of NIST 610 and comparison to published values, the relative error (%) were calculated relative to Jochum et al. [52]. Concentrations are in ppm, DL=detection limit.

Element	Isotope	This study	RSD (%)	Relative error (%)	Jochum et al. [52]	Gagnon et al. [55]	Gao et al. [58]	Pearce et al [47]	Rocholl et al. [44]	Dulski [59]
Li	7	475.3	3.6	-2.0	485.0	496.9	484.0	484.6	--	--
Be	9	465.7	2.9	-0.1	466.0	475.7	473.0	465.6	--	--
B	11	274.5	6.3	-22.9	356.0	363.0	--		--	--
Na	23	98717.5	5.9	--	--	99792.0	97174.0	99100.0	--	--
Mg	25	610.0	1.2	31.2	465.0	473.0	463.0	465.3	--	--
Al	27	10729.1	3.1	--	--	10950.0	11626.0	10800.0	--	--
Si	29	321857.6	2.4	--	--	330910.0	--	---	--	--
P	31	379.6	8.3	10.7	343.0	346.8	343.0	342.5	--	--
K	39	396.6	3.1	-18.4	486.0	487.0	--	--	--	--
Ca	43	81830.0	0.0	--	--	81830.0	--	--	--	--
Sc	45	460.1	1.7	4.3	441.0	446.1	442.0	441.1	--	---
Ti	47	467.3	1.1	7.7	434.0	438.0	434.0	434.0	--	--
V	51	441.1	4.6	-0.2	442.0	439.3	442.0	441.7	--	--
Cr	52	402.5	6.1	-0.6	405.0	404.8	404.0	405.2	--	--
Mn	55	454.6	4.2	-6.3	485.0	439.0	435.0	433.3	--	--
Fe	57	454.3	6.9	-0.8	458.0	465.3	--	--	--	--
Co	59	404.6	7.3	-0.1	405.0	408.0	405.0	405.0	--	--
Ni	60	455.4	7.5	-0.7	458.7	447.2	445.0	443.9	--	--
Cu	65	429.5	7.1	-0.1	430.0	433.2	430.0	430.3	--	--
Zn	68	452.6	4.9	-0.7	456.0	463.2	455.0	456.3	--	--
Ga	69	429.3	2.0	-2.0	438.0	442.2	437.0	438.1	--	--
Ge	72	424.4	5.6	-0.4	426.0	435.1	--	--	--	--
As	75	316.2	11.9	-0.2	317.0	424.1	--	--	--	--
Rb	85	412.0	2.9	-3.2	425.7	425.2	431.0	431.1	417.3	411.0
Sr	86	519.9	2.5	0.9	515.5	503.2	497.0	497.4	491.9	505.0
Y	89	452.8	3.7	0.6	450.0	452.4	450.0	449.9	458.0	454.0
Zr	90	450.2	3.2	2.3	440.0	443.2	439.0	439.9	436.8	456.0
Nb	93	460.9	2.8	10.0	419.0	423.7	420.0	419.4	--	--
Mo	95	410.2	4.8	0.0	410.0	379.9	378.0	376.8	--	--
Rh	103	1.3	12.0	-0.9	1.3	1.3	--	--	--	--
Pd	105	1.4	3.2	31.3	1.1	1.1	--	--	--	--
Ag	107	240.0	6.9	0.4	239.0	244.7	--	--	--	--
Cd	110	258.8	8.4	-0.1	259.0	268.4	--	--	--	--
In	115	438.8	8.3	-0.5	441.0	443.4	--	--	--	--
Sn	120	396.4	7.4	0.1	396.0	401.5	400.0	396.3	--	--
Sb	121	383.6	1.4	4.0	369.0	380.0	377.0	368.5	--	--
Cs	133	356.7	4.7	-1.2	361.0	362.3	360.0	360.9	357.3	372.0
Ba	136	446.2	2.5	2.6	435.0	435.9	425.0	424.1	430.7	452.0
La	139	457.0	2.7	0.0	457.0	470.0	457.0	457.4	426.1	440.0
Ce	140	452.2	2.2	0.9	448.0	457.7	448.0	447.8	446.8	456.0
Pr	141	434.0	2.2	0.9	430.0	442.2	430.0	429.8	442.9	472.0
Nd	146	434.8	2.1	0.9	431.0	442.5	430.0	430.8	429.4	430.0
Sm	147	455.3	2.1	1.0	451.0	463.4	449.0	450.5	449.5	446.0

Eu	153	459.2	3.7	-0.4	461.0	471.1	460.0	461.1	443.6	459.0
Gd	155	443.3	3.2	-0.2	444.0	429.2	420.0	419.9	441.6	466.0
Tb	159	445.8	2.8	0.6	443.0	452.0	442.0	442.8	439.9	457.0
Dy	163	454.6	2.1	6.5	427.0	435.4	426.0	426.5	429.8	437.5
Ho	165	449.4	1.6	0.1	449.0	458.7	448.0	449.4	439.8	451.0
Er	166	458.5	2.0	7.6	426.0	434.0	426.0	426.0	433.5	455.0
Tm	169	450.6	2.2	7.3	420.0	428.1	420.0	420.1	423.3	453.1
Yb	172	477.3	2.7	7.3	445.0	469.0	460.0	461.5	445.7	452.0
Lu	175	445.9	2.6	2.5	435.0	443.4	435.0	434.7	431.1	451.0
Hf	178	431.2	2.9	-0.2	432.0	427.8	418.0	417.7	421.2	443.0
Ta	181	478.2	2.4	5.8	452.0	386.8	376.0	376.6	--	--
W	182	446.8	4.8	0.4	445.0	452.1	--	--	--	--
Re	185	47.4	11.8	0.9	47.0	106.2	--	--	--	--
Pt	195	3.1	4.8	-1.9	3.2	3.3	--	--	--	--
Au	197	22.9	13.5	-0.6	23.0	23.3	--	--	--	--
Tl	205	61.0	4.2	0.1	61.0	63.4	--	--	--	--
Pb	206	423.5	5.8	-0.6	426.0	422.8	413.0	413.3	417.0	430.0
Bi	209	362.4	7.3	-20.9	458.0	371.6	--	--	--	--
Th	232	467.4	2.4	2.2	457.2	466.0	451.0	450.6	445.8	472.0
U	238	458.9	5.8	-0.6	461.5	460.1	457.0	457.1	451.8	464.0

Table 3.5: Analyses of BHVO-2 and comparison to published values, the relative error (%) were calculated relative to Jochum et al. [52]. Concentrations are in ppm, DL=detection limit.

Element	Isotope	This study	RSD (%)	Relative error (%)	Jochum et al. [52]	Gagnon et al. [55]	Gao et al. [58]	USGS [60]
Li	7	4.79	4.45	-0.19	4.80	4.80	5.00	5.00
Be	9	1.00	14.08	-0.34	1.00	--	1.40	--
B	11	6.84	5.96	--	--	--	--	--
Na	23	16703	7.42	--	--	13900	17672	16500
Mg	25	47808	1.26	--	--	48100	42682	43600
Al	27	71474	0.83	--	--	74300	--	--
Si	29	233456	4.98	--	--	231000	--	--
P	31	1539	10.10	28.22	1200	980	--	--
K	39	4065	5.65	-5.47	4300	4430	--	--
Ca	43	81700	0	--	--	71700	--	--
Sc	45	31.59	1.02	-1.28	32.00	32.00	31.00	32.00
Ti	47	16311	1.46	0.07	16300	16600	15621	16400
V	51	328.06	2.25	3.49	317.00	307.00	329.00	317.00
Cr	52	280.88	5.05	0.32	280.00	292.00	285.00	280.00
Mn	55	1187.69	2.32	-7.93	1290.00	1340.00	1345.00	1290.00
Fe	57	72070	1.47	-16.49	86300	89700	--	--
Co	59	45.13	5.00	0.30	45.00	47.00	47.00	45.00
Ni	60	122.83	5.05	3.22	119.00	113.00	112.00	119.00
Cu	65	119.02	4.56	0.01	127.00	121.00	142.00	127.00
Zn	66	124.43	4.18	20.81	103.00	96.00	107.00	103.00
Ga	69	22.50	5.91	2.29	22.00	23.00	21.00	21.70
Ge	72	2.40	11.33	50.30	1.60	--	--	--
As	75	< DL	--	--	--	--	--	--
Rb	85	9.08	6.54	-0.33	9.11	8.74	10.10	9.80
Sr	86	394.65	2.97	-0.34	396.00	410.00	382.00	389.00
Y	89	21.51	1.14	-17.25	26.00	22.00	23.00	26.00
Zr	90	151.43	1.11	-11.96	172.00	156.00	160.00	172.00
Nb	93	18.22	4.12	0.66	18.10	16.40	16.40	18.00
Mo	95	4.21	5.07	5.33	4.00	4.00	--	--
Rh	103	< DL	--	--	0.0007	--	--	--
Pd	105	< DL	--	--	0.0029	--	--	--
Ag	107	0.42	7.70	--	--	--	--	--
Cd	110	< DL	--	--	0.06	--	--	--
In	115	0.13	14.60	--	--	--	--	--
Sn	118	1.80	5.74	5.80	1.70	1.80	2.60	1.90
Sb	121	0.16	12.55	26.82	0.13	0.12	0.21	--
Cs	133	0.10	13.63	0.07	0.10	--	0.11	--
Ba	137	130.73	4.01	-0.21	131.00	137.00	128.00	130.00
La	139	14.79	1.93	-2.69	15.20	15.40	15.60	15.00
Ce	140	38.15	2.33	1.72	37.50	37.00	37.00	38.00
Pr	141	5.19	1.38	-2.92	5.35	4.90	5.00	--
Nd	146	24.28	2.07	-0.88	24.50	24.20	24.00	25.00
Sm	147	6.02	2.62	-0.83	6.07	5.93	5.80	6.20

Eu	153	2.05	1.95	-1.01	2.07	2.13	2.00	--
Gd	155	5.64	2.29	-9.60	6.24	5.62	5.90	6.30
Tb	159	0.81	1.56	-11.95	0.92	0.82	0.86	0.90
Dy	163	4.85	2.64	-8.63	5.31	4.59	4.90	--
Ho	165	0.87	2.94	-11.25	0.98	0.86	0.91	1.04
Er	166	2.27	2.69	-10.66	2.54	2.12	2.30	--
Tm	169	0.30	4.47	-8.98	0.33	0.29	0.30	--
Yb	172	1.93	4.52	-3.52	2.00	1.80	2.00	2.00
Lu	175	0.25	5.81	-8.39	0.27	025	0.26	0.28
Hf	178	3.83	1.68	-12.27	4.36	3.98	4.10	4.10
Ta	181	1.14	3.53	0.20	1.14	1.06	0.94	1.40
W	182	0.24	9.23	15.52	0.21	0.21	--	--
Re	185	< DL	--	--	0.0005	--	--	--
Pt	195	0.08	25.15	--	--	--	--	--
Au	197	0.42	8.66	--	--	--	--	--
Tl	205	0.02	22.02	--	--	--	--	--
Pb	206	1.84	2.35	14.76	1.60	1.70	1.40	--
Bi	209	< DL	--	--	--	--	--	--
Th	232	1.16	1.58	-5.29	1.22	1.16	1.18	1.20
U	238	0.44	3.09	9.96	0.40	0.393	0.44	--

Table 3.6: Analyses of BIR-1 and comparison to published values, the relative error (%) were calculated relative to Jochum et al. [52]. Concentrations are in ppm, DL=detection limit.

Element	Isotope	This study	RSD(%)	Relative error (%)	Jochum et al. [52]	Gagnon et al. [55]	Gao et al. [58]	USGS [60]	Eggins et al. [61]	Dulski [59]
Li	7	3.12	7.09	-2.59	3.20	3.50	3.60	3.60	--	--
Be	9	<DL	--	--	0.12	<DL	0.69	0.58	0.12	--
B	11	<DL	--	--	0.33	12.60	--	--	--	--
Na	23	13479	4.69	-0.15	13500	13369	14132	13500	--	--
Mg	25	66276	1.48	14.27	58000	57464	58471	58500	--	--
Al	27	81952	1.22	-0.06	82000	81817	--	--	--	--
Si	29	225138	2.71	0.42	224200	237429	--	--	--	--
P	31	91.89	8.22	-0.12	92.00	85.20	--	--	--	--
K	39	164.94	5.41	-28.29	230.00	211.00	--	--	--	--
Ca	43	95100	0.00	0.00	95100	73960	--	--	--	--
Sc	45	41.63	1.20	-3.18	43.00	43.90	41.00	44.00	43.80	--
Ti	47	6482.34	1.52	15.76	5600.00	6090.00	5532.0	5800.00	6036.00	--
V	51	332.27	1.85	4.16	319.00	331.80	338.00	310.00	322.00	--
Cr	52	390.57	3.75	-0.11	391.00	329.40	403.00	370.00	412.00	--
Mn	55	1202.92	1.81	-11.55	1360.00	1336.70	1417.0	1355.00	--	--
Fe	57	78286.16	3.75	-0.90	79000.	79628.00	--	--	--	--
Co	59	51.81	4.93	-0.37	52.00	50.80	57.00	52.00	53.00	--
Ni	60	166.42	4.59	0.25	166.00	164.50	190.00	170.00	175.00	--
Cu	65	109.63	2.95	-7.87	119.00	137.40	132.00	125.00	113.00	--
Zn	66	72.03	6.65	0.04	72.00	91.30	86.00	70.00	65.00	--
Ga	69	15.01	2.41	-1.92	15.30	16.40	17.00	--	15.20	--
Ge	72	1.69	16.19	20.60	1.40	2.4-3.3	--	--	--	--
As	75	<DL	--	--	0.44	2.31	--	--	--	--
Rb	85	0.20	9.23	-0.31	0.20	<DL	0.26	--	0.20	0.36
Sr	86	107.26	1.86	-1.60	109.00	116.90	104.00	110.00	106.40	110.00
Y	89	11.90	2.15	-23.72	15.60	14.10	13.30	16.00	16.20	14.90
Zr	90	11.96	4.18	-14.56	14.00	14.90	12.90	18.00	14.47	15.40
Nb	93	0.5396	2.3787	-1.88	0.5500	0.5300	0.4800	0.6000	0.5580	--
Mo	95	< DL	--	--	0.0700	<DL	--	--	0.0370	--
Rh	103	< DL	--	--	0.0003	0.03-0.04	--	--	--	--
Pd	105	< DL	--	--	0.0061	<DL	--	--	--	--
Ag	107	0.2515	25.5843	--	--	0.38-0.5	--	--	--	--
Cd	110	<DL	--	--	0.0970	0.36-0.1	--	--	0.0500	--
In	115	0.0560	7.2668	1.76	0.0550	0.06-08	--	--	--	--
Sn	118	0.6344	7.7063	5.73	0.6000	1.19-1.63	0.8400	--	0.8800	--
Sb	121	0.5013	8.1135	8.98	0.4600	0.5100	0.4700	0.5800	0.5000	--
Cs	133	< DL	--	--	0.0070	<DL	0.0069	--	0.0053	0.0060
Ba	136	6.6499	1.4095	-6.86	7.1400	7.5000	6.3000	7.0000	6.5200	6.4000
La	139	0.5435	1.3128	-11.63	0.6150	0.6700	0.6000	0.6300	0.6040	0.6200
Ce	140	1.9117	2.3363	-0.43	1.9200	2.1000	1.9000	1.9000	1.8970	1.8900
Pr	141	0.3528	2.9737	-4.64	0.3700	0.4100	0.3600	--	0.3780	0.3900
Nd	146	2.2766	2.4853	-4.35	2.3800	2.6000	2.3000	2.5000	2.3800	2.3500
Sm	147	1.0554	2.4737	-5.77	1.1200	1.2000	1.1000	1.1000	1.1170	1.0800

Eu	153	0.5068	4.8870	-4.38	0.5300	0.5900	0.5100	0.5500	0.5240	0.5300
Gd	155	1.5523	3.6176	-16.99	1.8700	1.8000	1.6000	1.8000	1.8500	1.9100
Tb	159	0.2901	2.1599	-19.43	0.3600	0.3500	0.3200	--	0.3790	0.3600
Dy	163	2.1615	1.7083	-13.88	2.5100	2.5000	2.3000	4.0000	2.5300	2.5500
Ho	165	0.4695	1.8813	-16.15	0.5600	0.5300	0.5100	--	0.5850	0.5600
Er	166	1.4102	3.6255	-15.05	1.6600	1.6000	1.5000	--	1.7340	1.7100
Tm	169	0.2105	6.4111	-15.80	0.2500	0.2400	0.2200	--	--	0.2500
Yb	172	1.4589	3.9388	-11.58	1.6500	1.7000	1.5000	1.7000	1.6490	1.6400
Lu	175	0.2107	3.2614	-15.71	0.2500	0.2300	0.2300	0.2600	0.2470	0.2500
Hf	178	0.4485	5.8299	-22.94	0.5820	0.6000	0.5300	0.6000	0.5620	0.6000
Ta	181	0.0351	5.2845	-1.74	0.0357	0.04-0.06	0.0320	--	0.0410	--
W	182	< DL	--	--	0.0700	<DL-.08	--	--	--	--
Re	185	< DL	--	--	0.0006	<DL-06	--	--	--	--
Pt	195	0.5642	13.0204	--	--	0.72-1.01	--	--	--	--
Au	197	0.0828	37.2942	--	--	0.09-0.12	--	--	--	--
Tl	205	< DL	--	--	0.0050	<DL	--	--	0.0040	--
Pb	206	3.2359	11.8873	4.38	3.1000	4.2000	3.6000	3.0000	2.9700	3.0000
Bi	209	< DL	--	--	0.0040	<DL-0.03	--	--	--	--
Th	232	0.0287	9.7085	-10.29	0.0320	<DL	0.0280	--	0.0302	0.0280
U	238	0.0133	13.7133	32.74	0.0100	<DL	0.0320	--	0.0100	0.0090

Table 3.7 : Analyses of BCR-2G and comparison to published values, the relative error (%) were calculated relative to Jochum et al. [52]. Concentrations are in ppm, DL=detection limit.

Element	Isotope	This study	RSD (%)	Relative error (%)	Jochum et al. [52]	Gagnon et al. [55]	Gao et al. [58]	Dulski [59]	USGS [60]	Jacob [57]
Li	7	8.77	5.63	-2.52	9.00	9.4-11.8	9.90	--	9.00	10.80
Be	9	2.27	5.12	-1.31	2.30	2.3--2.7	2.00	--	--	1.90
B	11	8.10	13.30	35.01	6.00	15.4-19.1	--	--	--	6.39
Na	23	23379	11.58	--	--	22268	23630	--	23400	23290
Mg	25	22604	0.96	--	--	20511	20980	--	21650	22490
Al	27	71373	1.58	--	--	73191	--	--	--	--
Si	29	250265	4.17	--	--	262519	--	--	--	--
P	31	1590	1.53	6.01	1500	1482	--	--	--	--
K	39	12868	5.36	-13.64	14900	15665	--	--	--	--
Ca	43	50900	0.00	--	--	42700	--	--	--	--
Sc	45	33.06	1.82	0.18	33.00	33.00	32.00	--	33.00	32.97
Ti	47	14033	2	-0.48	14100	14633	13005	--	13500	13728
V	51	424.13	3.66	-0.20	425.00	441.10	425.00	--	416.00	447.00
Cr	52	16.94	11.42	-0.36	17.00	16.50	17.00	--	18.00	18.40
Mn	55	1342	2.72	-13.44	1550	1500	1463	--	1520	1620
Fe	57	96612	2.29	0.01	96600	97152	--	--	--	--
Co	59	37.59	7.75	-1.07	38.00	36.00	38.00	--	37.00	38.92
Ni	60	11.86	11.96	-8.80	13.00	<DL	12.70	--	--	13.40
Cu	65	18.73	4.43	-10.82	21.00	<DL	18.00	--	19.00	22.00
Zn	66	140.26	4.33	12.21	125.00	143.20	153.00	--	127.00	169.00
Ga	69	26.93	3.64	17.08	23.00	30.00	24.00	--	23.00	--
Ge	72	1.91	6.21	27.08	1.50	2.9-3.5	--	--	--	--
As	75	<DL	--	--	--	<DL--2.4	--	--	--	--
Rb	85	47.28	8.00	0.59	47.00	50.30	51.00	46.90	48.00	47.80
Sr	86	341.34	3.54	-0.19	342.00	350.00	321.00	342.00	346.00	324.00
Y	89	31.34	2.53	-10.45	35.00	33.00	31.00	34.20	37.00	30.40
Zr	90	175.08	2.09	-4.85	184.00	186.10	167.00	194.00	188.00	161.00
Nb	93	12.63	3.32	1.05	12.50	10.1-12.6	10.90	--	--	12.40
Mo	95	268.75	6.64	-0.46	270.00	264.00	--	--	248.00	257.00
Rh	103	<DL	--	--	--	<DL	--	--	--	--
Pd	105	<DL	--	--	--	<DL	--	--	--	--
Ag	107	0.65	15.44	--	--	0.59-0.7	--	--	--	--
Cd	110	0.24	12.35	18.47	0.20	<DL	--	--	--	0.51
In	115	0.11	12.75	-1.47	0.11	0.13-0.16	--	--	--	0.12
Sn	118	2.31	8.51	-11.15	2.60	2.55-2.99	2.40	--	--	2.29
Sb	121	0.35	5.34	-0.41	0.35	0.31-0.37	0.51	--	--	0.38
Cs	133	1.14	8.54	-2.03	1.16	1.08	1.17	1.12	1.10	1.11
Ba	136	684.63	2.43	0.24	683.00	694.20	641.00	673.00	683.00	663.00
La	139	24.58	3.51	-0.48	24.70	27.40	25.00	24.80	25.00	24.10
Ce	140	53.09	3.87	-0.40	53.30	53.50	52.00	52.50	53.00	52.20
Pr	141	6.66	1.53	-0.59	6.70	6.70	6.30	6.94	6.80	6.42
Nd	146	28.66	2.57	-0.84	28.90	30.00	27.00	28.20	28.00	27.50
Sm	147	6.33	4.37	0.62	6.29	7.10	6.30	6.39	6.70	6.21
Eu	153	1.95	2.55	-0.87	1.97	2.00	1.91	1.98	2.00	1.88

Gd	155	6.54	2.50	-2.49	6.71	6.40	6.50	6.76	6.80	6.03
Tb	159	0.92	1.69	-9.43	1.02	1.10	0.95	1.05	1.07	0.91
Dy	163	6.17	1.51	-4.15	6.44	6.30	6.00	6.32		5.92
Ho	165	1.20	2.46	-5.64	1.27	1.24	1.20	1.30	1.33	1.14
Er	166	3.40	2.08	-8.11	3.70	3.40	3.30	3.64		3.19
Tm	169	0.49	2.45	-3.28	0.51	0.44	0.46	0.52	0.54	0.46
Yb	172	3.29	2.13	-2.86	3.39	3.60	3.20	3.52	3.50	3.25
Lu	175	0.46	2.26	-8.59	0.50	0.47	0.47	0.51	0.51	0.46
Hf	178	4.41	1.21	-8.92	4.84	4.90	4.50	5.18	4.80	4.24
Ta	181	0.78	2.60	0.31	0.78	0.63--0.88	0.63	--	--	0.75
W	182	0.51	6.98	2.04	0.50	0.72-0.92	--	--	--	0.57
Re	185	<DL	--	--	0.01	<DL	--	--	--	--
Pt	195	0.33	27.70	-57.87	0.78	0.31-0.38	--	--	--	--
Au	197	0.02	22.50	--	--	<DL-0.03	--	--	--	--
Tl	205	0.27	11.92	-10.94	0.30	0.25-0.31	--	--	--	--
Pb	206	11.15	4.57	1.32	11.00	11.80	10.90	10.00	11.00	11.70
Bi	209	0.05	20.95	-0.62	0.05	0.1-0.11	--	--	--	0.05
Th	232	5.86	1.57	-0.69	5.90	6.20	5.50	5.99	6.20	5.55
U	238	1.68	6.32	-0.37	1.69	1.60	1.70	1.66	1.69	1.77

Table 3.8: ^{206}Pb /^{238}U ratios of NIST and USGS reference materials

Sample	Measured Pb	Measured U	Measured 206Pb/238U	SD	RSD %	Reference [52] 206Pb/238U	% Deviation from Ref. [52]
NIST 610	423.53	462.69	0.232	0.012	5.2	0.234	-0.77
NIST 612	38.56	37.48	0.2606	0.008	3.0	0.2614	-0.30
NIST 614	2.35	0.83	0.712	0.029	3.2	0.717	-0.57
BHVO-2	1.84	0.44	1.050	0.031	2.9	1.013	3.64
BCR-2G	11.15	1.69	1.673	0.079	4.7	1.649	1.66
BIR-1G	3.02	0.01	76.43	1.76	2.3	78.53	-2.68

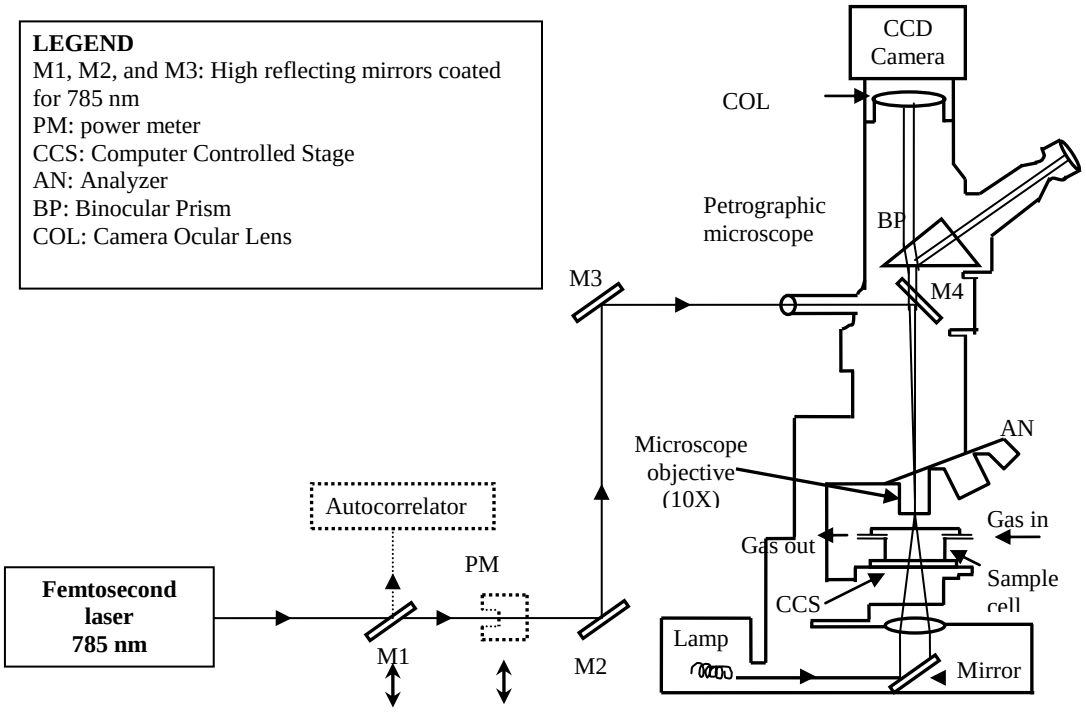

Figure 3.1: Experimental setup for laser beam bath and optics. A fs laser beam is steered onto the sample by dichroic mirrors M2, M3, and M4. The laser energy is measured by the power meter PM and the pulse width can be measured by the autocorrelator after being reflected when the mirror M1 is introduced into its path.

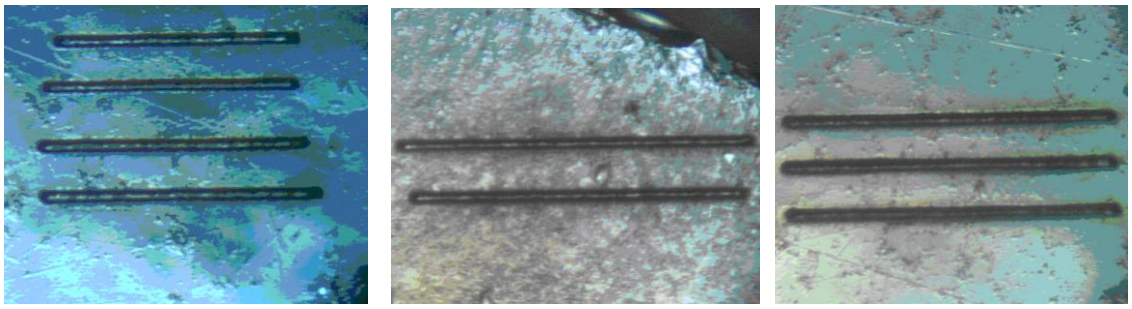

a :NIST 610 b: NIST 612 c: NIST 614

Figure 3.2: CCD camera images of NIR fs laser ablation of NIST 610, 612, and 614. It is clear from the image that fs laser ablate materials with different transparency equally well.

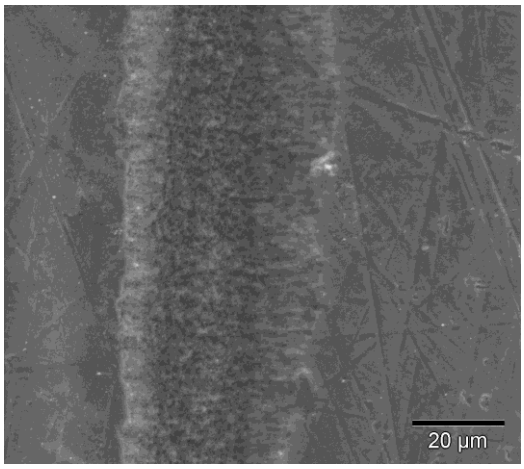

(a) Line scan

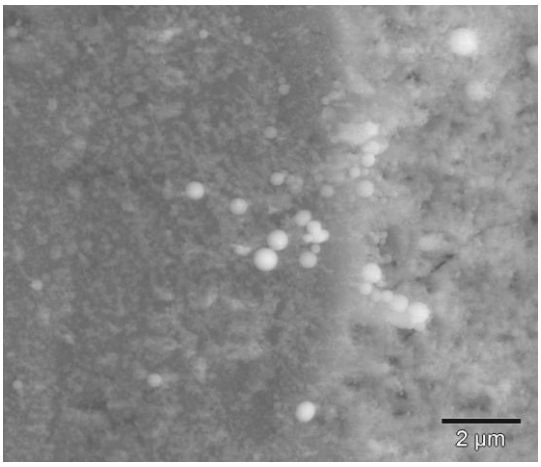

(b) Magnified image of (a)

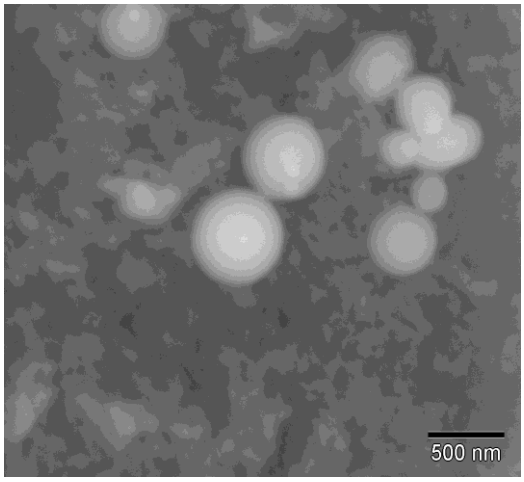

(c) Magnified image of (b)

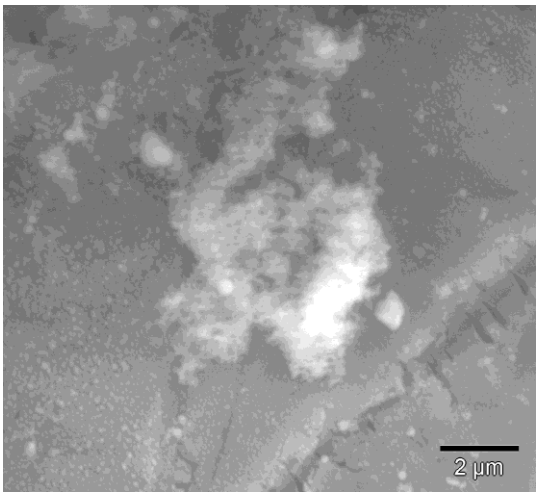

(d) fluffy particles

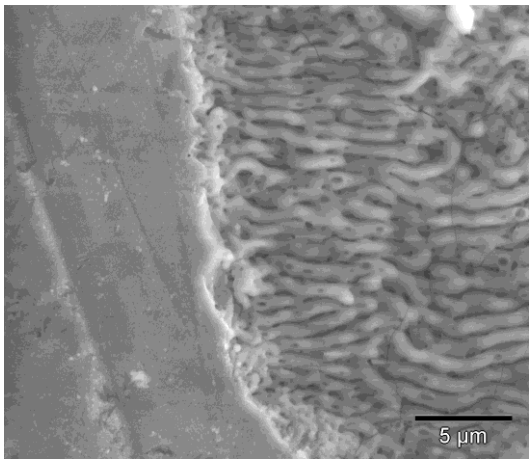

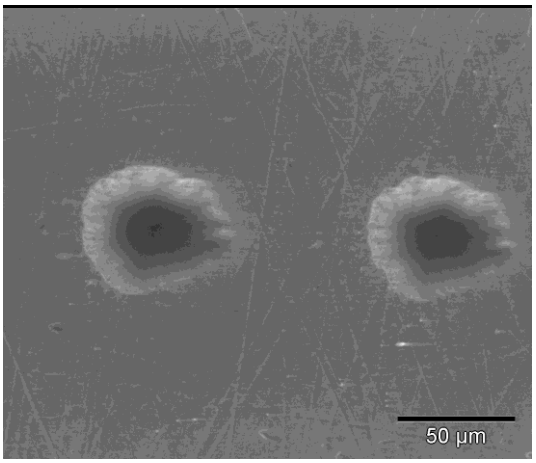

(e) A portion of NIR-fs laser-produced crater (f) Two similar laser-produced craters

Figure 3.3: SEM image of NIR femtosecond laser ablation of NIST 610: (a) a line scan at speed of 5µm s-1, energy =0.12 mJ, repetition rate = 10 Hz. (b) a magnified image of (a), (c) magnified image of (b), (d) cotton-like agglomerated particles, (e) a portion of a crater produced by 10 pulses of NIR-fs laser, (f) Two similar laser-produced holes.

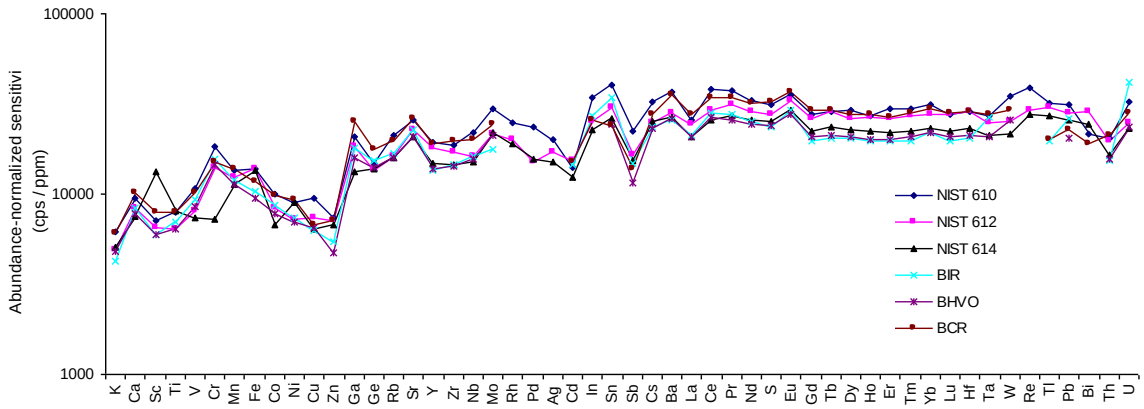

Figure 3.4: Abundance-normalized element sensitivity (cps /ppm) for elements obtained from fs-LA-ICP-MS of NIST 610, 612, 614, BCR-2G, BIR-1, and BHVO-2 under the tuning conditions in tables 1 and 2. The samples are moved at a speed of 5µm per second

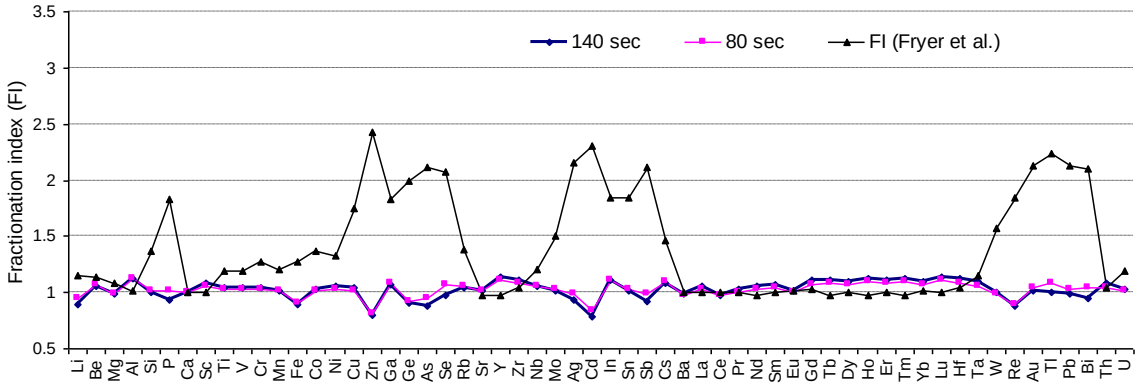

Figure 3.5: Elemental fractionation factors obtained from fs laser ablation drilling of NIST 610 at different ablation times in comparison to Fryer et al. 1995 [53], values obtained by ns laser ablation over 4 min time interval. Elements which tend to have higher fractionation factors (>1.5) in ns laser ablation, have fractionation indices very close to unity in fs laser ablation.

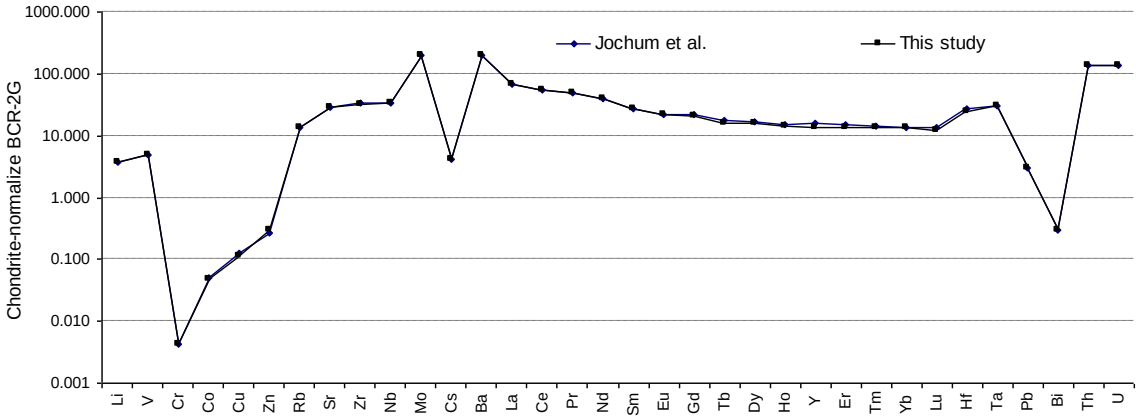

Figure 3.6: Comparison of chondrite- normalized concentrations of BCR-2G for Jochum et al. reference values and this study.

CHAPTER 4

Improving the Analytical Capabilities of Femtosecond Laser Ablation Multicollector ICP-Ms for High Precision Isotopic Analysis: The Role of Hydrogen and Nitrogen

4.1 INTRODUCTION

Over the last decades much work has been done to improve the analytical capabilities of ICP-MS since its first commercial introduction in 1983. Mixed-gas Inductively Coupled Plasma (ICP) has been extensively investigated to overcome analytical limitations of the Ar plasma [1-11]. Different gases such as helium [1], oxygen [12], nitrogen [1, 2, 4, 13, 14], hydrogen [1, 6], methane [5, 7] and other gases [10, 15, 16] that have been mixed with Ar showed different effects on enhancement and suppression of analyte sensitivity as well as oxide formation and matrix effects. Sesi et al. [1] studied the effect of adding helium, nitrogen, and hydrogen to the central and intermediate gas flow channels of an Ar-ICP. The effect of these gases on calcium ion emission and the fundamental plasma parameters (i.e. electron number density, electron temperature and gas kinetic temperature) has been shown to depend on the type and the amount of gas added to the plasma and whether the gas is introduced into the central or intermediate gas flow channel. Xiao et al. [13] investigated the effect of nitrogen addition (2-10%) to the outer gas flow of Ar ICP-MS on sensitivities, detection limits, mass discrimination and matrix effects for multi-element standard solutions containing different concentrations of Na. Improvement in sensitivities and detection limits were observed for some elements when nitrogen was added to the outer gas flow compared to pure Ar. Also mass discrimination and matrix effects were reduced with nitrogen addition. Beauchemin et al. [17] investigated addition of nitrogen (up to 10%) to Ar ICP-MS operating at constant flow and uptake rates and different power (from 1 to 1.4 kW). Although their results showed reduced sensitivities by

a factor of up to 5, the plasma stability and detection limits of Se and Fe were improved by a factor of 4. Other studies [18-23] have indicated reduction of molecular interferences ArCl and ArAr, ArO, ArOH, ClO and oxides by introducing a small amount of nitrogen into the central gas flow or the coolant gas flow.

As for solution ICP-MS, the addition of other gases to the Ar plasma in Laser ablation (LA)-ICP-MS has been studied by different authors [24-29]. Durrant [24] reported increased sensitivities of Ce and Th and reduced oxide to metal ratios (CeO/Ce and ThO/Th) upon the addition of 1% v/v or 12 % v/v of nitrogen to the coolant gas and cell flow, respectively. Crowe et al. [25] showed that adding 2 % v/v of nitrogen gas to the nebulizer gas flow before the sample cell resulted in a significant increase of sensitivity (by a factor of up to 2–3 times) and reduced mass bias in determination of Pb isotope ratios by quadrupole LA-ICP-MS. Iizuka et al. [26] reported that using a new design of sample cell and nitrogen mixing (at a rate of 4 ml/min) with the carrier gas has improved sensitivities of Hf, Lu and Yb by a factor of 2-3 as well as precision and accuracy of Hf isotope microanalysis in zircon by LA-Multicollector (MC)-ICP-MS. Recently Guillong et al. [28] studied the effect of mixing gases such as nitrogen, methane and hydrogen with He prior to the ablation cell using a 193 nm excimer LA-ICP-MS system. They reported an increase in sensitivity for the 47 investigated elements by a factor of 2-4 upon addition of 4-9 ml/min of hydrogen to the He carrier gas flow. In the same study, a weak sensitivity enhancement was reported for a few heavy elements like gold and uranium while other elements were not affected by nitrogen addition. In

another study, Hu et al. [29] reported an increase in the sensitivities for most of the 65 investigated elements upon the addition of 5-10 ml/min of nitrogen to the central channel gas (Ar + He) for a 193 nm excimer LA-ICP-MS system. They also reported a significant reduction in the oxide ratio ThO/Th and hydride ratio ArH/Ar with the nitrogen- Ar mixed plasma.

The introduction of multiple collectors to ICP-MS has produced a technique competitive to thermal ionization mass spectrometry (TIMS) which has been considered as the reference technique for high precision isotope ratio measurements [30-31]. Simultaneous detection of ions by Faraday detectors eliminates the effects of ion beam instabilities and allows accurate and high precision isotope ratio measurements. With the application of laser ablation to MC-ICP-MS, information at high spatial resolution can be obtained. However precise and accurate isotope ratio measurements by LA-MC-ICP-MS are affected by fractionation and mass bias effects. Many processes involved in LA-ICP-MS (particle formation, particle transport, atomization and ionization in the ICP) can contribute to elemental and isotopic fractionation. The proper choice of laser parameters (wavelength, pulse width, fluence) and ICP-MS operating conditions (RF power, gas flow, sampling depth) helps to minimize the extent of fractionation and mass bias. Recently, the use of femtosecond laser pulses has been reported to improve the analytical capabilities of LA-ICP-MS through reduction of fractionation and matrix effects [32-35]. Mass bias is an important factor affecting precision and accuracy of isotope ratio determinations by LA-MC-ICP-MS and must be minimized and/or robustly corrected for to obtain the most

precise and accurate isotope ratio analyses [30, 31, 36]. It is a significant feature of plasma source mass spectrometry and is related to preferential extraction and transmission of the heavier ions within the ICP-MS. Mass bias decreases with increasing atomic mass and its magnitude in ICP-MS is approximately an order of magnitude higher than that observed in TIMS [30, 36, 37]. Mass bias is generated within the plasma, in the interface region between the skimmer and the sampler cones, and in the ion extraction optics. The dominant source of mass bias is related to space charge effects which cause more repulsion and deflection of lighter ions compared to heavier ones [30, 31, 36, 38]. As a result, the measured isotope ratio of lighter to heavier isotopes is smaller than the true value. A number of different approaches have been used to correct for mass bias [31, 36-39]: i) Internal normalization: this method can be applied only to elements which have two or more stable (non-radiogenic) isotopes such as Sr, Nd, and Hf where the constant isotopic ratios of the two stable isotopes can be used to calculate the mass bias from the measured value. ii) External normalization: by using external standards to correct for mass bias assuming the mass bias for the external standard is identical to that of the sample. iii) Standard-sample standard bracketing: by alternate analysis of standards and samples assuming the mass bias is constant during the analysis period.

Few studies have been done to understand the effects of instrument operating conditions on mass bias [38, 40, 41]. Andrén et al. [40] concluded from isotope ratios determined for analytes deposited on the sampler and skimmer cones and on extraction lenses that ion extraction from the plasma and

processes in the interface region alter isotopic composition and contribute to mass bias. They also reported that any factor affecting the ion distribution (i.e. instrumental parameters and operating conditions) in the plasma will affect the mass bias. Fontaine et al. [41] reported the presence of systematic variation in mass bias in MC-ICP-MS with changes of the operating conditions (carrier gas flow rate, sampling depth, and extraction lens voltage), sample introduction and matrix effects.

The aim of this work is to investigate whether the effect of hydrogen and nitrogen additions on sensitivities of a number of elements across the entire mass range is the same for femtosecond laser ablation as it is with nanosecond lasers and to investigate the effect of nitrogen addition on sensitivity enhancement and mass bias corrections for fs-LA-MC-ICP-MS using Pb isotope ratio measurements as an example.

4.2 EXPERIMENTAL SET UP

4.2.1 LA-ICP-MS

Experiments were carried out using a Quantronix Integra C® femtosecond laser ablation system located at Great Lakes Institute for Environmental Research (GLIER), University of Windsor, Canada. It is a regenerative and multi-pass Ti:sapphire laser ablation system based on the Chirped Pulse Amplification (CPA) technique. The maximum energy that can be obtained from this laser system is 2 mJ (at 1KHz) in the near infrared (NIR, λ=795 nm). Ar was used as a carrier gas and mixed with nitrogen or hydrogen before the ablation cell using a

T-shaped connector (Figure 4.1). The ablated material was detected using ThermoElectron X7-II® ICP-MS. The instrument was optimized using pure Ar and NIST 610 for maximum sensitivity and low oxide formation (ThO/Th <0.5 %). After each gas addition, the instrument was re-optimized for maximum sensitivity. All data were acquired on NIST 610 and NIST 612 SRMs in line scan ablation mode at a speed of 5µm per second with sample surface at the focus of the laser beam. The measurements were carried out using time resolved analysis in fast peak jumping mode. Each line scan analysis consists of 60 seconds gas background collection followed by another 60 seconds ablation for signal collection. Each analyte signal was corrected for background by subtracting the background signal from the corresponding gross signal (signal obtained after firing the laser). The ablation cell was flushed for 2 minutes (no ablation) between analyses to reduce memory effects and allow the instrument to stabilize after each gas addition. A summary of the laser system and ICP-MS specifications and operating conditions is shown in Table 4.1.

4.2.2 LA-MC-ICP-MS

Lead isotope measurements of NIST 610 and NIST 612 were carried out by fs-LA-MC-ICP-MS using the previously described femtosecond laser ablation system coupled with a Finnigan™ Neptune MC-ICP-MS. The Finnigan™ Neptune is a double-focusing high resolution MC-ICP-MS with a movable multicollector array consisting of nine faraday detectors and five ion counters. A Thallium solution of 100 ppb concentration in 3 % HNO_3 was introduced (to

correct for mass bias) before the ablation cell at a flow rate of 100 µl/min using the Apex® system. The Apex® is an inlet system that can be connected directly to the torch injector and allows for self-aspiration at rates from 20µl/min to 1000µl/min. The Apex® also allows the addition of other gases such as nitrogen (in this study, nitrogen was added to Ar gas before the ablation cell). The laser energy used to ablate NIST 610 was 0.3 mJ but was increased to 0.8 mJ for NIST 612 (Pb concentration in NIST 612 is about 10 times lower than its concentration in NIST 610) to increase the amount of ablated material and consequently the signal intensity. The repetition rate of fs laser pulses was kept at 100 Hz and data were acquired in line scan ablation mode with the laser focus at the sample surface. Data was acquired for 300 seconds; the first 100 seconds for background collection (no laser ablation) and the remaining 200 seconds for signal collection. After each ablation, the cell was flushed for five minutes to minimize memory effects. Isotopes ^{202}Hg, ^{203}Tl, ^{204}Hg, ^{204}Pb, ^{205}Tl, ^{206}Pb, ^{207}Pb and ^{208}Pb were measured using the Faraday detector configuration shown in Table 4. 2.

4.2.2.1 DATA REDUCTION

The raw mass spectrometric intensity data were processed offline using a spreadsheet application by subtracting the average background (average of background integrations obtained during the first 100 seconds while the laser was off) from the signal integrations of each isotope. The first few cycles (in the background and signal obtained after laser ablation commenced) were rejected

for more stable signals. The interference of ^{204}Hg on ^{204}Pb was corrected by subtracting the ^{204}Hg intensity (calculated from the measured background-corrected ^{202}Hg intensity, by assuming ^{204}Hg/^{202}Hg =0.2299) from the background-corrected ^{204}Pb intensity. Isotope ratios (^{205}Tl/^{203}Tl, ^{206}Pb/^{204}Pb, ^{207}Pb/^{204}Pb, ^{208}Pb/^{204}Pb, ^{208}Pb/^{206}Pb and ^{207}Pb/^{206}Pb) were calculated from background- and interference-corrected isotopic data.

Pb isotopic determinations are not straightforward due to the fact that Pb has only one stable (non-radiogenic) isotope, ^{204}Pb, which prevents the application of an internal normalization approach to correct for mass bias. However, as suggested by Longerich et al.[42], Tl can be used as a surrogate to correct for mass bias provided that Tl mass bias can be related to Pb. In our calculations we used the power law [31]:

$$R_{True} = R_{Meas}(1+\alpha)^{\Delta m}$$

And the mass bias per atomic mass unit α:

$$\alpha = \left[\frac{R_{Tl,True}}{R_{Tl,Meas.}}\right]^{1/\Delta M} - 1$$

Where R_{True} and R_{Meas} are the true and measured Pb isotope ratios, respectively; $\Delta m = (M_i - M_j)$ is the mass difference between masses M_i and M_j of Pb. $R_{Tl,True}$ and $R_{Tl,Meas.}$ are the true and measured Tl isotope ratios, respectively; and $\Delta M = 2$ is the mass difference of Tl isotopes (i.e. ^{205}Tl - ^{203}Tl).

4.3 RESULTS AND DISCUSSIONS

4.3.1 HYDROGEN ADDITION (FS-LA-ICP-MS)

The addition of hydrogen to the Ar carrier gas before the ablation cell increased the intensity of most investigated elements by a factor of 1.5-2.5. The degree of intensity enhancement is higher for elements with high first ionization potentials such as Be, P, S, As, Se and Au (factor of 3-5). Figure 4.2 shows the background-corrected intensity normalized to pure Ar for selected elements as a function of hydrogen flow rates. The oxide ratios marginally decreased with hydrogen addition from 0.1 % and 0.35 % (pure Ar) to 0.09 % and 0.25 % (6 ml/min H_2) for UO/U and ThO/Th, respectively. The slight decrease in the oxide ratios may be an indication of increased plasma gas temperature. Hydrogen has higher thermal conductivity than argon and the plasma gas temperature has been reported to increase by 2000 K when hydrogen was added to the central gas flow [1]. The introduction of hydrogen into the central gas flow increased hydride ratios from 0.001 % and 0.002 % (pure Ar) to 0.002 % and 0.005% (6 ml/min H_2) for UH/U and ThH/Th, respectively. Figure 4.3 shows the background signal intensities acquired for pure Ar and 6 ml/min hydrogen in fs-LA-ICP-MS of NIST 612. Higher backgrounds are observed for masses with polyatomic species of hydrogen. The addition of hydrogen also leads to an increase of doubly charged ions from 0.44 to 0.79 % and from 0.93 to 1.36 % for $^{++}$U/U and $^{++}$Ce/Ce, respectively.

4.3.2 Nitrogen addition

Figure 4.4 shows the effect of nitrogen flow rates on signal intensity normalized to pure Ar of selected elements across the entire mass spectrum. The addition of nitrogen before the ablation cell enhanced the sensitivities of most investigated elements by a factor of 2-3. The enhanced sensitivity could be related to the increased thermal conductivity since nitrogen has a thermal conductivity higher than that of Ar by a factor of 32 at 7000 K[24]. Backgrounds were found to increase with nitrogen addition only for some lighter isotopes such as ^{29}Si, ^{31}P, ^{39}K, ^{55}Mn and ^{66}Zn (Figure 4.5). The oxide ratios decreased with nitrogen addition from 0.28 % and 0.46 % (pure Ar) to 0.19 % and 0.26 % (5 ml/min N_2) for UO/U and ThO/Th, respectively. An increase of doubly charged ions from 0.01 to 0.02 % and from 0.01 to 0.04 % for $^{++}$U/U and $^{++}$Ce/Ce, respectively, is also observed with nitrogen addition.

Sensitivity enhancement can be beneficial for some applications that require analysis of limited amounts of materials or analysis of materials with low elemental concentrations. The addition of nitrogen or hydrogen can benefit isotope ratio determinations using LA-MC-ICP-MS where high spatial resolution sampling and large ion beams are required for high precision isotopic analysis. The next section investigates the role of nitrogen addition as an effective means for improving sensitivity and reducing mass bias in Pb isotope measurements using fs-LA-MC-ICP-MS.

4.3.3 Pb ISOTOPE MEASUREMENTS

4.3.3.1 EFFECT of NITROGEN ON Pb and Tl SENSITIVITIES IN LA-MC-ICP-MS

The addition of nitrogen to Ar before the ablation cell enhanced the signal intensity of Tl by a factor of 4 and Pb by a factor of 3 (at nitrogen flow rate of 5 ml/min) in fs-LA-MC-ICP-MS of NIST 610 (Figure 4.6 a-b) which is similar to the results with the quadrupole mass spectrometer. This intensity enhancement is important for isotopic analysis using Faraday detectors where large ion beams are necessary for high precision analysis. During the Pb isotopic analyses, the Tl solution was continuously aspirated and desolvated into the laser ablation cell where it mixed with the laser ablated material. The behavior of Tl from the desolvated liquid might be different from that of Tl in the dry ablated material as a result of different transport efficiencies or changed plasma conditions. This is clear from figure 4.7 where the intensity variation of the Tl isotopes and the $^{205}Tl/^{203}Tl$ ratio at constant nitrogen flow rate (8ml/min) during data acquisition of 300 seconds on NIST 612 are shown. The intensity drop for the Tl isotopes when the laser was fired may be related to changes in the plasma conditions as a result of ablated material being introduced into the ICP. A reduction in the plasma temperature as a result of plasma loading may be the reason for the observed drop in intensity. However the $^{205}Tl/^{203}Tl$ ratio was not affected by the signal intensity changes or the source of Tl (simple desolvated liquid or a mixture with ablated NIST glass) and was stable during the whole data acquisition time.

4.3.3.2 EFFECT OF NITROGEN ON MASS BIAS

Figure 4.8 shows the calculated mass bias of $^{205}Tl/^{203}Tl$ and $^{208}Pb/^{206}Pb$ as a function of nitrogen flow rate during fs-LA-MC-ICP-MS of NIST 610. The addition of nitrogen decreased the mass bias coefficient (α) from -0.76% and -0.75% for $^{208}Pb/^{206}Pb$ and $^{205}Tl/^{203}Tl$ to -0.67% and -0.65, respectively (reduction of about 13 % at 5ml/min nitrogen). The negative sign indicates that the measured isotope ratios are higher than the true values due to the loss of light isotopes. The power law was used to calculate mass bias coefficients using the values of $^{208}Pb/^{206}Pb$ =2.168 and $^{205}Tl/^{203}Tl$ =2.3889 as obtained from references [43] and [44], respectively. It is clear from Figure 4.8 that the mass bias coefficient α_{Pb} of $^{208}Pb/^{206}Pb$ is not identical to α_{Tl} of $^{205}Tl/^{203}Tl$ and in contrast to the common mass bias-mass relationship where heavier elements have lower mass bias than lighter elements, inspection of figure 4.8 shows the reverse (Tl, a lighter element has lower mass bias than Pb, a heavier element) but there is consistency in the mass bias behavior of both isotopes as a function of nitrogen flow rate. We do not know the reason for this discrepancy but it could be related to incorrect isotope ratios of $^{205}Tl/^{203}Tl$ and $^{208}Pb/^{206}Pb$ that have been used for normalization or some other effects. In LA-ICP-MS analyses, nitrogen from air will always be entrained in variable amounts into the system through tubing and connections, from the ablation cell and in the ICP. Under these “standard” conditions, the mass bias is not stable as can be seen from figure 4.8 at “zero” nitrogen flow rate. The addition of more nitrogen helps to improve and stabilize mass bias for both Tl and Pb (Figure 4.8, plateau region). Figure 4.9 shows the

relationship between $^{205}Tl/^{203}Tl$ and $^{208}Pb/^{206}Pb$ mass bias factors calculated from power law at constant nitrogen flow rates (8 ml/min), for 6 replicate measurements of NIST 610, where a strong linear correlation (R^2=0.9998) between both factors is clear. The ratio of mass bias factors α_{Pb}/α_{Tl} was found to equal 1.0214 for $^{208}Pb/^{206}Pb$ in this study. This ratio is higher than that of White et al. [45] who reported a mass bias ratio α_{Pb}/α_{Tl} of 0.9746 for NBS981in solution using the exponential law. The difference in mass bias coefficients between Pb and Tl was interpreted as the reason why Tl was unable to provide accurate normalization of most SRM981 solutions and about 30% of silicate samples measured by Isoprope MC-ICP-MS [44]. In this study, as well, the use of Tl as a surrogate for Pb mass bias would not give accurate determinations of Pb isotope ratios if mass bias differences between Pb and Tl were not taken into account. In our calculations of isotope ratios we corrected for this difference by determining the ratio of mass bias factor of $^{208}Pb/^{204}Pb$, $^{207}Pb/^{204}Pb$, $^{206}Pb/^{204}Pb$, $^{207}Pb/^{206}Pb$ and $^{208}Pb/^{206}Pb$ to that of $^{205}Tl/^{203}Tl$ (i.e. $\alpha_{Pb} = 1.03\,\alpha_{Tl}$ for $^{208}Pb/^{206}Pb$) for each measurement and then applied the power law to get the corrected isotope ratios instead of renormalizing to a different Tl isotopic composition (i.e. adjustment of $^{205}Tl/^{203}Tl$ to provide the closest values of Pb isotope ratio to the reference values) as done in other studies [46--48]. In this way we obtained accurate isotope ratios as listed in Table 4.3. Figure 4.10 shows the effect of mass bias correction (using different $^{205}Tl/^{203}Tl$ ratios) on $^{208}Pb/^{206}Pb$ ratio of NIST 610 as measured by fs-LA-ICP-MS. Tl normalization has greatly corrected the measured isotope ratio compared to the raw ratios.

In this study we also applied the standard-sample-standard bracketing technique as another method to correct for mass bias. NIST 612 was used as a bracketing standard for Pb isotope ratio determinations in NIST 610. Alternate measurements of NIST 612 and NIST 610 were carried out using high laser energy on NIST 612 (0.8 mJ) and low laser energy on NIST 610 (0.3 mJ) to get more similar ion intensities for both matrices when switching between NIST 610 and NIST 612. The isotope ratio was calculated according to the following equation [31]

$$R_{True} = R_{Meas} \frac{R_{Std}}{\sqrt{r_{Std}^{1} \times r_{Std}^{2}}}$$

Where R_{True} and R_{Meas} represent the true and measured isotope ratios of the sample, respectively; R_{Std} is the true isotope ratio of the bracketing standard; and r_{Std}^{1} and r_{Std}^{2} are the isotope ratios of the bracketing standard measured before and after the sample.

Table 4.3 lists the measured Pb isotope ratios after being corrected for mass bias using both Tl normalization and standard-sample-standard bracketing together with published values. For Tl normalization, the Pb isotope ratios from each analytical event (single analysis of 300 seconds) were reported as the average of 185 integrations with the error reported as 1 standard deviation. The gross means of 6 measurements with 1 standard deviation are: $^{206}Pb/^{204}Pb$=17.0472 ± 0.0045, $^{207}Pb/^{204}Pb$ =15.5087 ± 0.0048, $^{208}Pb/^{204}Pb$ =36.9715 ± 0.0137, $^{208}Pb/^{206}Pb$ = 2.1685 ± 0.0003 and $^{207}Pb/^{206}Pb$ =0.9097 ± 0.0001. These values are in good agreement with published data. For standard-

sample-standard bracketing, twelve raw isotope ratios (after being corrected for background and ^{204}Hg interferences on ^{204}Pb) of alternate NIST 610 and NIST 610 were used to get five values of each isotope ratio in NIST 610 with means: ^{206}Pb/^{204}Pb=17.0608 ± 0.0132, ^{207}Pb/^{204}Pb =15.5219 ± 0.0124, ^{208}Pb/^{204}Pb =37.0076 ± 0.0300, ^{208}Pb/^{206}Pb = 2.1692 ± 0.0002 and ^{207}Pb/^{206}Pb =0.9098 ± 0.0001.

4.4 DISCUSSION

The idea of using mixed gas plasma is not new. It was originally used with ICP-MS and ICP-AES to improve their sensitivities, stabilities and analytical capabilities. However, there are contradictions in published data regarding enhancement or depression of sensitivities under different gas mixture conditions. For example, in some studies [11, 24, 25, 26, 29] whether based on solution- or LA-ICP-MS, addition of nitrogen to Ar gas was found to enhance sensitivity whereas in some other studies [17, 20, 28] a depression or little enhancement in sensitivity was reported. This wide variation in published data can be attributed to differences in instrumentation, experimental conditions and different ways of optimization among different laboratories. In this study, the addition of hydrogen and nitrogen to Ar carrier gas has improved elemental sensitivities, likely due to the higher thermal conductivities of these gases which results in higher plasma temperature and increased excitation and ionization efficiency of many elements. Nitrogen and hydrogen were added before the ablation cell. Therefore, the observed sensitivity enhancement could also be

related to processes occurring not only in the ion source (ICP) but also in the ablation cell and transport system. For example the ablation process could be affected by the added gases and consequently lead to changes in the amount of ablated material and particle size distribution. This would affect the transport efficiency and the degree of ionization inside the ICP with a subsequent enhancement or suppression of signal intensity. It should also be mentioned that consistent optimization of the large number of potential focusing parameters in ICP-MS after each gas addition is difficult. Thus accounting for the effect of all parameters to study the effect of gas addition is not possible.

Accurate and precise isotopic measurements are hindered by many obstacles in LA-ICP-MS such as elemental and isotopic fractionation, mass bias, abundance sensitivity, matrix effects and interferences. Careful optimization of experimental conditions can reduce these problems. The use of femtosecond laser pulses for ablation has been reported to minimize fractionation and matrix effects. Introduction of multicollectors with double focusing high resolution sector field analyzers has minimized ion beam instabilities, improved abundance sensitivity and eliminated some interferences when used at high resolution. Use of mixed gas plasmas is another way to reduce these effects. Addition of nitrogen to the Ar carrier gas, as indicated in this study, has reduced mass bias by about 13 %, robustly stabilized the mass bias ratios of Tl/Pb and increased sensitivity of Tl and Pb by a factor of 3-4. There do not appear to be any negative effects for Pb isotope analyses by introducing nitrogen to the plasma.

For other isotope systems, the increase in sensitivity achieved with addition of hydrogen or nitrogen will generally enhance precision of the measured isotope ratios. However the production of hydride ions in the ICP will introduce new interferences that may degrade precision and accuracy. For example in LA-MC-ICP-MS analyses of Sr isotopes, the presence of significant quantities of KrH^+, RbH^+ and SrH^+ in the analyzed ion beam will require significant inter element and inter isotope corrections that will be difficult to quantify with potential serious degradation in the ability to measure both Sr mass bias (from $^{86}Sr/^{88}Sr$) and the isotope ratio ($^{87}Sr/^{86}Sr$) which varies naturally by radioactive decay of ^{87}Rb. The increase of doubly charged ions with the hotter plasmas produced with hydrogen or nitrogen addition, e.g. of rare earth elements (REE), can be a problem in the determination of the isotopic composition of elements of interest such as Sr (interferences from $^{172}Yb^{+2}$ on $^{86}Sr^{+1}$; $^{176}Yb^{+2}$, $^{176}Lu^{+2}$ and $^{176}Hf^{+2}$ on $^{88}Sr^{+1}$) and Rb (interferences from $^{170}Er^{+2}$, $^{170}Yb^{+2}$ on $^{85}Rb^{+1}$; $^{174}Yb^{+2}$ and $^{174}Hf^{+2}$ on $^{87}Rb^{+1}$). Therefore it may become important to make a compromise between the benefits of enhanced sensitivity and the drawbacks of increased doubly charged ions and other interferences induced by addition of different gases to the plasma.

4.5 CONCLUSIONS

It has been shown in this study that addition of nitrogen and hydrogen to Ar carrier gas has improved signal intensity of most investigated elements in fs-LA-ICP-MS. At the same time there was an increase of polyatomic species of

nitrogen and hydrogen. The observed decrease in the oxide ratios and increase of doubly charged ions can be related to the increase of the plasma temperature as a result of high thermal conductivities of these gases. Careful optimization of instrumental parameters after gas addition is important since adding a gas will alter the plasma conditions, therefore it is important to make sure that the changes in sensitivities are caused only by gas addition and not by changes of optimum conditions.

We have also shown that adding nitrogen to Ar carrier gas before the ablation cell in fs-LA-MC-ICP-MS has improved the intensity of Tl and Pb by a factor of 3-4. This enhancement of sensitivity is important for isotopic analysis using Faraday detectors where large ion beams are necessary for precise and accurate isotopic analysis. Femtosecond laser systems with controllable energy and repetition rates (up to few kHz) can also be a tool for achieving the high count rates. The mass bias was reduced by about 13 % when nitrogen was added to Ar carrier gas. This reduction can be related to improvement of ion transmission as a result of more robust plasma in the presence of nitrogen. It has been also shown that Tl and Pb do not have identical mass bias and the mass bias difference should be taken into account for accurate and precise isotope ratios determination based on Tl normalization.

4.6 REFERENCES

[1] N. N. Sesi, A. M. Mackenzie, K. E. Shanks, P. Y. Yang and G. M. Hieftje, Fundamental studies of mixed gas inductively coupled plasmas Spectrochim. Acta B, 1994, **49**, 1259-1282.

[2] R. S. Houk, A. Montaser and V. A. Fassel, Mass-spectra and ionization temperatures in an argon-nitrogen inductively coupled plasma Appl. Spectrosc., 1983, **37**, 425–428.

[3] D. Hausler, Trace element analysis of organic solutions using inductively coupled plasma-mass spectrometry Spectrochim. Acta, Part B, 1987, **42**, 63–73.

[4] E. H. Choot and G. Horlick, Vertical spatial emission profiles in Ar-N_2 mixed gas inductively coupled plasmas, Spectrochim. Acta, Part B, 1986, **41**,889–906.

[5] K. S. Park, S. T. Kim, Y. M. Kim, Y. J Kim and W. Lee, Application of methane mixed plasma for the determination of Ge, As, and Se in serum and urine by ICP/MSBull. KoreanChem. Soc., 2003, **24**, 285–290.

[6] M. Murillo and J. M. Mermet, Improvement of the energy transfer with added-hydrogen in inductively coupled plasma atomic emission spectrometry Spectrochim. Acta, Part B, 1989, **44**,359–366.

[7] I. Rodushkin, P. Nordlund, E. Engstro¨m and D. C. Baxter, Improved multi-elemental analyses by inductively coupled plasma-sector field mass spectrometry through methane addition to the plasmaJ. Anal. At. Spectrom., 2005, **20**, 1250–1255.

[8] A. Montaser and R. L. Vanhoven, Crit. Rev. Anal. Chem., Mixed-gas, molecular-gas, and helium inductively coupled plasmas for analytical atomic spectrometry - a critical-review1987, **18**, 45–103.

[9] A. Montaser, S. K. Chan and D. W. Koppenaal, Anal. Chem. Inductively Coupled Helium Plasma as an Ion Source for Mass Spectrometry , 1987, **59**, 1240–1242.

[10] L. Ebdon, M. J. Ford, R. C. Hutton and S. J. Hill, Evaluation of ethene addition to the nebulizer gas in inductively-coupled plasma-mass spectrometry for the removal of matrix-gas-derived, solvent-gas-derived, and support-gas-derived polyatomic ion interferences, Appl. Spectrosc.,1994, **48**, 507–516.

[11] Z. Hu, S. Gao, Y. Liu, S. Hu, H. Chen and H. Yuan, Signal enhancement in laser ablation ICP-MS by addition of nitrogen in the central channel gas, J. Anal. At. Spectrom., 2008, **23**, 1093–1101.

[12] R. C. Hutton, Application of inductively Coupled Plasma Source Mass Spectrometry (ICP-MS) to the Determination of Trace Metals in Organics, J. Anal. At. Spectrom., 1986, **1**, 259-263.

[13] G. Xiao and D. Beauchemin, Reduction of Matrix Effects and Mass Discrimination in Inductively Coupled Plasma Mass Spectrometry With Optimized Argon-Nitrogen Plasmas, J. Anal. At. Spectrom., 1994, **9**, 509-518.

[14] A. E. Holliday and D. Beauchemin, Preliminary investigation of direct sea-water analysis by inductively coupled plasma mass spectrometry using a

mixed-gas plasma, flow injection and external calibration, J. Anal. At. Spectrom., 2003, **18**, 1109–1112.

[15] Z. Hu, S. Hub, S. Gao,Y. Liua and S. Lin, Volatile organic solvent-induced signal enhancements in inductively coupled plasma-mass spectrometry: a case study of methanol and acetone, Spectrochimica Acta B 2004, **59**, 1463–1470.

[16] Z. Hu. S. Gao,. S. Hu,. H. Yuan,. X. Liua and Y. Liu, Suppression of interferences for direct determination of arsenic in geological samples by inductively coupled plasma mass spectrometry , J. Anal. At. Spectrom., 2005, **20**, 1263-1269.

[17] D. Beauchemin and J. M. Craig, Investigations on mixed-gas plasmas produced by adding nitrogen to the plasma gas in ICP-MS, Spectrochimica Acta B, 1991, **46**, 603-614.

[18] E. H. Evans and L. Ebdon, Simple Approach To Reducing Polyatomic Ion Interferences On Arsenic And Selenium In Inductively Coupled Plasma Mass-Spectrometry, J. Anal. At. Spectrom., 1989, **4**, 299-300.

[19] E. H. Evans and L. Ebdon, Effect Of Organic-Solvents And Molecular Gases On Polyatomic Ion Interferences In Inductively Coupled Plasma Mass-Spectrometry J. Anal. At. Spectrom., 1990, **5**, 425 -430.

[20] J. M. Craig and D. Beauchemint, Reduction Of The Effects Of Concomitant Elements In Inductively Coupled Plasma Mass-Spectrometry By Adding Nitrogen To The Plasma Gas , J. Anal. At. Spectrom., 1992, **7**, 937-942.

[21] J. W. Lam and G. Horlick, A Comparison Of Argon And Mixed Gas Plasmas For Inductively Coupled Plasma Mass-Spectrometry, Spectrochim Acta B, 1990, **45**, 1313-1325.

[22] S. J. Hill, M. J. Ford and L. Ebdon, Simplex Optimization Of Nitrogen Argon Plasmas In Inductively Coupled Plasma Mass-Spectrometry For The Removal Of Chloride-Based Interferences, J. Anal. At. Spectrom., 1992, **7**, 719 -725.

[23] H. Louie and S. Y. P. Soo,Use Of Nitrogen And Hydrogen In Inductively Coupled Plasma Mass-Spectrometry , J. Anal. At. Spectrom., 1992, **7**, 557-564.

[24] S. F. Durrant, Feasibility of improvement in analytical performance in laser ablation inductively coupled plasma-mass spectrometry (LA-ICP-MS) by addition of nitrogen to the argon plasma, Fresenius J Anal Chem., 1994, **349**, 768-771.

[25] S. A. Crowe, B. J. Fryer, I. M. Samson and J. E. Gagnon, Precise isotope ratio determination of common Pb using quadrupole LA-ICP-MS with optimized laser sampling conditions and a robust mixed-gas plasma, J. Anal. At. Spectrom., 2003, **18**, 1331-1338.

[26] T. Iizuka and T. Hirata, Improvements of precision and ccuracy in in situ Hf isotope microanalysis of zircon using the laser ablation-MC-ICPMS technique, Chem. Geol., 2005, **220**, 121– 137.

[27] Q. Ni, Z. C. Hu, Z. Y. Bao and Y. F. Zhang, Improved Cd determination in glasses by laser ablation inductively coupled plasma mass spectrometry using nitrogen as a matrix modifier, Chin. Chem. Let., 2009, **20**, 92–95.

[28] M. Guillong and C. A. Heinrich, Sensitivity enhancement in laser ablation ICP-MS using small amountsof hydrogen in the carrier gas, J. Anal. At. Spectrom., 2007, **22**, 1488–1494.

[29] Z. Hu, S. Gao, Y. Liu, S. Hu, H. Chen and H. Yuan, Signal enhancement in laser ablation ICP-MS by addition of nitrogen in the central channel gas, J. Anal. At. Spectrom., 2008, **23**, 1093–1101.

[30] I. T. Platzner, Modern isotope ratio mass spectrometry, volume 145 in chemical analysis: a series of monographs on analytical chemistry and its applications, John Wiely , England, 1997.

[31] F. Albarede and B. Beard, Analytical methods for non traditional isotopes, Reviews in Mineralogy and Geochemistry, **55** (2004)113-152.

[32] R.E. Russo, X. Mao, J. J. Gonzalez and S. S. Mao, Femtosecond laser ablation ICP-MS, J. Anal. At. Spectrom., 2002, **17**,1072-1075.

[33] M. Shaheen, J. E. Gagnon, Z. Yanga and B. J. Fryer, Evaluation of the analytical performance of femtosecond laser ablation inductively coupled plasma mass spectrometry at 785 nm with glass reference materials**,** J. Anal. At. Spectrom., 2008, **23**, 1610–1621.

[34] I. Horn and F. von Blanckenburg, Investigation on elemental and isotopic fractionation during 196 nm femtosecond laser ablation multiple collector

inductively coupled plasma mass spectrometry, Spectrochim. Acta B, 2007, **62**, 410–422.

[35] J. Chmeleff, I. Horn, G. Steinhoefel, F. von Blanckenburg, In situ determination of precise stable Si isotope ratios by UV-femtosecond laser ablation high-resolution multi-collector ICP-MS, Chem. Geol., 2008, **249**, 155–166.

[36] M. Rehkamper, F. Wombacher and J. K. Aggarwal, Stable isotope analysis by multiple collector ICP-MS, in handbook of stable isotope analytical techniques, volume 1, P. A. de Groot, Elsevier, 2004.

[37] J. S. Becker, Inorganic mass spectrometry: principles and applications, John Wiley &Sons Ltd, 2007.

[38] N. J. Pearson, W. L. Griffen and S. Y. O'Reilly, Mass fractionation correction in laser ablation multiple-collector ICP-MS: implication for overlap correction and precise and accurate in situ isotope ratio measurement, in Laser ablation in earth sciences: current practices and outstanding issues, short course series, volume 40, Paul Sylvester, Vancouver, BC, 2008.

[39] H. Zou, Mass fractionation in ionization processes, in Quantitative geochemistry, Imperial college press, London, 2007.

[40] H. Andrén, I. Rodushkin, A. Stenberg, D. Malinovsky and D. C. Baxter, Sources of mass bias and isotope ratio variation in multi-collector ICP-MS: optimization of instrumental parameters based on experimental observations, *J. Anal. At. Spectrom.***,** 2004, **19**, 1217 – 1224.

[41] G. H. Fontaine, B. Hattendorf, B. Bourdon and D. Gunther, Effects of operating conditions and matrix on mass bias in MC-ICPMS, J. Anal. At. Spectrom., 2009, **24**, 637–648.

[42] H.P. Longerich,B. J. Fryer, D. F. Strong, Determination of lead isotope ratios by inductively coupled plasma-mass spectrometry (ICP-MS). Spectrochim. Acta, Part B: Atom. Spectrosc. 1987, **42** (1– 2), 39–48.

[43] http://georem.mpch-mainz.gwdg.de/sample_query_pref.asp

[44] M.F. Thirlwall, Multicollector ICP-MS analysis of Pb isotopes using a 207Pb-204Pb double spike demonstrates up to 400 ppm/amu systematic errors in Tl-normalization, Chem. Geol. 2002, **184**, 255–279.

[45] W. M. White, F. Albarede and P. Telouk, High-precision analysis of Pb isotope ratios by multi-collector ICP-MS, Chem. Geol. 2000, **167**, 257–270.

[46] M. Rehkamper and A. N. Halliday, Accuracy and long-term reproducibility of lead isotopic measurements by multiple-collector inductively coupled plasma mass spectrometry using an external method for correction of mass discrimination, Int. J.Mass Spec. Ion. Proc., 1998, **181**, 123–133.

[47] N.S. Belshaw, P.A. Freedman, R. K. O'Nions, M. Frank and Y. Guo, A new variable dispersion double-focusing plasma mass spectrometer with performance illustrated for Pb isotopes **,** Int. J. Mass Spec. Ion. Proc., 1998, **181**, 51-58.

[48] C. Gallon, J. Aggarwal and A. R. Flegal, Comparison of Mass Discrimination Correction Methods and Sample Introduction Systems for the Determination

of Lead Isotopic Composition Using a Multicollector Inductively Coupled Plasma Mass Spectrometer, Anal. Chem. 2008**, 80**, 8355–8363.

[49] A. J. Walder, I. D. Abell and I .Platzener, Lead isotope ratio measurement of NIST 610 glass by laser ablation inductively coupled plasma mass spectrometry, Spectrochim. Acta B, 1993, **48**(3), 397-402.

[50] J. D. Woodhead and J. M. Hergt, Strontium, Neodymium and Lead Isotope Analyses of NIST Glass Certified Reference Materials: SRM 610, 612, 614, Geostand. Newsl.,2001, **25**, 261-266.

[51] J. Baker, D. Peate, T. Waight., C. Meyzen,Pb isotopic analysis of standards and samples using a 207Pb– double spike and thallium to correct for mass bias with double-focusing MC-ICP-MS, Chem.Geol., **2004**, 211, 275–303.

[52] I. Platzner, S. Ehrlich and L. Halicz**,** Isotope-ratio measurements of lead in NIST standard reference materials by multiple-collector inductively coupled plasma mass spectrometry, Fres. J Anal.Chem., 2001, **370**, 624–628.

[53] N. S. Belshaw, R. K. O'Nions, D. J. Martel and K. W. Burton, High-resolution SIMS analysis of common lead, Chem. Geol., 1994, **112**, 57-70.

[54] N. Machado and G. Gauthier, Determination of 207Pb/206Pb ages on zircon and monazite by laser ablation ICP-MS and application to a study of sedimentary provenance and metamorphism in southeastern Brazil, Geochim. Cosmochim Acta, 1996, **60**, 5063-5073.

Table 4.1: LA –ICP-MS, MC-ICP-MS specifications and operating conditions

Laser ablation system	
Manufacture:	Quantronix
Model:	Integra C®
Type:	Ti:sapphire based on the Chirped Pulse Amplification (CPA) technique
Wavelength:	Fundamental: 785 nm
Repetition rate:	Up to 1kHz, experiment: 20 Hz for quadruple ICP-MS and 100 Hz for MC-ICP-MS
Pulse energy:	Maximum: 2mJ/pulse, experiment: 0.2, 0.3, 0.8 mJ
Pulse width:	<130 fs
Fluence:	12.3 Jcm^{-2} for quadruple ICP-MS and 7.4 Jcm^{-2} for MC-ICP-MS
Crater size:	47µm for quadruple ICP-MS and 67µm for MC-ICP-MS
Objective lens:	10X
ICP-MS	
Manufacture:	ThermoElectron®
Model:	X7-II®
Detector type:	ETP® dual mode (pulse and analogue counting)
Dynamic range:	~1.3 x 10^9 ICPS
Sensitivity (sol.):	~350× 10^6 ICPS/ppm
Cone type:	High Performance Interface (HPI)
Resolution:	Standard (125), High (160)
RF power:	1400 W
Plasma gas:	13 L min^{-1}
Auxiliary gas:	0.98 L min^{-1}
Nebulizer gas:	0.88-1.02 L min^{-1}
MC-ICP-MS	
Manufacture:	ThermoElectron®
Model:	Finnigan™ Neptune
Coolant gas	15 l/min
Sample gas	0.91 l/min
Auxiliary gas	0.7 l/min
Rf power	1200 W
Integration time	1.049 sec
Tl flow rate	100 µl/min

Table 4.2: Faraday cup configurations used for Pb ratios measurements

Collector	L3	L2	L1	Center	H1	H2	H3
MassIsotope	202 Hg	203 Tl	204 Pb Hg	205 Tl	206 Pb	207 Pb	208 Pb

Table 4.3: Measured Pb isotope ratios of NIST 610 using Tl normalization and standard-sample-standard bracketing

	$^{206}Pb/^{204}Pb$	$^{207}Pb/^{204}Pb$	$^{208}Pb/^{204}Pb$	$^{208}Pb/^{206}Pb$	$^{207}Pb/^{206}Pb$
Tl normalization (this study)					
#1	17.0547 ± 0.0673	15.5173 ± 0.0645	36.9968 ± 0.1705	2.1691 ± 0.0045	0.9099 ± 0.0017
#2	17.0480 ± 0.0321	15.5097 ± 0.0287	36.9724 ± 0.0694	2.1684 ± 0.0015	0.9098 ± 0.0004
#3	17.0466 ± 0.0348	15.5076 ± 0.0312	36.9691 ± 0.0754	2.1684 ± 0.0014	0.9097 ± 0.0005
#4	17.0465 ± 0.0354	15.5073 ± 0.0315	36.9681 ± 0.0774	2.1684 ± 0.0014	0.9097 ± 0.0004
#5	17.0469 ± 0.0298	15.5075 ± 0.0267	36.9678 ± 0.0644	2.1683 ± 0.0011	0.9097 ± 0.0004
#6	17.0405 ± 0.0318	15.5026 ± 0.0281	36.9551 ± 0.0674	2.1684 ± 0.0011	0.9097 ± 0.0004
Average ± SD	**17.0472 ± 0.0045**	**15.5087 ± 0.0048**	**36.9715 ± 0.0137**	**2.1685 ± 0.0003**	**0.9097 ± 0.0001**
Standard-sample bracketing (this study)					
#1	17.0468	15.5073	36.9706	2.1688	0.9097
#2	17.0756	15.5352	37.0416	2.1693	0.9097
#3	17.0607	15.5218	37.0094	2.1693	0.9098
#4	17.0487	15.5122	36.9851	2.1694	0.9098
#5	17.0722	15.5333	37.0315	2.1691	0.9098
Average ± SD	**17.0608 ± 0.0132**	**15.5219 ± 0.0124**	**37.0076 ± 0.0300**	**2.1692 ± 0.0002**	**0.9098 ± 0.0001**
Reference Values [43] (used in this study)	17.0450 ± 0.0080	15.5040 ± 0.0090	36.9640 ± 0.0220	2.1680 ± 0.0010	0.90960 ± 0.0003
Walder et al. [49]	17.0510 ± 0.0160	15.5090 ± 0.0180	36.9480 ± 0.0380	2.1670 ± 0.0018	0.9096 ± 0.0008
Woodhead et al. [50]	17.0470 ± 0.0018	15.5090 ± 0.0001	36.9750 ± 0.0026	2.1699 ± 0.0003	0.9101 ± 0.0001
Baker et al. [51]	17.0520 ± 0.0020	15.5150 ± 0.0020	36.9910 ± 0.0050	2.1694 ± 0.0001	0.9099 ± 0.0005
Platzner Et al. [52]	17.0510 ± 0.0090	15.5070 ± 0.0080	36.9650 ± 0.0160	2.1677 ± 0.0006	0.9095 ± 0.0002
Belshaw et al. [53]	17.0490 ± 0.0120	15.5060	36.9790	2.1690 ± 0.0010	0.9095 ± 0.0006
Machado et al. [54]	17.0640 ± 0.0070	15.5250	37.0460	2.1710 ± 0.0010	0.9098 ± 0.0002

For Tl normalization, data are reported for 6 measurements as the mean ± 1 standard deviation (SD). This data represents the mean of 200 integrations (1 second each integration) after background correction. For standard-sample-standard bracketing, NIST 612 was used as a bracketing standard for NIST612. All isotope ratio measurements were carried out by adding 8ml/min N_2 to Ar before the ablation cell.

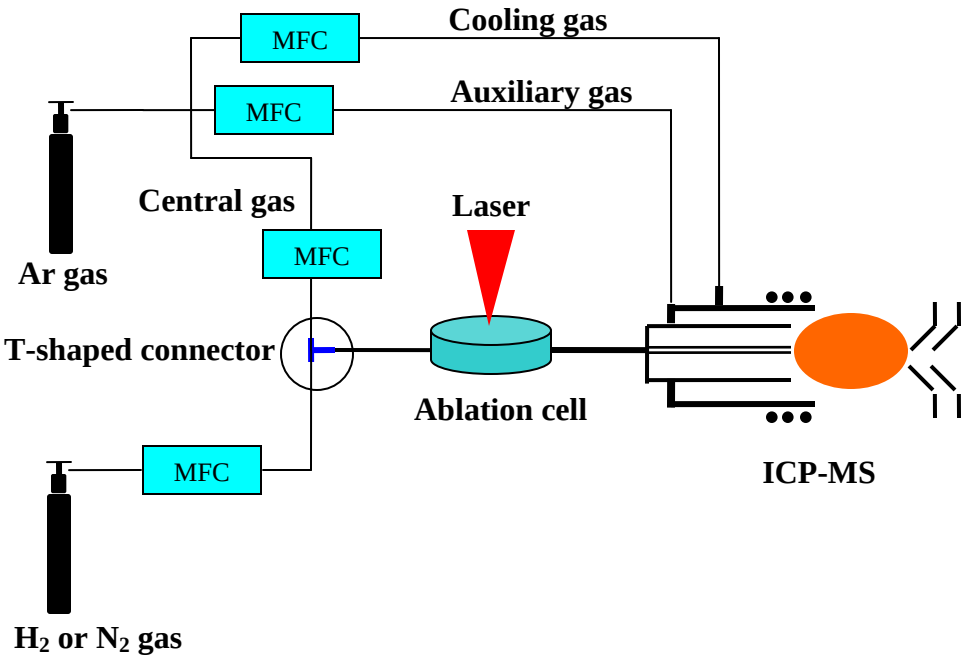

Figure 4.1: A schematic set-up of LA-ICP-MS for the addition of small amounts N_2 or H_2. MFC: mass flow controller.

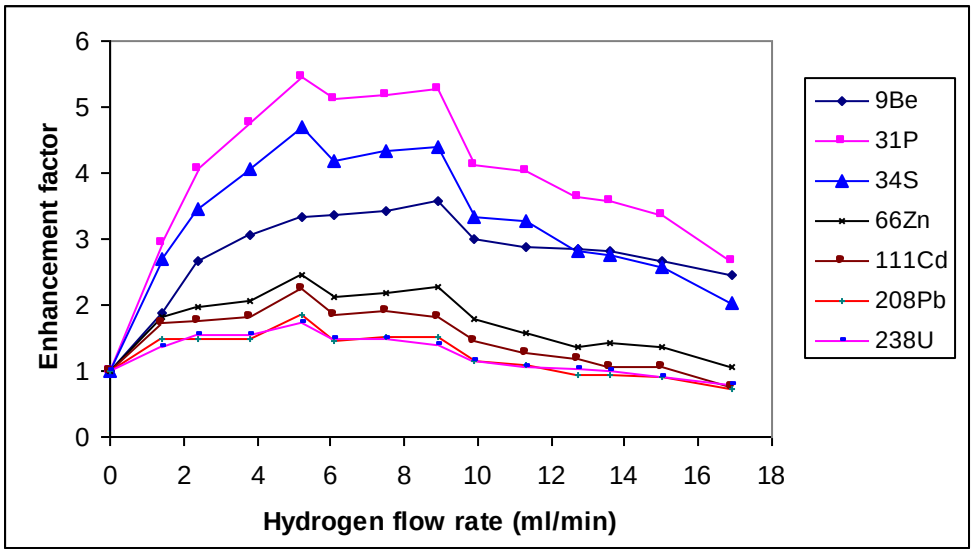

Figure 4.2: the effect of hydrogen flow rates on signal enhancement factor relative to pure Ar in fs-LA-ICP-MS of NIST 612.

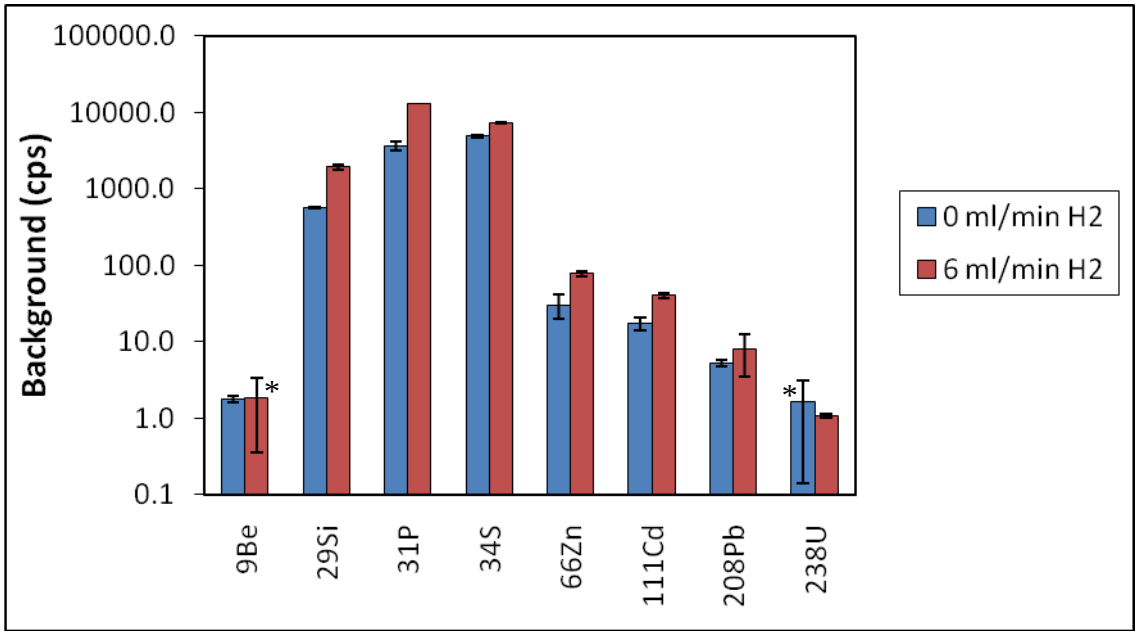

Figure 4.3: background intensities (cps) obtained at 0 and 6 ml/min hydrogen added to Ar carrier gas before the ablation cell in fs-LA-ICP-MS of NIST 612. * ^{238}U at 0 ml/min H_2 and 9Be at 5 ml/min H_2 have standard deviations greater than the average values.

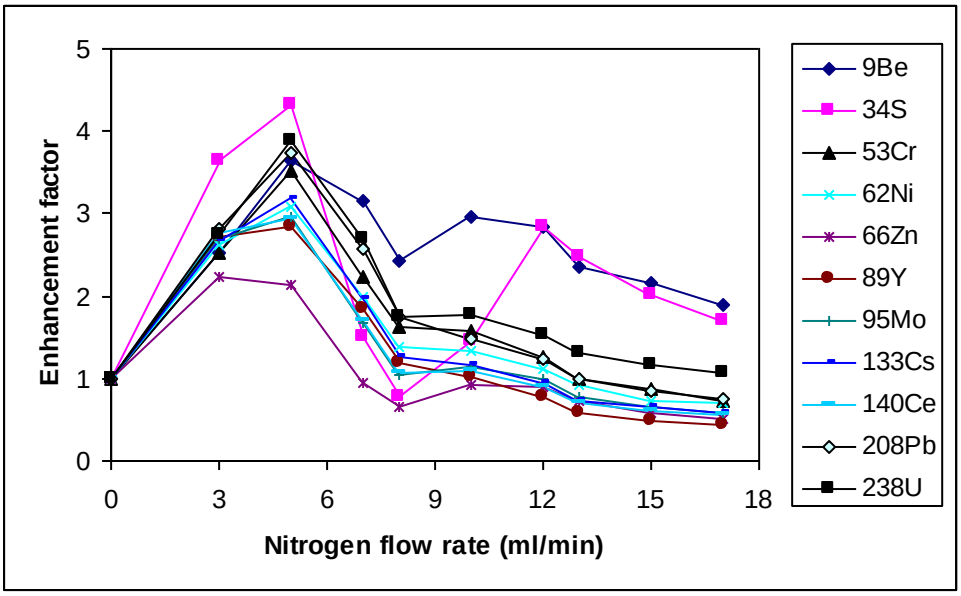

Figure 4.4: the effect of nitrogen flow rate on the signal enhancement factor relative to pure Ar in fs-LA-ICP-MS of NIST 612.

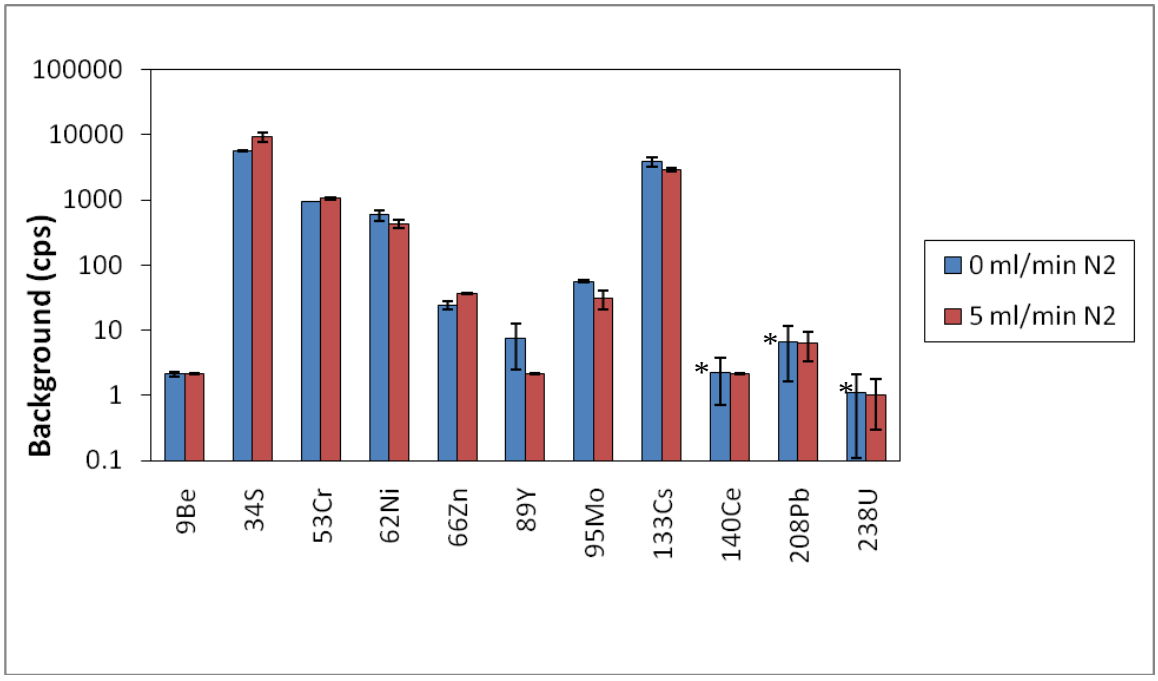

Figure 4.5: background intensity in the absence and presence of 5ml/min nitrogen obtained in fs-LA-ICP-MS of NIST 612. *^{140}Ce, ^{208}Pb and ^{238}U at 0 ml/min N_2 have standard deviations greater than the average values.

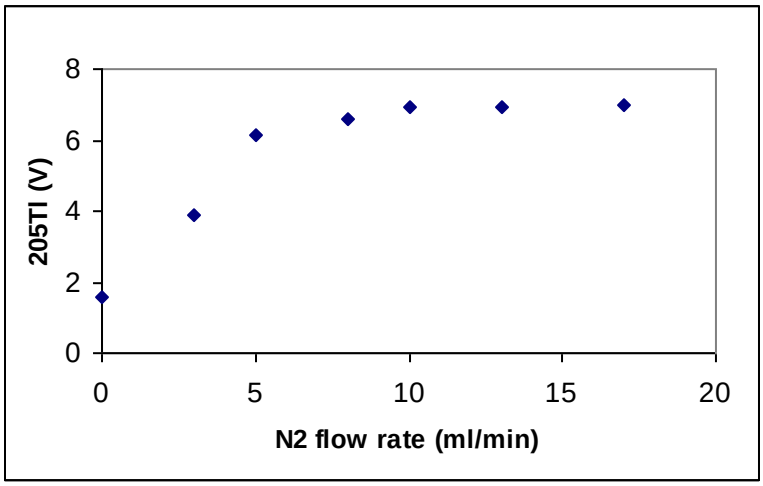

Figure 4.6a: effect of nitrogen flow rate on signal intensity of ^{205}Tl in fs-LA-MC-ICP-MS.

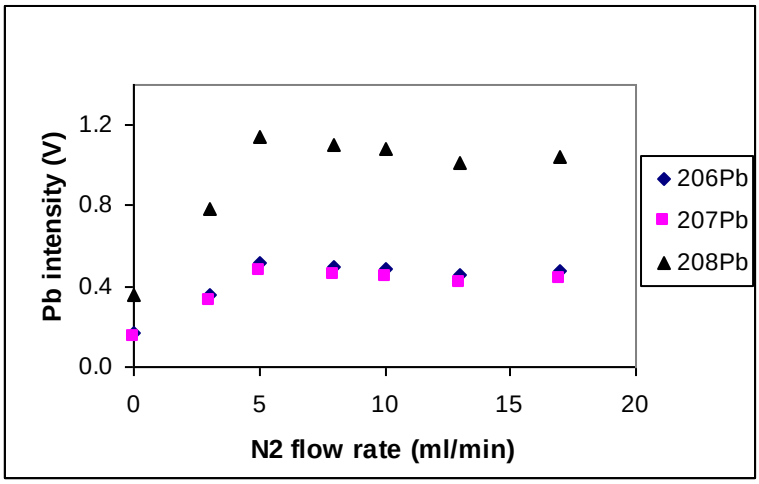

Figure 4.6b: Effect of nitrogen flow rate on signal intensity of Pb isotopes in fs-LA-MC-ICP-MS.

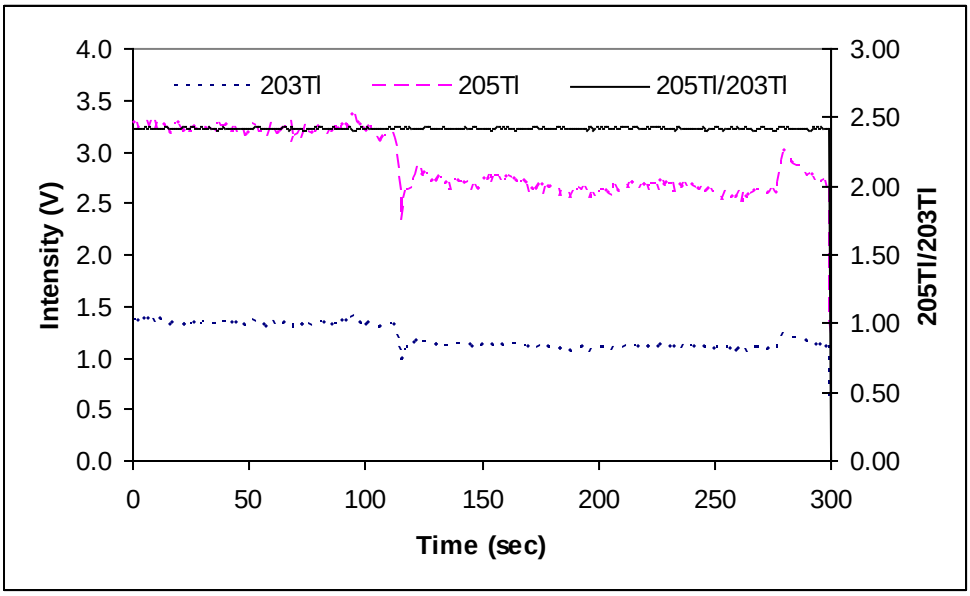

Figure 4.7: intensity variation of Tl isotopes and $^{205}Tl/^{203}Tl$ during data acquisition of 300 seconds on NIST 612. The first 100 seconds represents Tl solution (no laser ablation) while the last 200 seconds represents Tl solution and laser ablation.

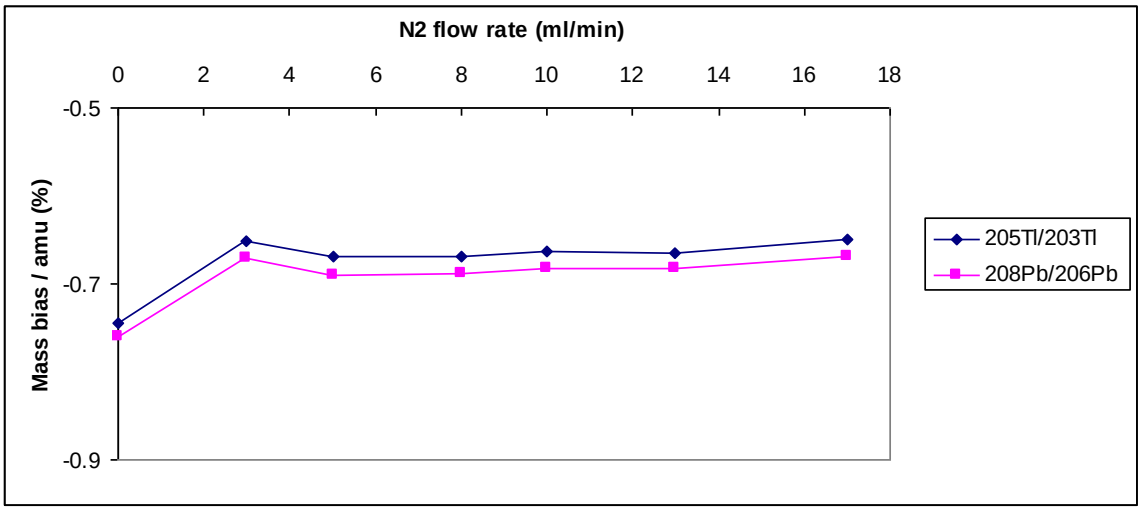

Figure 4.8: Mass bias of $^{205}Tl/^{203}Tl$ and $^{208}Pb/^{206}Pb$ as a function of nitrogen flow rate in fs-LA-MC-ICP-MS of NIST 610. The nitrogen and Tl were added before the ablation cell.

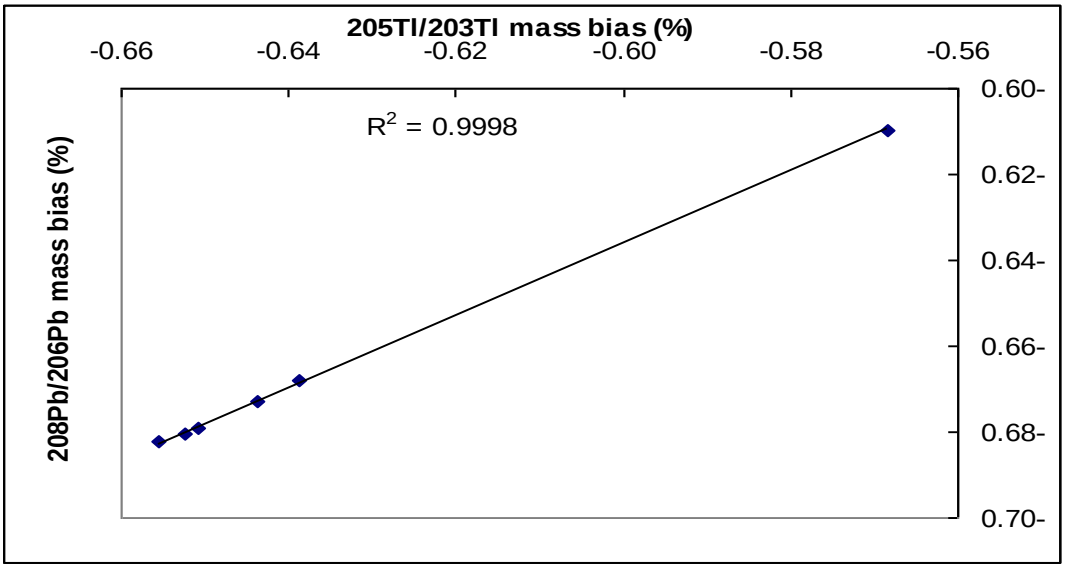

Figure 4.9: the relationship between $^{205}Tl/^{203}Tl$ and $^{208}Pb/^{206}Pb$ mass bias factors calculated from power law at constant nitrogen flow rates (8 ml/min), for 6 replicate measurements of NIST 610, a strong linear correlation (R^2=0.9998) exist between both factors. Values of $^{205}Tl/^{203}Tl$ =2.3889 and $^{208}Pb/^{206}Pb$=2.168 were obtained from references [44] and [43], respectively.

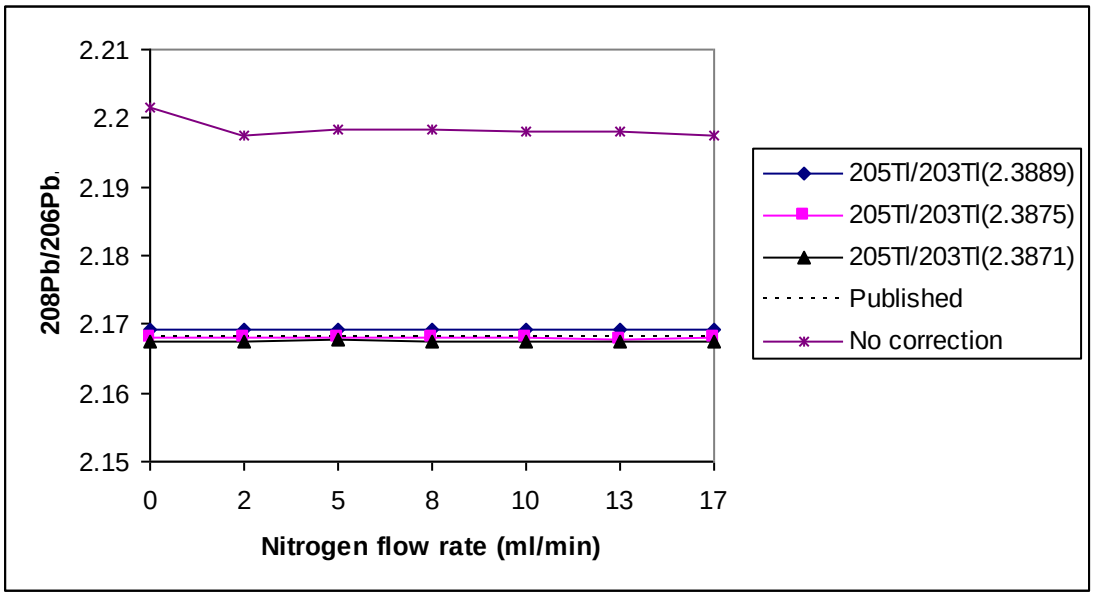

Figure 4.10: effect of mass bias correction using different $^{205}Tl/^{203}Tl$ ratios on $^{208}Pb/^{206}Pb$ ratio of NIST 610 as measured by fs-LA-ICP-MS. $^{208}Pb/^{206}Pb$ published value was obtained from reference [43].

CHAPTER 5

ELEMENTAL ANALYSIS OF SEDIMENT REFERENCE MATERIALS: A COMPARISON BETWEEN FEMTOSECOND LASER ABLATION- AND SOLUTION- INDUCTIVELY COUPLED PLASMA MASS SPECTROMETRY

5.1 INTRODUCTION

Solution-based (SO) Inductively coupled plasma mass spectrometry (ICP-MS) has gained wide acceptance in elemental and isotopic analysis of a wide range of matrices [1-8]. Capability of multi-element analysis, wide linear dynamic range, high sensitivity, low detection limits, and the ease of coupling with different sample introduction systems are advantages of this technique. Tedious sample preparations (especially those of refractory matrices such as sediments and soils) and the risk of contamination are often disadvantages [3, 7, 9]. Sediments are complex structures composed of mineral constituents, organic matter, living organisms, air and water. They can be a source or a sink of contaminants in aquatic systems. Therefore, identification of sediment chemical compositions is important to understand the behavior of contaminants in aquatic systems and can also give valuable information about environmental changes. Sample preparation for sediment analysis by SO-ICP-MS is a critical step for accurate analysis because of the complex and often refractory nature of sediments. Various digestion techniques such as open-vessel, closed-vessel digestions using mixed acid attacks and fusion procedures have been used for sediment digestion [10]. Wet digestion procedures without using hydrofluoric acid (HF) are incomplete and are only useful for the determination of the acid-extractable fraction of an element and do not adequately represent its total abundance in the sediment [11-12].

The coupling of direct solid sample introduction techniques such as laser ablation (LA) with ICP-MS has minimized the problems of sample preparation

and increased sample throughput [5, 13-19]. LA-ICP-MS has been applied for bulk elemental and isotopic analyses of soils and sediments prepared in different forms such as pressed pellets or fused disks [20-30]. Most studies by LA-ICP-MS have been based on nanosecond laser (ns) systems (Nd:YAG and excimer lasers) [31-35]. Excimer lasers working at deep ultraviolet (DUV) have been reported to give controlled ablation in terms of crater geometry, particle size distributions and chemistry of the laser-produced aerosols. While Nd:YAG laser systems are less expensive and easier to maintain, the thermal characteristics of these systems can lead to elemental and isotopic fractionation, matrix effects, and less-representative sampling. Recently, femtosecond (fs) laser pulses have been suggested for chemical analysis by LA-ICP-MS to eliminate the problems associated with nanosecond laser systems [36-44]. Femtosecond laser pulses minimize the thermal effects generated during laser-solid interactions and consequently have minimized fractionation and matrix effects. Compared to ns-LA-ICP-MS, fs-LA-ICP-MS has narrower particle size distributions, better transport efficiencies, and better vaporization, atomization and ionization of laser-produced aerosols in the ICP [36-44]. Because elemental analysis by SO-ICP-MS and LA-ICP-MS, like many other analytical techniques, necessitate comparisons to reference materials of known chemical compositions, it is important to have well-identified reference materials, which are not readily available for sediments.

In this work we report the chemical composition of seven sediment reference materials (Lake sediments: LKSD-1, LKSD-2, LKSD-3, Stream sediments: STSD-2, STSD-3, and Marine sediments: PACS-2, MESS-3) after

digestion in a mixture of hydrofluoric and nitric acids and analysis by SO-ICP-MS. We also investigated the analytical capabilities of femtosecond (fs)- LA-ICP-MS of sediments prepared in the form of solid disks using Spurr low viscosity epoxy resin. The goal was to validate the capability of LA-ICP-MS for the analysis of natural sediment cores extracted from a lake or a river and prepared in a similar way (as the sediment reference materials) for high spatial resolution analysis.

5.2 EXPERIMENTAL

5.2.1 SAMPLE DIGESTION FOR SO-ICP-MS ANALYSIS

Seven sediment reference materials (Lake sediments: LKSD-1, LKSD-2, LKSD-3, Stream sediments: STSD-2, STSD-3, and Marine sediments: PACS-2, MESS-3) were prepared for solution analysis by ICP-MS. These reference materials (provided in a powder form) represent typical lake, stream and marine sediments from various locations within the Canadian Shield and were collected by the Geological Survey of Canada. The samples were prepared, blended and bottled at Canada Centre for Mineral and Energy Technology (CANMET). Hydrofluoric acid is the only acid that will dissolve silica-based materials by forming volatile SiF_6 [7], therefore it was used in our sediment digestion method together with concentrated nitric acid. About 100 mg of the sample (used as supplied) was accurately weighted into a clean screw top Savillex PFA bottle (30 ml) and mixed with 1 ml distilled hydrofluoric acid and 2 ml concentrated nitric acid. Each bottle was tightly sealed and heated to a temperature of 100 °C using a hotplate for two days. The cover of each bottle was removed and the solutions

were dried at a temperature of 70 °C for about 12 hours to ensure complete evaporation of the acids. This process was repeated two times until clear solutions were obtained. Free HF acid even at low concentrations must be removed prior to analysis as it attacks glassware used in ICP-MS nebulizers, spray chambers and injectors [7]. Residual hydrofluoric acid was removed from solution by twice re-evaporating the digested samples following addition of nitric acid. We preferred evaporation to addition of Boric acid (H_3BO_3) for HF removal because the later increases total dissolved solids in solution that leads to matrix effects and deteriorated analytical capabilities of the ICP-MS. The internal standard elements Be, In and Tl at concentrations of 10, 1 and 2 ppm, respectively, were added to samples after being filtered and diluted by 1% HNO_3 to correct for matrix effects, drift and variable sensitivity.

5.2.2 SAMPLE PREPARATION FOR LASER ABLATION

A simple and fast method was used to prepare sediment reference materials for LA-ICP-MS. About 2 grams of each sediment reference material were moistened with acetone and shaken for a few minutes to allow stacking of sediment particles and reducing interstitial air. The sediment was then impregnated with a freshly prepared Spurr low-viscosity epoxy resin [45] and left at room temperature for eight hours to give a chance for the resin to infiltrate the sample. This embedding medium was reported to have good penetration qualities and has previously been successfully used for preparation of sediments [45-48]. The components of the resin and their mixing ratios that provide useful

properties with a variety of hardness characteristics are shown in Table 5.1. In this work we used the standard medium resin for sediment preparation but we reduced the cure temperature to 60 °C and increased the cure time to 16 hours since a higher temperature was found to increase gas generation in the sediment during curing. Sediment disks were prepared for analysis by fs-LA-ICP-MS by polishing and cleaning the surface.

5.2.3 SO-ICP-MS

All measurements (laser ablation or solution) were carried out using the ThermoElectron X7-II® ICP-MS (Table 5.2) at the Great Lakes Institute for Environmental Research, University of Windsor, Canada. Solutions were aspirated into Conical nebulizer and cyclonic spray chamber by a peristaltic pump at a rate of 2 ml/min. The instrument was tuned for maximum sensitivity and minimum oxide ratio ($^{254}UO/^{238}U$=2-3%). Reference solutions were prepared from custom-made multielement standards (Inorganic Ventures, Inc. and in-house). Nominal concentration of 5 ppb standard solutions were prepared and used for quantification of 44 elements in sediment reference materials.

5.2.4 LA-ICP-MS

The laser ablation system consists of a Quantronix Integra C® fs laser operating at its fundamental wavelength of 785 nm and a pulse width less than 130 fs. The description of the laser system can be found in Shaheen et al. [43]. The effect of heterogeneity of sediment reference materials was reduced by

using large laser spot sizes (~110 µm) and scan ablation mode (5µm/s). With this sampling strategy, larger volumes of sample were ablated leading to improved precisions and detection limits. The ICP-MS was optimized for maximum sensitivity and minimum oxide formation (ThO/Th <0.1 %) using NIST 612 as a standard. LKSD-3 sediment reference material (prepared in a form of a solid disk) was used as an external standard for quantification of elements in other sediment reference materials (LKSD-1, LK-SD-2, STSD-2 and STSD-3) which have been treated as unknowns. Silicon, based on literature values, was used as an internal standard to correct for matrix effects and amount of material ablated. All samples were polished and then cleaned by sonication for 15 minutes in MilliQ® water. Immediately before analysis, the surface of each sample was cleaned with ultrapure ethanol. Five scan ablations were carried out on each unknown to calculate precisions with each ablation consisting of one minute for gas blank signal collection (i.e. the laser is off) followed by two minutes of analyte signal collection. LA-ICP-MS data manipulation was performed off-line using commercial spreadsheet software and in-house written software based on Longerich et al. [49]. The operating conditions of the laser system are shown in Table 5.3.

5.3 RESULTS AND DISCUSSION

Figure 5.1 shows disks prepared from a sediment reference material (LKSD-3) and a blank resin using Spurr low viscosity epoxy resin. The blank resin was prepared by mixing the components of the embedding media (Table

5.1) to obtain a standard medium resin which was cured at a temperature of 60 °C. Due to the presence of interstitial air between sediment particles, bubbles can form during the curing process as can be seen for LKSD-3 from Figure 5.1, however there are still large areas on the pellet surface available for ablation. Interstitial air can be reduced by pressing the sediment powder before impregnation with the resin with a subsequent improvement in the disk quality. Figure 5.2 shows scanning electron micrographs (SEM) of ablation tracks in: a) blank resin and b) LKSD-3 impregnated with Spurr low viscosity epoxy resin. Sediment grains are seen to have sizes up to ~ 100µm in this material therefore utilization of a large laser spot size and scanning the laser beam over the sample surface are important to reduce the effect of sample heterogeneity on ablation behavior and results.

An important issue that must be taken into account when using an epoxy resin as an embedding medium for sediment preparation is contamination that can be introduced to the sediment from the resin. The major components of the blank resin (as we measured by Energy Dispersive X-ray flourescence) are C, O and Cl with concentrations of 78.84 wt %, 19.94 wt % and wt 1.22 %, respectively. Figures 5.3 and 5.4 show signal intensities of representative elements obtained from fs-LA-ICP-MS of a blank resin and sediment reference material LKSD-3, respectively. For most elements, there are insignificant changes in intensities upon ablation of the blank resin. This indicates that the chemical contribution of the resin to sediment metal concentrations is extremely small and can be neglected for these elements. Some masses (such as ^{52}Cr,

^{63}Cu, ^{66}Zn and ^{93}Nb) have shown an increase in signal intensity upon ablation of the blank resin. Such increase in intensity can be related to interferences on ^{52}Cr from $^{40}Ar^{12}C$; on ^{63}Cu from $^{40}Ar^{23}Na$; on ^{66}Zn from $^{14}N^{40}Ar^{12}C$, and on ^{93}Nb from $^{40}Ar^{40}Ar^{13}C$. Reduction of these interferences was made by selecting masses that show minimum interferences and by subtraction of the blank signal (i.e. the signal obtained from laser ablation of blank resin) from sediment signals.

5.3.1 QUANTIFICATION OF SEDIMENT REFERENCE MATERIALS

Tables 5.4-5.8 list the concentrations of 44 elements in sediment reference materials (LKSD-1, LKSD-2, LKSd-3, STSD-2, STSD-3, PACS-2 and MESS-3) as determined by SO-ICP-MS and fs-LA-ICP-MS. The concentrations reported are the average of four (SO-ICP-MS) and five (fs-LA-ICP-MS) replicate analyses. The precisions of the measurements are reported as % RSD (Relative Standard Deviation). For comparison, the compiled published values (obtained from GeoReM, Max-Planck-Institute database for reference materials of geological and environmental interest) [50] are also listed.

Table 5.4 lists concentration values of 44 elements in lake (LKSD-3) and marine (PACS-2 and MESS-3) sediments as determined by SO-ICP-MS. For more than 30 elements the precisions are better than 2 % for all matrices. The concentrations of LKSD-3 lie within 15 % of the published values for all elements except for Ni, Zn, Ge, Cd and Sb. The good precision of the measured concentrations of elements in LKSD-3 and the generally good agreement with the published values indicate that the choice of LKSD-3 as an external standard

for LA-ICP-MS was appropriate since any error in the quantification of concentrations in LKSD-3 would affect accuracy of quantification of other samples. High deviation (>30 %) from published values is observed for some elements in MESS-3. Figure 5.5 shows chondrite-normalized REE concentrations of published and measured values. In general, there is good agreement between all values although occasionally the LA-ICP-MS values are slightly and systematically different (higher or lower) suggesting that sample heterogeneity is an issue.

The concentrations of 43 elements in lake sediment (LKSD-1) are shown in Table 5.5. The RSDs for most elements determined by SO-ICP-MS and fs-LA-ICP-MS are better than 5% and 10%, respectively. For some elements, elemental concentrations measured by fs-LA-ICP-MS deviate by more than 30% from those measured by SO-ICP-MS. This deviation can be seen from the chondrite-normalized concentrations in Figure 5.5. The poor agreement between solution ICP-MS, fs-LA-ICP-MS and the published values is likely related to heterogeneity problems. Table 5.6 lists the measured element concentrations in LKSD-2 reference material. Concentration values obtained from fs-LA-ICP-MS lie within ± 6 % of those obtained from solution ICP-MS for most elements. The measured concentrations by both methods agree with or lie within the GeoReM published values. The agreement between the measured and published values can be clearly seen from chondrite-normalized concentrations shown in Figure 5.5. The RSDs for solution ICP-MS are better than 2% for most elements indicating a good homogeneity of LKSD-2. For fs-LA-ICP-MS, the precision is not

as good as that of solution ICP-MS but still better than 15% for most elements. The lower precision observed in LA-ICP-MS is related to counting statistics and the noisy signal of laser ablation which could be the results of many factors including sample heterogeneity, sample surface morphology and grain size.

Elemental concentrations in stream sediment reference materials (STST-2 and STSD-3) are shown in tables 5.7 and 5.8, respectively. For solution ICP-MS, precisions are better than 2% for most elements in both matrices with the exception of Cd which has a slightly lower precision (6.5 % in STSD-2 and 3.2% in STSD-3). In case of fs-LA-ICP-MS, the precisions are better than 12% and 15 % for most elements in STSD-2 and STSD-3, respectively. Concentration values obtained by fs-LA-ICP-MS agree (within ± 10% (STSD-2) and ± 15% (STSD-3)) with those obtained by solution ICP-MS. Compared to published values, the ICP-MS measured concentrations are lower but still lie within ± 20% of the published values for most elements in both matrices. This can be shown in figure 5.5 where chondrite-normalized concentrations of measured and published values are plotted.

Zinc showed lower concentration in all sediment reference materials compared to published values. Some other elements such as Cr, Ni and Cd show higher concentrations than published values for all sediment reference materials whether measured by solution ICP-MS or fs-LA-ICP-MS. A reason for this could be contamination or memory effects or inadequate information on the reference materials. All sediment reference materials appear to have good homogeneity for solution analysis since precisions better than 2 % were obtained

for most elements when measured by SO-ICP-MS. Only LKSD-1 shows slightly high RSD (5%) in case of SO-ICP-MS but better precision than all other sediment reference materials when measured by fs-LA-ICP-MS. S. Revillon et al. [10] reported a similar behavior (high RSD) on Japanese lake sediment (JLK-1) and attributed the reason to the high organic content of JLK-1 (the organic content of LKSD-1 is 12.3% (GeoReM))[50].

5.3.2 APPLICATION TO HIGH SPATIAL RESOLUTION ANALYSIS OF LAKE SEDIMENTS

A unique advantage of LA-ICP-MS is the ability of high spatial resolution chemical analysis. Such ability can be used to extract important information about environmental change from sediment cores if the cores were extracted and prepared carefully to preserve spatial integrity of the sediment. As an example of the applicability of the method described in this paper to high spatial resolution analysis, we prepared a sediment core (extracted from Lake Erie, Ontario, Canada) for LA-ICP-MS following a method modified from Jilbert et al. [48]. A plastic U-channel was carefully used to extract sediment from the plastic sleeve with minimal disturbance. The sediment containing U-channel was left to dry and then impregnated with low viscosity epoxy resin for a day and then cured at 60 ^{0}C for another day. Segments of the sediment were prepared for LA-ICP-MS by cutting the prepared portion into slices of suitable sizes to fit the ablation cell and cleaned immediately before ablation by wiping the surface with ethanol.

Figure 5.6-a shows a SEM image of two ablation tracks produced by fs-LA-ICP-MS on a sediment section prepared from the sediment core. Figure 5.6-b shows the agreement between signal intensities of ^{27}Al obtained from two ablation line scans of a sediment core section. Good reproducibility exists between the two ablations. Each data point is the average of 50 mass scans which is equivalent to the average over 1 mm on the spatial scale. Figure 5.7 shows the distribution of Cr and Ba along sediment core as measured by fs-LA-ICP-MS. The deeper sediment has much less Cr than the more recent one, which indicates the variation of Cr input with time (related to recent industrial activity in the vicinity of this site). Barium concentration is almost constant along the core reflect constant geological sources. By knowing the sediment accumulation rate, it would be possible to link the variation in elemental concentrations to particular events happening at specific times.

5.4 CONCLUSIONS

Sample preparation is a critical step in analysis of complex matrices such as sediments and soils by either SO-ICP-MS or LA-ICP-MS. Complete sample digestion of such matrices is difficult and requires special precautions to avoid contamination or loss of volatile elements during sample preparation. In this work we determined the chemical compositions of seven sediment reference materials (Lake sediments: LKSD-1, LKSD-2, LKSD-3, Stream sediments: STSD-2, STSD-3, and Marine sediments: PACS-2, MESS-3) using both SO-ICP-MS and fs-LA-ICP-MS. Elemental concentrations of sediment reference materials determined

by fs-LA-ICP-MS lie within 15 % of those determined by solution ICP-MS for most investigated elements. Precisions obtained by fs-LA-ICP-MS (better than 20 %) are not as good as those obtained by solution ICP-MS (better than 2 %) but can be considered acceptable for matrices that have complex and heterogeneous compositions such as sediments. LKSD-1 has slightly higher RSD values (but still better than 5 %) compared to other sediment reference material and this could be related to heterogeneity, high organic content or incomplete digestion of this reference material. The good agreement between fs-LA-ICP-MS and solution ICP-MS indicates that the method used for sample preparation for LA-ICP-MS (i.e. impregnation with Spurr low viscosity epoxy resin) can be successfully applied to natural sediment cores. This method of sample preparation can maintain sediment spatial integrity which is essential for extracting useful information about environmental changes over short periods of time.

High spatial resolution analysis is an important advantage of LA-ICP-MS. With this technique, it is possible to investigate the chemical composition of samples at resolution down to few tens of micrometers. For sediments, as an example, chemical behaviour across different layers of sediment can be studied allowing investigation of chemical changes related to issues such as redox reactions and changing sediment sources.

5.5 REFERENCES

[1] J.S. Becker and H. J Dietze, Inorganic trace analysis by mass spectrometry, Spectrochim.Acta Part B, 1998, **53**, 1475–1506.

[2] J.S. Becker and H. J Dietze, Inorganic mass spectrometric methods for trace, ultra-trace, isotope and surface analysis, Int.J.Mass Spectrom. 2000, **195/196**, 1–35.

[3] J.S. Becker, inorganic mass spectrometry principles and applications, 2007, John Wiley & Sons Ltd, The Atrium, Southern Gate, Chichester, England.

[4] D. Beauchemin, Inductively Coupled Plasma Mass Spectrometry, Anal. Chem., 2004, **76**, 3395-3416.

[5] O. T. Butler, J. M. Cook, C. F. Harrington, S. J. Hill, J. Rieuwerts and D. L. Miles, Atomic spectrometry update. Environmental analysis, J. Anal. At. Spectrom., 2006, **21**, 17–243.

[6] J.A.C Broekaert, Mass spectrometry with plasma sources at atmospheric pressure state-of-the-art and some developmental trends, Fresenius J.Anal.Chem. 2000, **368**, 15–22.

[7] K. E. Jarvis, A. L. Gray, and R. S. Houk , Handbook of inductively coupled plasma mass spectrometry, ,1992 Blackie Academic & Professional, Chapman & Hall.

[8] R. Thomas, Practical Guide to ICP-MS, 2004, Dekker M., Inc. New York.

[9] A. Montaser, Inductively coupled plasma mass spectrometry,1998, Wiley-VCH, INC., New York.

[10] S. Revillon and Hureau-Mazaudier, Improvements in Digestion Protocols for Trace Element and Isotope Determinations in Stream and Lake Sediment Reference Materials (JSd-1, JSd-2, JSd-3, JLk-1 and LKSD-1), Geostand. Geoanal. Res., 2009, **33**, 397-413.

[11] P. Krause, B. Erbsloh, R. Niedergesass, R. Pepelnik, and A. Prange, Comparative study of different digestion procedures using supplementary analytical methods for multielement-screening of more than 50 elements in sediments of the river Elbe, Fresenius J Anal Chem., 1995, **353** : 3-11.

[12] I. L. Marr, P. Kluge, L. Main, V. Margerin, and C. Lescop, Digests or Extracts?- Some Interesting but Conflicting Results for Three Widely Differing Polluted Sediment Samples, Mikrochim. Acta , 1995, **119**, 219-232.

[13] A. L. Gray, Solid Sample Introduction by Laser Ablation for Inductively Coupled Plasma Source Mass Spectrometry, Analyst,1985, **110**, 551-556.

[14] S.F. Durrant, Laser ablation inductively coupled plasma mass spectrometry: achievements, problems, prospects, J. Anal. At. Spectrom., 1999, **14**, 1385–1403.

[15] J. R. Bacon, J. C. Greenwood, L. V. Vaeck and J. G. Williams, Atomic spectrometry update. Atomic mass spectrometry, J. Anal. At.. Spectrom., 2004, **19**, 1020-1057.

[16] J. S Becker. (2002), Applications of inductively coupled plasma mass spectrometry and laser ablation inductively coupled plasma mass spectrometry in materials science, Spectrochimica Acta Part B, 2002, **57**, 1805–1820.

[17] D. Günther, B. Hattendorf, Solid sample analysis using laser ablation inductively coupled plasma mass spectrometry, Trends in Analytical Chemistry, 2005, **24**, 255-265.

[18] R. E. Russo, X. Mao, J. Gonzalez and S.S. Mao, Femtosecond laser ablation ICP-MS, J. Anal. At. Spectrom. 2002, **17**, 1072-1075.

[19] C. C.Garcia, H. Lindner, and K. Niemax, Laser ablation inductively coupled plasma mass spectrometry—current shortcomings, practical suggestions for improving performance, and experiments to guide future development, J. Anal. At. Spectrom., 2009, **24**, 14–26.

[20] Y. L. Lee, C. C. Chang, S. J. Jiang, Laser ablation inductively coupled plasma mass spectrometry for the determination of trace elements in soil, Spectrochimica Acta Part B, 2003, **58**, 523–530.

[21] S. F. Boulyga, M. Tibi, K. G. Heumann, Application of isotope-dilution laser ablation ICP–MS for direct determination of Pu concentrations in soils at pg g–1 levels, Anal Bioanal Chem., 2004, **378** , 342–347.

[22] S. F. Boulyga, , J. S Becker, Determination of uranium isotopic composition and 236U content of soil samples and hot particles using inductively coupled plasma mass spectrometry, Fresenius J Anal Chem., 2001, **370**, 612-617.

[23] S. A Baker, M.Bi , R. Q. Aucelio, B. W. Smith and J. D. Winefordner, Analysis of soil and sediment samples by laser ablation inductively coupled plasma mass spectrometry, J. Anal. At. Spectrom.,1999, **14**, 19–26.

[24] P. M.,C. Bruneau, N. Ostle, D. A Davidson, I. C. Grieve, A. E. Fallick, determination of rhizosphere ^{13}C pulse signals in soil thin sections by laser

ablation isotope ratio mass spectrometry, Rapid Commun Mass Spectrom., 2002, **16**, 2190-2194.

[25] S. Rauch, H. F. Hemond and D. J. Brabander, High spatial resolution analysis of lake sediment cores by laser ablation inductively coupled plasma-mass spectrometry (LA-ICP-MS), *Limnol. Oceanogr. : Methods, 2006, **4***, 268-274.

[26] S. Rauch, H. F. Hemond and B. Ehrenbrink, Recent Changes In Platinum Group Element Concentrations And Osmium Isotopic Composition In Sediments From An Urban Lake, Environ. Sci. Technol., 2004, **38**, 396-402.

[27] B. Fernandez, F. Claverie, C. Pecheyran and O. F. X. Donarda, Solid-spiking isotope dilution laser ablation ICP-MS for the direct and simultaneous determination of trace elements in soils and sediments, J. Anal. At. Spectrom., 2008, **23**, 367–377.

[28] G. Tao, Y. Fujikawa, M. Mitsui and R. Yamada, Determination of mercury in sediment samples by laser ablation inductively coupled plasma mass spectrometry, J. Anal. At. Spectrom., 2002,**17**, 560–562.

[29] X. Guo and F. E. Lichte, Analysis of Rocks, Soils and Sediments for the Chalcophile Elements by Laser Ablation-Inductively Coupled Plasma Mass Spectrometry, Analyst, 1995, **120**, 2707-2711.

[30] L. Arroyo, T. Trejos, P. R. Gardinali and J. R. Almirall, Optimization and validation of a Laser Ablation Inductively Coupled Plasma Mass Spectrometry method for the routine analysis of soils and sediments, Spectrochim. Acta Part B, 2009, **64**, 16–25.

[31] H. R. Kuhn and D. Günther, The agglomeration state of nanosecond laser-generated aerosol particles entering the ICP, Anal Bioanal Chem.,2005, 383, 434–441.

[32] R. Delmdahl and, G. Oldershausen, Quantitative solid sample analysis by ArF excimer laser ablation, Journal of Molecular Structure, 2005, **744/747**, 255–258.

[33] Z. Hu, S. Gao, L. Liu, H. Chen and S. Hu, Accurate Determination of Rare Earth Elements in USGS, NIST SRM, and MPI-DING Glasses by Excimer LA-ICP-MS at High Spatial Resolution, Spectroscopy Letters, 2008, **41**, 228–236.

[34] S. A. Crowe, B. J. Fryer, I. M. Samson and J. E. Gagnon, Precise isotope ratio determination of common Pb using quadrupole LA-ICP-MS with optimized laser sampling conditions and a robust mixed-gas plasma, J. Anal. At. Spectrom., 2003, **18**,1331-1338.

[35] B. J. Fryer, S.E. Jackson and H. P. Longerich, The application of laser ablation microprobe-inductively coupled plasma-mass spectrometry (LAM-ICP-MS) to the in situ (U)-Pb geochronology, Chem. Geol., 1993, **109**,1-8.

[36] T. Hirata and Y. Kon, Evaluation of the Analytical Capability of NIR Femtosecond Laser Ablation–Inductively Coupled Plasma Mass Spectrometry, Analytical Sciences , 2008, **24**, 345-353.

[37] I. Horn, F. Blanckenburg , Investigation on elemental and isotopic fractionation during 196 nm femtosecond laser ablation multiple collector inductively coupled plasma mass spectrometry, Spectrochim. Acta Part B, 2007, **62**, 410–422.

[38] C. C. Garcia, M. Wälle, H. Lindner, J. Koch, K. Niemax and D. Günther, Femtosecond laser ablation inductively coupled plasma mass spectrometry: Transport efficiencies of aerosols released under argon atmosphere and the importance of the focus position, Spectrochim. Acta Part B , 2008, **63**, 271–276.

[39] F. Poitrasson, M. Mao, S. S. Mao, R. Freydier R. E. Russo, Comparison of Ultraviolet Femtosecond and Nanosecond Laser Ablation Inductively Coupled Plasma Mass Spectrometry Analysis in Glass, Monazite, and Zircon, Anal. Chem., 2003, **75**, 6184-6190.

[40] Q. Bian, C. C. Garcia, J. Koch K. Niemax, Non-matrix matched calibration of major and minor concentrations of Zn and Cu in brass, aluminium and silicate glass using NIR femtosecond laser ablation inductively coupled plasma mass spectrometry, J. Anal. At. Spectrom., 2006, **21**,187-191.

[41] J. Koch, M. Wälle, J. Pisonero and D. Günther, Performance characteristics of ultra-violet femtosecond laser ablation inductively coupled plasma mass spectrometry at 256 and 200 nm, J. Anal. At. Spectrom., 2006, **21**, 932-940.

[42] R. E. Russo, X. Mao X, H. Liu, J. Gonzalez and S.S Mao, Laser ablation in analytical chemistry—a review, Talanta, 2002, **57**, 425–451.

[43] M. Shaheen, J. E. Gagnon, Z. Yang and B. J. Fryer, Evaluation of the analytical performance of femtosecond laser ablation inductively coupled plasma mass spectrometry at 785 nm with glass reference materials, J. Anal. At. Spectrom., 2008, **23**, 1610–1621.

[44] J. Gonzalez, C. Liu, X. Mao and R. E. Russo, UV-femtosecond laser ablation-ICP-MS for analysis of alloy samples, J. Anal. At. Spectrom., 2004,**19**, 1165-1168.

[45] Polysciences©,, Spurr Low-Viscosity Embedding Media *For Biological, Material and Mineralogical Specimen*,. Spurr low-viscosity embedding media, 1992, data sheet #127. Warrington, PA, 2 pp.

[46] S. E. Lamoureux, Embedding unfrozen lake sediments for thin section preparation, Journal of Paleolimnology , 1994, **10**, 141-146.

[47] X. Boes and N. Fagel, Impregnation method for detecting annual laminations in sediment cores: An overview, Sedimentary Geology, 2005, **179**, 185–194.

[48] T. Jilbert, D. De Lange and G. J. Reichart, Fluid displacive resin embedding of laminated sediments: preserving trace metals for high-resolution paleoclimate investigations, Limnol. Oceanogr.: Methods, 2008, **6**, 16–22.

[49] H. P Longerich., S. E. Jackson and D.Günther, Laser Ablation Inductively Coupled Plasma Mass Spectrometric Transient Signal Data Acquisition and Analyte Concentration Calculation, J. Anal. At. Spectrom., 1996, 11, 899-904.

[50] GeoReM , Max-Planck-Institute database for reference materials of geological and environmental interest, http://georem.mpch-mainz.gwdg.de/sample_query_pref.asp

Table 5.1: Spurr low-viscosity epoxy resin [Polysciences©, (1992)]

	Standard medium	Suggested Modifications of the Medium	
Ingredient	A Firm	B Hard	C Soft
ERL 4221	4.10 g	4.10 g	4.10 g
Diglycidyl ether of polypropylene glycol (D.E.R. 736) (d)	1.43 g	0.95 g	1.90 g
Nonenyl succinic anhydride (NSA)	5.90 g	5.90 g	5.90 g
Dimethylaminoethanol (DMAE) (c)	0.1 g	0.1g	0.1 g
Cure schedule (hr) at 70°C (a)	8	8	8
Pot life (days) (b)	3.4	3.4	3.4

(a) Cure for minimum hours indicated or longer, generally overnight. (b) Time between initial mixing and end point for convenient use, store at room temperature in a closed container. (c) As dimethylaminoethanol increases, color increases. (d) Reducing D.E.R. 736 lightly improves the color.

Table 5.2: ICP-MS instrumentation and operating conditions

Manufacture:	ThermoElectron®	
Model:	X7-II®	
Detector type:	ETP® dual mode (pulse and analogue counting)	
Dynamic range:	~1.3 x 10^9 ICPS	
Sensitivity (sol.):	~350× 10^6 ICPS/ppm	
Cone type:	High Performance Interface (HPI)	
	LA-ICP-MS):	ICP-MS
Plasma conditions		
Resolution:	Standard (125), High (170)	
RF power:	1400 W	1400 W
Plasma gas:	13 L min^{-1}	13 L min^{-1}
Auxiliary gas:	0.98 L min^{-1}	0.98 L min^{-1}
Nebulizer gas:	1.04 L min^{-1}	0.9 L min^{-1}
Sampling depth:	140 mm	150 mm

Table 5.3: LA system specifications and operating conditions

Manufacture:	Quantronix
Model:	Integra C®
Type:	Ti:sapphire based on the Chirped Pulse Amplification (CPA) technique
Wavelength:	Fundamental: 785 nm
Repetition rate:	Up to 1kHz, experiment: 20 Hz
Pulse energy:	Maximum: 2mJ/pulse, experiment: 0.51 mJ
Pulse width:	<130 fs
Spot size	110 µm
Objective lens:	10X

Table 5.4: element concentrations in sediment reference materials (LKSD-3, PACS-2 and MESS-3) as determined by solution ICP-MS. RSDs are calculated based on four replicate analyses.

	LKSD-3			PACS-2			MESS-3		
	Compiled [50]	ICP-MS	RSD (%)	Compiled [50]	ICP-MS	RSD (%)	Compiled [50]	ICP-MS	RSD (%)
Li	25	22.98	1.1	32.2	26.77	3.4	73.6	64.11	0.6
B	25	20.15	1.3	--	24.25	4.6	--	87.66	2.5
Sc	13	12.79	1	--	13.81	1	--	16.37	0.7
Ti	3330	2998	0.5	4430	4457	0.9	4400	4478	1.2
V	55-82	74.73	0.3	133	122.01	1.7	243	196.79	0.5
Cr	46-87	94.80	2.9	90.7	84.36	3.9	105	103.73	4.3
Mn	1220-1440	1230	0.8	440	391.97	0.9	324	293.43	1.1
Co	30	31.64	0.6	11.5	11.70	0.7	14.4	13.88	0.5
Ni	44-50	92.40	4	39.5	40.14	1.3	46.9	44.94	1.1
Cu	33-35	36.05	2.2	310	302.24	3.5	33.9	33.79	0.2
Zn	132-152	88.67	1.8	364	193.18	2	159	104.02	2.3
Ge	1.6	11.81	2.1	--	10.30	2.5	--	12.92	1.6
As	23-28.6	22.17	2.1	26.2	28.36	3.7	21.2	23.71	0.3
Rb	--	74.77	0.5	--	41.48	0.2	--	162.76	0.6
Sr	240	245.53	0.3	276.0	262.64	0.4	129	132.68	0.7
Y	30	25.24	0.7	--	14.40	1.3	--	23.26	0.3
Nb	7.4-10	10.62	1.7	--	9.44	1.2	--	16.54	1.6
Rh	--	0.008	4.7	--	0.014	3.7	--	0.004	5
Pd	--	1.91	1.9	--	1.19	2	--	1.66	0.8
Cd	0.4-0.9	1.65	2.6	2.1	4.58	5.2	0.2	0.74	4.6
Sn	2-2.8	2.45	4.2	19.8	22.17	1.4	2.5	2.998	3.2
Sb	1.3-1.4	2.04	5.1	11.3	20.41	2.3	1.2	1.91	1
Cs	2	2.13	1.1	--	2.02	0.4	--	8.37	0.5
Ba	680	594.08	0.5	802	828.63	1.5	--	909.16	3.2
La	52	44.07	1.2	--	15.03	2	32.3	36.04	0.8
Ce	90	81.68	0.8	22	30.30	2.2	66.6	68.77	0.5
Pr	11.3-12	10.89	0.9	--	3.87	2.4	--	8.36	0.8
Nd	44	40.59	0.9	--	15.37	1.8	27.9	30.64	0.8
Sm	8	7.27	0.9	--	3.25	1.7	5.1	5.68	1.2
Eu	1.5	1.47	0.6	--	1.07	1.2	1.1	1.39	0.9
Gd	6.4-7.5	8.72	0.5	--	4.23	1.3	4.2	7.13	0.4
Tb	1	0.92	0.5	--	0.51	1.1	0.6	0.80	1.1
Dy	4.9	4.58	0.9	--	2.75	1	3.2	4.13	0.7
Ho	1.02-1.1	0.90	0.7	--	0.55	1.4	0.6	0.82	1.3
Er	3-3.03	2.75	0.4	--	1.61	0.8	1.9	2.50	0.8
Tm	0.41-0.57	0.37	0.6	--	0.22	1.4	0.3	0.35	0.7
Yb	2.7	2.49	0.8	--	1.47	1.5	1.9	2.35	0.7
Lu	0.4	0.38	1.4	--	0.22	1.4	0.3	0.35	1.6
Re	--	0.005	3.4	--	0.007	3.4	--	0.006	3.7
Pt	--	0.052	5.5	--	0.027	1.4	--	0.039	2.5
Pb	21-32	27.93	3.7	183	155.83	1.4	21.1	20.01	1.3
Bi	2.8	2.75	0.8	--	0.31	7.2	0.3	0.29	0.3
Th	11.4	10.10	1.7	--	3.97	4.1	--	11.18	0.8
U	4.6	3.92	1.7	2	2.16	0.5	4	3.26	1.2

Table 5.5: element concentrations in sediment reference material LKSD-1 as determined by solution ICP-MS and fs-LA-ICP-MS, n refers to the number of replicate analyses.

	Compiled [50]	ICP-MS (n=4)		fs-LA-ICP-MS (n=5)	
	ppm	ppm	RSD (%)	ppm	RSD %
Li	7	4.57	3.4	6.77	12.6
B	49	31.15	3.4	30.08	40
Sc	9	7.48	1.7	10.85	6.5
Ti	620-3010	2911	1.4	2570	3.8
V	27-50	45.14	1.3	53.42	9.4
Cr	11--31	44.97	5.7	46.51	10.8
Mn	410-700	600.61	4	862.96	4
Co	8.0-11	11.69	0.7	12.36	9.1
Ni	11--16	60.1	8.5	51.61	18.7
Cu	42-44	43.41	1.8	52.15	2.8
Zn	311-337	160.37	2.1	217.64	5.3
Ge	--	5.24	1.9	9.71	5.2
As	30-40	19.04	3.8	8.61	7.6
Rb	24	22.15	1.6	26.25	9
Sr	250	249.71	1.3	306.9	7.3
Y	19	17.32	2.2	27.28	7.6
Nb	7	5.24	4.1	3.83	1.7
Pd	--	1.43	4.9	1.91	7.7
Cd	1.2	2.76	6	4.54	24.5
Sn	16	4.19	4.7	5.74	28.9
Sb	1.2	1.93	8.2	2.09	13.2
Cs	1.5	0.66	1.2	1.02	9.2
Ba	85-430	351.12	1	435	9.3
La	16	13.84	5.2	15.85	9.8
Ce	27	24.56	5.1	24.58	19.9
Pr	--	3.72	5.4	3.83	23.7
Nd	16	15.54	4.8	20.97	6.1
Sm	4	3.42	4	4.82	5.3
Eu	0.9	0.94	2.5	1.22	10.7
Gd	3.6	4.32	2.8	7.28	2.6
Tb	0.6	0.54	1.8	0.86	3.7
Dy	3.4	3.03	0.9	4.38	0.8
Ho	1	0.63	1.5	0.89	7.8
Er	--	1.89	1.5	3.03	6.2
Tm	0.35	0.263	1.4	0.44	6.8
Yb	2	1.8	1	2.29	6
Lu	0.4	0.27	2.6	0.41	8.8
Re	--	0.023	4.2	0.03	3
Pt	--	0.029	3.9	0.015	19.2
Pb	81-84	76.21	2.8	89.83	14.7
Bi	0.95	0.85	2.3	0.86	8
Th	2.2	2.16	5.9	2.03	10.8
U	9.7	8.47	3.5	14.34	5.9

Table 5.6: element concentrations in sediment reference material LKSD-2 as determined by solution ICP-MS and fs-LA-ICP-MS, n refers to the number of replicate analyses.

	Compiled [50]	ICP-MS (n=4)		fs-LA-ICP-MS (n=5)	
	ppm	ppm	RSD (%)	ppm	RSD %
Li	20	18.02	1.2	17.66	8.2
Sc	13	12.76	2.3	12.91	11.2
Ti	3460	3274	1.7	3339	8.2
V	48-77	72.37	2.6	75.45	13
Cr	29-57	68.78	3.4	66.6	4.8
Mn	1840-2020	1690	0.5	1698	16.4
Co	15-17	18.41	0.9	18.37	7.1
Ni	23-26	68.54	2	60.41	9.5
Cu	34-37	37.66	2.7	38.89	19.1
Zn	188-209	120.94	2.8	111.37	7.1
Ge	--	13.05	1.6	13.73	6.1
As	11	12.58	1.8	11.55	18.2
Rb	85	79.78	0.6	76.61	14.5
Sr	220	232.34	0.6	232.27	12.7
Y	46	37.75	1.1	42.86	12.7
Nb	11	11.59	3.5	11.03	17
Pd	--	2.74	0.8	2.74	14.3
Cd	0.6-1	2.08	2.3	2.13	5.5
Sn	3.1	3.12	1.5	3.29	5.4
Sb	1.02-1.2	1.77	4.5	1.71	26.2
Cs	3	2.61	0.8	2.43	9.5
Ba	206-780	677.45	0.4	588.9	10.4
La	68	59.33	0.9	58.67	12.2
Ce	120	127.99	0.8	115.06	16.6
Pr	18	14.78	0.6	35.37	6.4
Nd	58	55.46	0.7	58.04	14.2
Sm	11	10.06	1	10.49	17
Eu	1.9	1.94	0.5	1.98	12.2
Gd	9-9.4	12.12	1	11.85	15.7
Tb	1.4	1.32	0.4	1.32	17.6
Dy	7.3	6.68	0.7	6.25	19.1
Ho	1.5-2.1	1.34	0.6	1.22	17.7
Er	4.4	4.04	0.5	3.89	18.1
Tm	0.6-0.79	0.54	0.5	0.63	10.6
Yb	4.4	3.66	0.6	3.62	18.8
Lu	0.64	0.55	0.4	0.63	12.7
Re	--	0.006	1.9	< DL	--
Pt	--	0.057	2.2	< DL	--
Pb	34-36	41.72	0.8	42.35	11.2
Bi	1.07	1.07	0.7	0.99	15.8
Th	13.4	11.62	0.7	11.4	9.7
U	7.4	6.49	1.1	7.29	10.4

Table 5.7: element concentrations in sediment reference material STSD-2 as determined by solution ICP-MS and fs-LA-ICP-MS, n refers to the number of replicate analyses.

	Compiled [50]	ICP-MS (n=4)		fs-LA-ICP-MS (n=5)	
	ppm	ppm	RSD (%)	ppm	RSD (%)
Li	65	60.49	1	59.65	8.3
B	42	26.12	1.8	25.12	5.3
Sc	16	14.72	0.6	13.54	5.4
Ti	1720-4870	4491	0.8	3937	5.3
V	58-104	92.91	0.3	85.7	2.3
Cr	43-116	119.12	3.1	124.84	4.4
Mn	670-1060	905.63	0.6	856.29	7
Co	16-19	20.31	0.5	19.02	8.8
Ni	47-60	91.88	1.5	107.88	9.5
Cu	43-49	47.77	2.5	59.68	16.6
Zn	216-246	124.74	3	172.1	13.5
Ge	--	13.52	0.6	14.72	3.7
As	32-42.1	40.21	1.6	40.84	6.7
Rb	104	97.33	0.4	106.18	10.7
Sr	400	463.1	0.8	467.1	13
Y	37	31.12	1.3	31.16	8.8
Nb	20	24.39	2.9	23.23	8
Rh	--	0.014	3.5	0.017	19.9
Pd	--	2.44	1.2	2.49	7.1
Cd	0.7-0.9	2.07	6.5	2.05	18.3
Sn	5	4.41	1.3	4.65	13.8
Sb	2.6-4.8	7.65	3.9	8.22	18.8
Cs	12	10.48	0.8	12.38	4.7
Ba	100-540	459.6	0.4	439.4	25
La	59	48.49	2	47.97	15.7
Ce	93	81.51	1.7	65.86	9.6
Nd	43	40.69	1.7	37.71	3.3
Sm	8	7.75	1.2	7.72	12.7
Eu	2	1.92	0.6	2.18	7.3
Gd	7.4	9.8	0.3	9.95	11.1
Tb	1.3	1.12	1.2	1.16	9.8
Dy	6.5	5.73	1.3	5.55	8.6
Ho	2.1	1.11	0.9	0.96	10.4
Er	--	3.25	0.6	3.41	6.8
Tm	0.75	0.43	1.8	0.43	12.5
Yb	3.7	2.91	1.4	3.07	11.1
Lu	0.7	0.43	1.5	0.42	6.3
Pb	63-67	66.82	0.7	87.37	15.2
Bi	3.86	3.52	0.8	3.33	10.6
Th	16.1	14.99	3.9	15.36	13
U	15.8	15	0.4	19.8	12.8

Table 5.8: element concentrations in sediment reference material STSD-3 as determined by solution ICP-MS and fs-LA-ICP-MS, n refers to the number of replicate analyses.

	Compiled [50]	ICP-MS (n=4)		fs-LA-ICP-MS (n=5)	
	ppm	ppm	RSD (%)	ppm	RSD (%)
Li	23-28	26.51	1.5	26.10	4.5
B	82	51.17	2.8	49.91	11.1
Sc	13	11.71	1.6	12.87	10.4
Ti	610-4400	3874	1.3	4269	77.6
V	61-134	120.32	1.9	122.32	9
Cr	29-80	68.05	2.6	75.88	10.6
Mn	2520-2730	2345	1.5	1425	19.3
Co	14-16	16.09	1.7	15.23	11.6
Ni	25-30	33.01	1.1	43.03	3
Cu	36-40	39.18	1.8	37.58	15.3
Zn	184-204	142.44	1.1	120.14	7.1
Ge	--	11.09	1.2	12.13	9.4
As	22-28.3	26.75	2.8	29.54	12.3
Rb	68	62.63	2.1	68.04	5.4
Sr	230	240.65	1.5	259.31	10.1
Y	36	28.79	1.6	26.82	9.3
Nb	12	13.19	2.8	9.15	4.6
Pd	--	2.21	0.7	2.33	1.9
Cd	0.8-1.1	2.85	3.2	2.18	7.8
Sn	4	3.76	2.5	2.99	13
Sb	2.4-4	6.45	1.2	4.65	22.9
Cs	2.4-4	4.69	1.5	4.41	5.9
Ba	1490	2051	1.4	1121	17.4
La	39	31.69	2.3	27.71	11.7
Ce	63	55.42	2.6	42.57	4.6
Nd	33	31.23	2.4	29.79	10.2
Sm	7	6.2	1.5	7.06	17.5
Eu	1.3	1.72	1.3	1.51	15.6
Gd	6.5	8.01	1.5	6.79	15.5
Tb	1.1	0.94	1.5	1.05	8.3
Dy	5.4	4.93	0.7	5.51	1
Ho	1.3	0.99	1.2	1.01	14.3
Er	--	2.97	1.6	3.03	14.1
Tm	0.67	0.405	1.5	0.443	11
Yb	3.4	2.77	2.1	2.54	11.2
Lu	0.8	0.42	2.1	0.46	10.3
Pb	39-42	41.04	2	39.43	10.4
Th	8.5	7.22	3	8.93	12.5
U	10.5	8.43	2	9.22	13.2

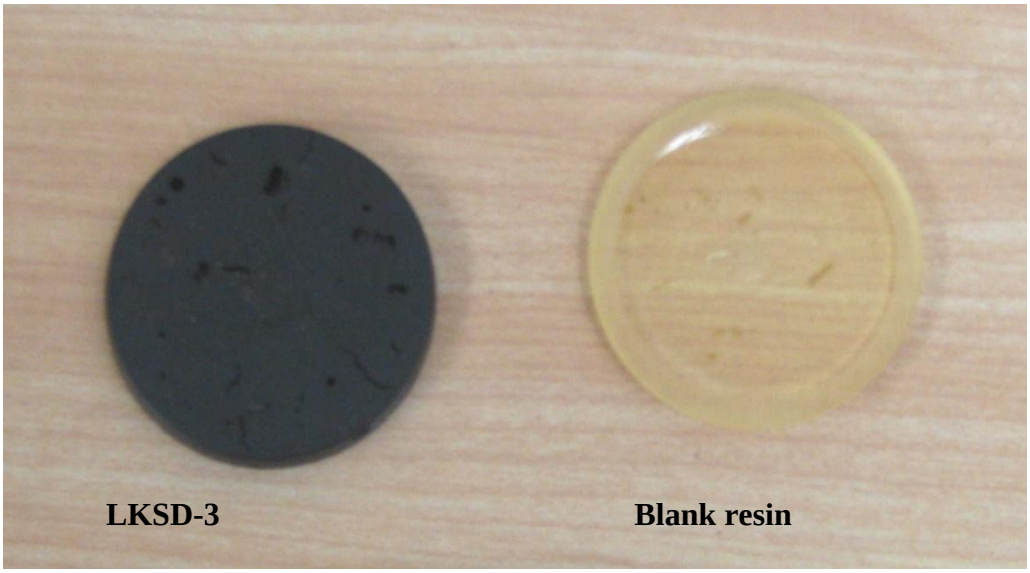

Figure 5.1: LKSD-3 and blank disks prepared by using Spurr low viscosity epoxy resin

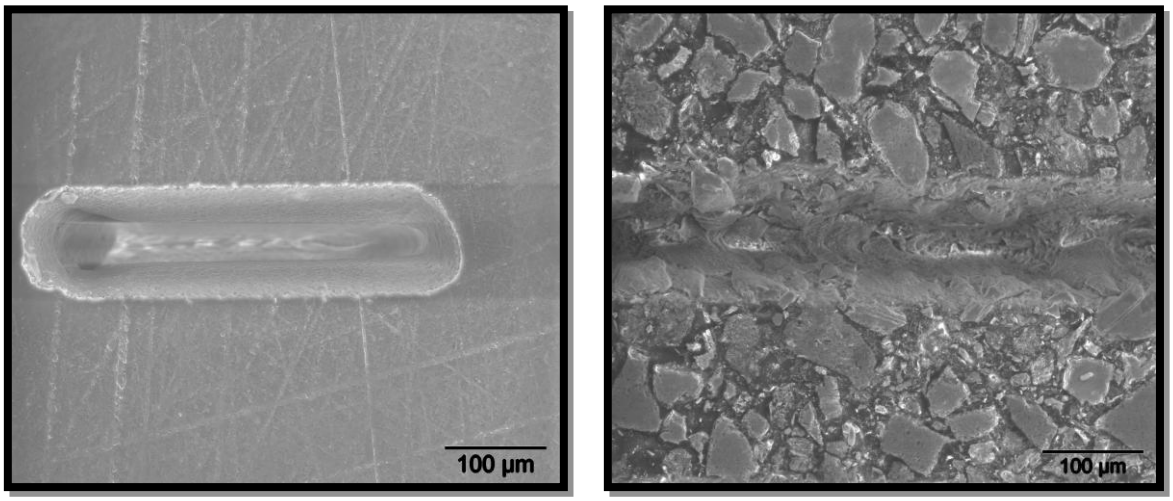

a b

Figure 5.2: scanning electron micrographs (SEM) of: a) blank resin and b) LKSD-3, prepared by using Spurr low viscosity epoxy resin. Sediment grains are seen to have grain sizes up to~ 100µm, therefore utilization of a large laser spot size and scanning the laser beam over the sample surface are important to reduce the effect of sample heterogeneity on ablation behavior.

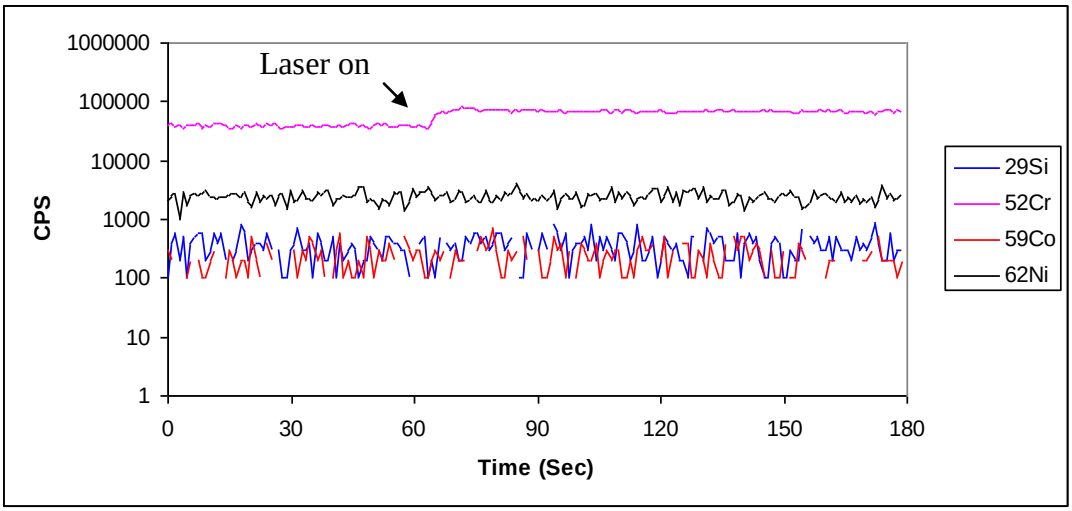

Figure 5.3: signal intensity obtained by fs-LA-ICP-MS of blank resin. The laser was fired after 60 seconds of gas blank collection. For most elements, there are insignificant changes in intensities upon ablation of the blank resin which indicates that the chemical contribution of the resin to sediment metal concentrations is extremely small and can be neglected for these elements.

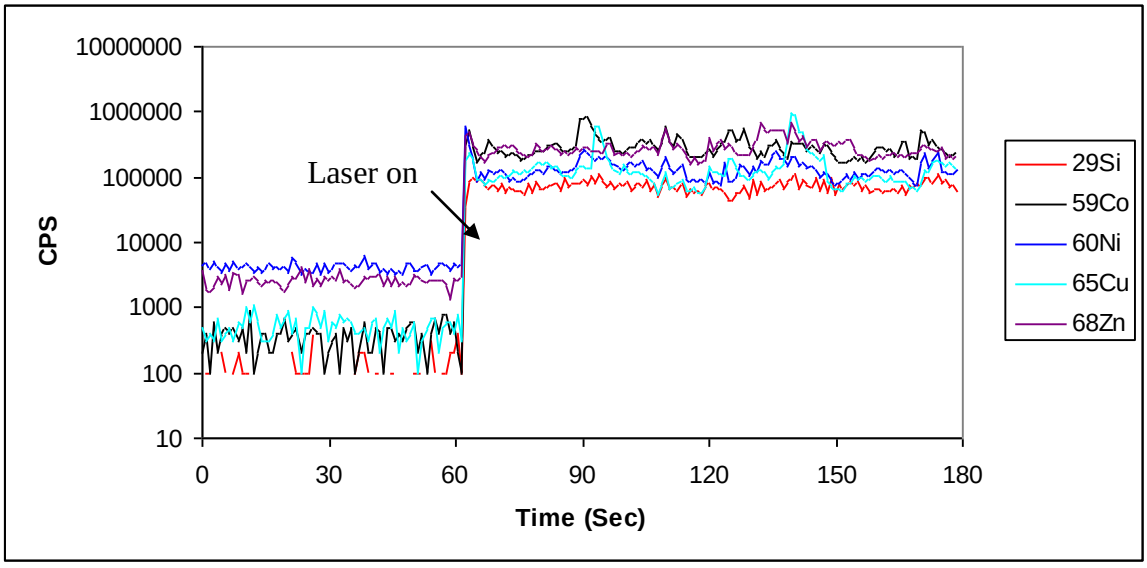

Figure 5.4: signal intensity obtained by fs-LA-ICP-MS of sediment reference material LKSD-3. LKSD-3 was used as a calibration standard for quantification of other sediment reference materials which have been treated as unknowns.

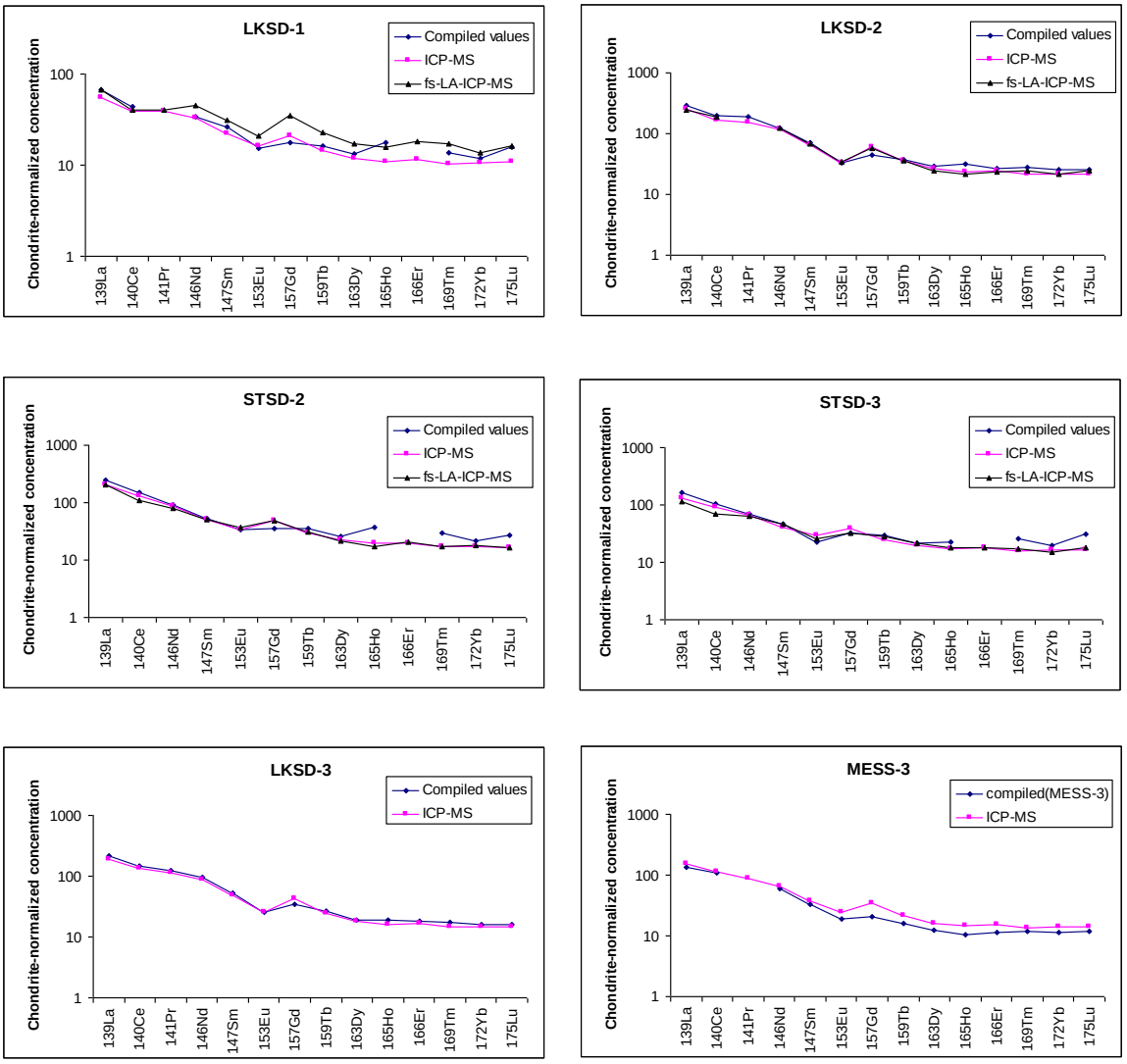

Figure 5.5: Chondrite-normalized concentration of sediment reference materials (LKSD-1, LKSD-2, LKSD-3, STSD-2, STSD-3 and MESS-3) for solution ICP-MS and fs-LA-ICP-MS in comparison to compiled values obtained from GeoReM.

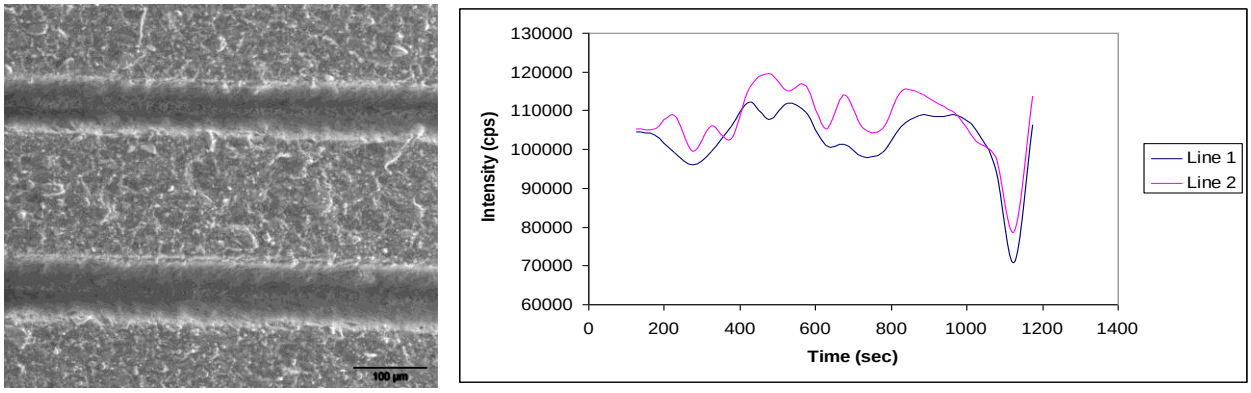

a b

Figure 5.6, a: SEM image of two ablation tracks in a sediment core, b: agreement between signal intensities of ^{27}Al obtained from two ablation line scans of a sediment core section. Good reproducibility exists between the two ablations. Each data point is the average of 50 mass scan.

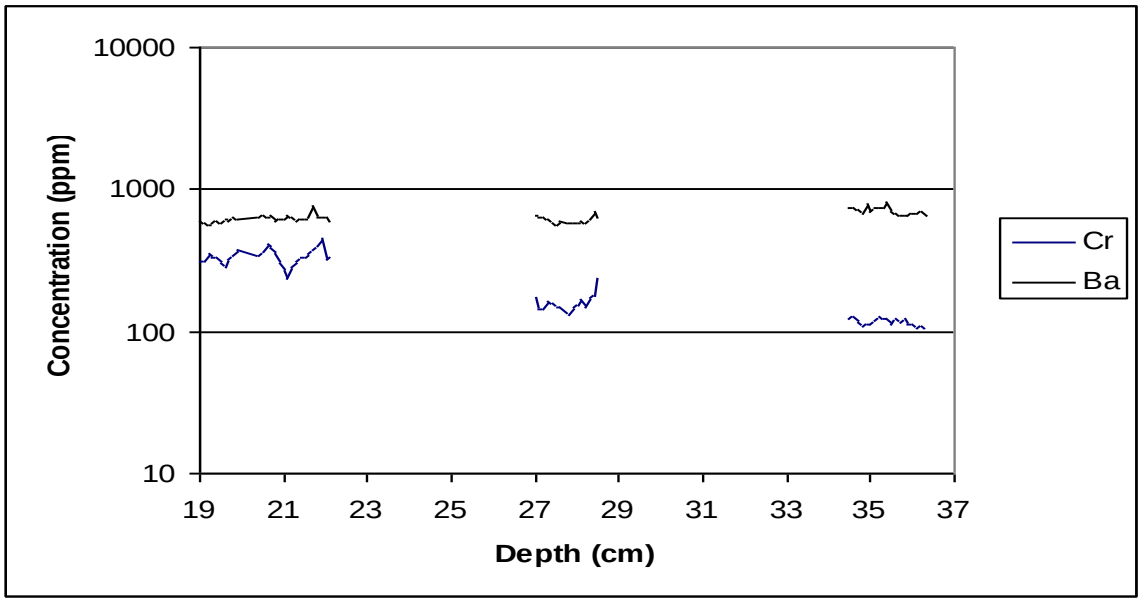

Figure 5.7: distribution of Cr and Ba along sediment core extracted from Lake Erie, Ontario, Canada, as measured by fs-LA-ICP-MS. The deepest sediment has less Cr than the most recent one which indicates the variation of industrial Cr input with time. Ba concentration is almost constant along the core reflecting constant geological sources.

CHAPTER 6

SUMMARY OF THE THESIS

6.1 INTRODUCTION

LA-ICP-MS is a powerful analytical technique that has been applied to multi-element analysis of trace, minor and major elements of solids in many areas of science including geological, environmental, medical, biological and forensic [11-12]. Many parameters affect the analytical capabilities of this technique and make its optimization difficult [13-26]. This includes parameters related to the laser beam (wavelength, pulse with, energy, repetition rate and beam profile), ablation cell and transport tubing (design and geometry of the ablation cell, tubing properties and ablation cell gas) and mass spectrometer (interface pressure, design and geometry of the cones, type of analyzer and type of detector).

Despite the advantages of LA-ICP-MS, there are a number of drawbacks that limit its application to routine analysis. Elemental and isotopic fractionation [27] is an issue that occurs during LA-ICP-MS and limits accurate analysis of different types of samples. For accurate and precise analysis, the ablated materials must be representative of the sample (i.e. has the same chemical composition as the sample) and must be completely transported to the ICP and completely ionized in the ICP. These criteria for accurate analysis are generally not completely attained during analysis since laser-induced fractionation can occur as a result of thermal effects in the irradiated volume which can cause segregation of elements depending on their thermal properities. Fractionation can also occur due to particle loss in the ablation cell or during transport if the chemical composition of particles is size dependent. Incomplete vaporization and

atomization of particles in the ICP is another source of fractionation. The use of matrix-matched standards for calibration is normally required to eliminate laser-induced fractionation but the lack of appropriate standards of a wide variety of samples of interest currently restricts the accurate and precise applications of this technique. Different laser sampling strategies [28] (such as active focusing, soft ablation, and scanning ablation) have been used to reduce laser-induced fractionation.

Matrix effects are another drawback of LA-ICP-MS [29]. The amount of ablated material depends on the properties of the sample being ablated. An internal standard is usually used to correct for variation of the ablation yield between sample and the standard reference material. An internal standard is an element that has a known concentration and homogeneous distribution in both the sample and the standard. The internal standard should have similar properties to the elements being quantified for accurate and precise characterization of the unknown.

Most of the work done to improve the analytical capabilities of LA-ICP-MS has concentrated on developing lasers that can provide controlled ablation where the laser energy is efficiently absorbed by the sample and the ablated material is representative of the sample [24-27]. Laser wavelength is an important parameter in nanosecond laser systems since it affects the degree of laser energy absorption by matrices of different transparency. Laser systems operating at UV wavelengths (frequency quadrupled: 266 nm, frequency quintupled: 213 nm Nd:YAG and 193 nm ArF excimer laser) have better ablation characteristics than

those operating at IR wavelength (fundamental 1064 nm Nd:YAG). The utilization of femtosecond laser pulses probably represents the most promising instrumental advancement toward the idea of controlled ablation. Application of femtosecond lasers has greatly improved the analytical capabilities of LA-ICP-MS. The drawbacks observed in nanosecond LA-ICP-MS (fractionation and matrix effects) have been very much reduced when femtosecond lasers are used for ablation.

6.2 SUMMARY OF THE THESIS

In my thesis I investigated aspects of the interactions of lasers with solids. Understanding the mechanisms of these interactions is an important step to reach the full potential of LA-ICP-MS as an analytical technique. In chapter 2 I summarized a method commonly used to generate femtosecond laser pulses. It is important for people working with such laser systems to understand how they work. This will be of great help to solve problems that can arise during experimental work. For example our early investigations on interaction of femtosecond lasers with solids (by studying the surface morphology of ablated materials using scanning electron microscope) showed a distortion of the laser beam (i.e the laser beam was not a Gaussian but had some hot spots across it, see chapter 2). Such distorted laser energy profiles can not achieve the precise and accurate analyses by LA-ICP-MS required for some applications. Our understanding of the femtosecond laser system has helped us to determine the likely reasons responsible for this distortion and to reduce their effects by proper

alignment of optics (both inside and outside the laser system) and proper selection of the objective lens used to focus the laser beam on the sample.

Chapter 2 also summarized in brief the mechanisms of laser-solid interactions and the differences between femtosecond and nanosecond laser ablation. Minimum thermal effects and minimum laser-plasma interactions are characteristics of femtosecond laser ablation. As a result lower laser ablation thereshold, higher energy absorption, narrower particle size distribution, better transport efficiency and better atomization and ionization in the ICP-MS are advantages of femtosecond compared to nanosecond LA-ICP-MS.

Evaluation of the analytical capabilities of fs-LA-ICP-MS was done by the analysis of 6 standard reference materials (NIST and basalt glasses) under optimum operating conditions, chapter 3. We found from this study that fractionation (a severe problem for some elements in nanosecond LA-ICP-MS) and matrix effects have been very much reduced when ablation was carried out using femtosecond laser pulses. Materials of different transparency (NIST 610 vs NIST 614) were found to have similar ablation behavior under femtosecond laser ablation. Matrix effects were also reduced. In this chapter we analyzed 5 standard reference (NIST 610, NIST 612, BHVO-2G, BIR-1G and BCR-2G) materials using fs-LA-ICP-MS and NIST 612 as an external standard. There was a good agreement between the measured concentrations and the published values for most investigated elements. The precisions were better than 10% for most investigated elements in all matrices. The data published in this chapter can be considered as a valuable data base for analytical laboratories since it lists the

concentrations of 63 elements found in 5 standard reference materials commonly used for calibration of LA-ICP-MS.

Mixed gas plasmas were investigated in chapter 4 by adding different gases such as hydrogen and nitrogen to the Ar gas in fs-LA-ICP-MS. The addition of small amounts of these molecular gases changes the plasma properties by affecting the electron number density and plasma temperature since these gases have higher thermal conductivities than Ar. Enhancement of sensitivities was observed for many elements across the mass spectrum. The effect of nitrogen on sensitivity and mass bias in Pb isotope determination by fs-LA-MC-ICP-MS was also investigated. Nitrogen was used instead of hydrogen since hydrides formed as a result of hydrogen addition can cause interferences on isotopes of interest (i.e. $^{203}Tl^{1}H$ on ^{204}Pb, $^{204}Pb^{1}H$ on ^{205}Tl, $^{205}Tl^{1}H$ on ^{206}Pb, $^{206}Pb^{1}H$ on ^{207}Pb and $^{207}Pb^{1}H$ on ^{208}Pb). We found that the mass bias of Tl is not identical to that of Pb and this difference must be taken into consideration to get accurate and precise isotope ratio determination. A reduction of mass bias by a factor of ~13 % was observed upon addition of small amount of nitrogen to the Ar gas before the ablation cell. Also mass bias stability was achieved when the nitrogen flow rate exceeded 5 ml/min. More precise and accurate Pb isotope ratios in NIST 610 were obtained when Tl was used to correct for mass bias compared to the standard sample standard bracketing correction method.

Chemical analysis of sediments and soils are important applications of LA-ICP-MS. Analyses of these matrices using solution ICP-MS require time consuming digestion procedures using hazardous acids like HF with increased

risk of contamination or loss of volatile elements. In chapter 5 we reported elemental concentrations of 7 sediment reference materials (lake sediments: LKSD-1, LKSD-2, LKSD-3; stream sediments: STSD-2 and STSD-3; marine sediments:PACS-2 and MESS-3) determined by both solution ICP-MS and fs-LA-ICP-MS. Sediment reference materials were prepared for LA-ICP-MS by impregnation with Spurr low viscosity epoxy resin in a form of solid disks suitable for laser ablation. Solution ICP-MS gave precisions better than 2 % for most investigated elements in all sediment reference materials except LKSD-1 which showed slightly higher RSD (but better than 5%). The precision obtained in fs-LA-ICP-MS was better than 15 % for most investigated elements in all matrices. The good agreement between concentrations determined by fs-LA-ICP-MS and solution ICP-MS indicates the success of the method used to prepare sediment for LA-ICP-MS and the possibility of extending this method to the preparation of sediment cores for high spatial resolution analysis.

6.3 FUTURE WORK

A problem associated with LA-ICP-MS is the lack of suitable standard reference materials (SRMs) for most samples that can by analyzed by this tecnique. In sediment analysis, as an example, homogeneous and certified reference materials do not exist, appropriate for analyses at the micro meter scale. Therefore working on development of SRMs is important to improve LA-ICP-MS. Different methods to prepare sediment cores in ways that keep their

integtity are needed to get better quality and faster sediment preparation for LA-ICP-MS.

Accurate and precise isotopic analyses using surrogates (e.g. Tl to correct for mass bias of Pb) need more investigation. It is important to study the effect of opereatiing conditions of MC-ICP-MS and laser sampling conditions on mass bias in a systematic way to determine to improve isotope ratio measurements.

An issue that needs to be addressed in femtosecond LA-ICP-MS is the effect of wavelength on the ablation characteristics of a wide variety of matrices with different absorption behavior. So far, it seems that wavelength in fs-LA-ICP-MS has minor effects (in contrast to nanosecond LA-ICP-MS where wavelength is a dominant parameter affecting ablation behavior) on ablation behavior in terms of particle size distribution, matrix effects and ablation yield. Robust studies of wavelength effects are not yet possible due to insufficient fluence obtained after frequency conversion from IR to UV due to the limited output energy of current femtosecond laser systems and poor energy conversion efficiency. The continuous progress in femtosecond laser technology will probably lead to a new generation of high power femtosecond laser systems that have high energy in the UV range. At that point more studies using UV femtosecond laser pulses can reveal the current unknown wavelength dependency of fs-LA-ICP-MS. The main benefit of using UV femtosecond laser pulses for ablation could be the improvement of spatial resolution (small crater size), as was discussed in Chapter 2.

6.4 REFERENCES

[1] D. Gunther, R. Frischknecht , C. A. Heinrich and H-J Kahlert, Capabilities of an Argon Fluoride 193 nm Excimer Laser for Laser Ablation Inductively Coupled Plasma Mass Spectometry Microanalysis of Geological Materials, J. Anal. At. Spectrom., 1997, **12**, 939-944.

[2] C. Geerstein., A. Briand, F. Chartier, J.-L. Lacour, P. Mauchient and S. Sjöström, Comparison between infrared and ultraviolet laser ablation at atmospheric pressure—implications for solid sampling inductively coupled plasma spectrometry**,** J. Anal. At. Spectrom., 1994, **9**, 17-22.

[3] E. V. Putten, F. Dehairs,E. Keppens and W. Baeyens, High resolution distribution of trace elements in the calcite shell layer of modern *Mytilus edulis*: Environmental and biological controls, Geochim. Cosmochim. Acta, 2000, **64,** 997–1011.

[4] W. R. Berti and L. W. Jacobs, Distribution of Trace Elements in Soil from Repeated Sewage Sludge Applications, J. Environ. Qual. 1998, **27,**1280-1286.

[5] S. F. Durrant, Multi-elemental Analysis of Environmental Matrices by Laser Ablation Inductively Coupled Plasma Mass Spectrometry, Analyst, 1992, **117,** 1585-1592.

[6] E. Hoffmann, H. Stephanowitz, E. Ullrich, J. Skole, C. Ludke and B. Hoffmann, Investigation of mercury migration in human teeth using spatially resolved analysis by laser ablation-ICP-MS , J. Anal. At. Spectrom., 2000, **15,** 663-667.

[7] F. Lochner, J. Appleton, F. Keenan and M. Cooke, : Multi-element profiling of human deciduous teeth by laser ablation-inductively coupled plasma-mass spectrometry, Anal. Chem. Acta, 1999, **401,** 299-309.

[8] J. Feldmann, A. Kindness and P. Ek, Laser ablation of soft tissue using a cryogenically cooled ablation cell, J. Anal. At. Spectrom., 2002, **17**, 813-818.

[9] S. Wang, R. Brown and D. J. Gray, Application of laser ablation_ICP-MS to the spatially resolved microanalysis of biological tissue, Appl. Spectrosc., 1994, **48,** 1321-1325.

[10] R. J. Watling, Novel applications of laser ablation inductively coupled plasma mass spectrometry in forensic sciene and forsenic archeology, , Spectroscopy, 1999, **14**, 16-34.

[11] L. Fuhe, M.K. Balazs and R. Pong, Total dose measurement for ion implantation using laser ablation ICP-MS , J. Anal. At. Spectrom., 2000, **15**, 1139-1141.

[12] V. Kanicky, V. Otruba and J. M. Mermet, Depth profiling of tin-coated glass by laser ablation inductively coupled plasma emission spectrometry with acoustic signal measurement, Fres. J. Anal. Chem., 2000, **366,** 228-233.

[13] D. Günther and B. Hattendorf, Solid sample analysis using laser ablation inductively coupled plasma mass spectrometry, Trends in Anal. Chem., 2005, **24,** 255-265.

[14] R. Russo, Laser ablation, Appl. Spectrosc., 1995, **49**, 14A-A28.

[15] A. Bogaerts , Z. Chen , R. Gijbels and A. Vertes, Laser ablation for analytical sampling: what can we learn from modeling?, Spectrochim. Acta, Part B, 2003, **58,** 1867-1893.

[16] S. Amoruso, Modeling of UV pulsed-laser ablation of metallic targets**.** Appl. Phys. A, 1999, **69**, 323-332.

[17] N. Bityurin and A. Malyshev, UV-laser ablation of absorbing dielectrics by ultra-short laser pulses, , Appl. Surf. Sci ., 1998, **127–129,** 199-205.

[18] A. Bogaerts, Z. Chen, Nanosecond laser ablation of Cu: modeling of the expansion in He background gas, and comparison with expansion in vacuum, J. Anal. At. Spectrom., 2004, **19**, 1169-1176.

[19] N.M. Bulgakova and A.V. Bulgakov, Pulsed laser ablation of solids: transition from normal vaporization to phase explosion, , Appl. Phys. A, 2001, **73,** 199-208.

[20] B.N. Chickov, C. Momma, S. Nolte, F. yon Alvensleben and A. Tiinnermann, Femtosecond, picosecond and nanosecond laser ablation of solids**,** Appl. Phys. A, 1996, **63**, 109-115.

[21] R. E. Russo, X. L. Mao, O. V. Borisov and H. Liu, Infuence of wavelength on fractionation in laser ablation ICP-MS, J. Anal. At. Spectrom., 2000, **15**, 1115-1120.

[22] J. S. Becker and D. Tenzler, Studies of LA-ICP-MS on quartz glasses at different wavelengths of a Nd:YAG laser, , Fres. J Anal. Chem., 2001, **370,** 637-640.

[23] T.V. Kononenko S.V. Garnov , S.M. Klimentov, V.I. Konov, E.N. Loubnin, F. Dausinger, A. Raiber and C. Taut, Laser ablation of metals and ceramics in picosecond–nanosecond pulsewidth in the presence of different ambient atmospheres, , Appl. Surf. Sci., 1997, **109-110**, 48-51.

[24] J. Koch, H. Lindner, A. von Bohlen, R. Hergenroder and K. Niemax, Elemental fractionation of dielectric aerosols produced by near-infrared femtosecond laser ablation of silicate glasses, J. Anal. At. Spectrom., 2005, **20**, 901-906.

[25] F. Poitrasson,, X.i Mao, S. S. Mao,. Freydier and R. Russo, Comparison of Ultraviolet Femtosecond and Nanosecond Laser Ablation Inductively Coupled Plasma Mass Spectrometry Analysis in Glass, Monazite, and Zircon, Anal. Chem., 2003, **75,** 6184-6190.

[26] J. Gonzalez, C. Liu, X. Mao and R. E. Russo, UV-femtosecond laser ablation-ICP-MS for analysis of alloy samples, J. Anal. At. Spectrom., 2004, **19**, 1165-1168.

[27] B.J. Fryer, S.E. Jackson, and H.P. Longerich, The design, operation and role of the laser ablation microprobe coupled with an inductively coupled plasma-mass spectrometer (LAM-ICP-MS) in the earth sciences. Can. Min., 1995, **33**, 303-312.

[28] T. Hirata, Soft Ablation Technique for Laser Ablation– Inductively Coupled Plasma Mass Spectrometry, J. Anal. At. Spectrom.1997, **12**, 1337-1342

[29] M. Motelica-Heino P. Le Coustumerb and F. X. Donard, Micro- and macro-scale investigation of fractionation and matrix effects in LA-ICP-MS at 1064 nm and 266 nm on glassy materials, . Anal. At. Spectrom.2001,**16**, 542-547

APPENDIX A

RE: Permission Request Form: Mohamed Shaheen

Tuesday, December 15, 2009 8:51 AM

From:

"CONTRACTS-COPYRIGHT (shared)" <Contracts-Copyright@rsc.org>
Add sender to Contacts

To:

"'mshaheen73@yahoo.com'" <mshaheen73@yahoo.com>

Dear Mohamed Shaheen

The Royal Society of Chemistry (RSC) hereby grants permission for the use of your paper(s) specified below in the printed and microfilm version of your thesis. You may also make available the PDF version of your paper(s) that the RSC sent to the corresponding author(s) of your paper(s) upon publication of the paper(s) in the following ways: in your thesis via any website that your university may have for the deposition of theses, via your university's Intranet or via your own personal website. We are however unable to grant you permission to include the PDF version of the paper(s) on its own in your institutional repository. The Royal Society of Chemistry is a signatory to the STM Guidelines on Permissions (available on request).

Please note that if the material specified below or any part of it appears with credit or acknowledgement to a third party then you must also sec ure permission from that third party before reproducing that material.

Please ensure that the thesis states the following:

Reproduced by permission of The Royal Society of Chemistry

and include a link to the article on the Royal Society of Chemistry's website.

Please ensure that your co-authors are aware that you are including the paper in your thesis.

Regards

Gill Cockhead

Contracts & Copyright Executive

Gill Cockhead (Mrs), Contracts & Copyright Executive

Royal Society of Chemistry, Thomas Graham House

Science Park , Milton Road, Cambridge CB4 0WF , UK

Tel +44 (0) 1223 432134, Fax +44 (0) 1223 423623

http://www.rsc.org

-----Original Message-----
From: mshaheen73@yahoo.com [mailto:mshaheen73@yahoo.com]
Sent: 15 December 2009 00:19

To: CONTRACTS-COPYRIGHT (shared)
Subject: Permission Request Form: Mohamed Shaheen

Name : Mohamed Shaheen
Address :

Great Lakes Institute for Environmental Research
University of Windsor
Ontario , Canada

Tel : 519-253-3000 Ext. 4245
Fax :
Email : mshaheen73@yahoo.com

Journal/Book Title : JAAS
Editor/Author(s) : M. Shaheen, J. E. Gagnon, Z.yang and B. J. Fryer
Volume Number : 23
Year of Publication : 2008
Description of Material : Article
Page(s) : 1610-1621

Any Additional Comments :

Dear Sir,
I am finishing my Ph.D. thesis and I need JAAS permission to include the material we have published in JASS:
"Evaluation of the analytical performance of femtosecond laser ablation inductively coupled plasma mass spectrometry at 785 nm with glass reference materials"

Authors:
Mohamed Shaheen, Joel E. Gagnon, Zhaoping Yang and Brian J. Fryer

J. Anal. At. Spectrom., 2008, 23, 1610 - 1621,

APPENDIX B

Detection limits in ppm obtained using fs-LA-ICP-MS of NIST and Basalt reference materials.

Element	Isotope	NIST 610	NIST 612	NIST 614	BCR-2G	BHVO-2G	BIR-2G
Li	7	0.6	1.1	1.0	2.1	2.1	1.5
Be	9	0.3	0.5	0.4	0.4	0.6	0.4
B	11	0.6	1.1	1.0	1.3	1.5	1.1
Na	23	23.2	46.9	40.6	39.3	52.9	42.9
Mg	25	2.1	3.8	3.4	4.2	5.9	5.7
Al	27	5.6	11.1	7.9	10.8	12.8	11.2
Si	29	396.4	770.2	684.8	794.4	963.9	790.9
P	31	10.1	20.1	18.8	26.4	39.9	28.8
K	39	2.9	6.4	5.5	6.7	8.0	6.9
Ca	43	307.3	611.7	467.7	547.3	636.4	498.4
Sc	45	0.4	0.8	0.7	0.7	0.8	0.7
Ti	47	2.4	4.8	3.3	4.0	4.6	3.7
V	51	0.4	0.8	0.6	0.9	1.0	0.8
Cr	52	0.3	0.7	0.6	0.7	0.8	0.7
Mn	55	0.2	0.3	0.2	0.3	0.3	0.2
Fe	57	8.7	17.7	16.2	23.2	20.2	21.1
Co	59	0.150	0.275	0.267	0.380	0.472	0.421
Ni	60	0.486	1.041	0.941	1.156	1.407	1.027
Cu	65	0.449	1.007	0.777	1.029	1.201	0.951
Zn	66	0.175	0.396	0.286	0.466	0.515	0.447
Ga	69	0.055	0.111	0.084	0.110	0.123	0.094
Ge	72	0.132	0.303	0.233	0.277	0.299	0.229
As	75	0.422	0.818	0.767	1.252	1.452	1.151
Rb	85	0.069	0.128	0.123	0.101	0.136	0.105
Sr	86	0.293	0.524	0.412	0.713	0.884	0.714
Y	89	0.011	0.024	0.016	0.018	0.019	0.014
Zr	90	0.016	0.036	0.025	0.017	0.027	0.017
Nb	93	0.012	0.024	0.017	0.017	0.020	0.015
Mo	95	0.085	0.170	0.142	0.171	0.195	0.164
Rh	103	0.008	0.016	0.011	0.013	0.016	0.013
Pd	105	0.042	0.096	0.075	0.085	0.089	0.078
Ag	107	0.030	0.061	0.044	0.048	0.050	0.041
Cd	110	0.112	0.213	0.171	0.154	0.171	0.131
In	115	0.008	0.017	0.014	0.019	0.021	0.016
Sn	118	0.029	0.064	0.047	0.050	0.061	0.043
Sb	121	0.045	0.094	0.065	0.065	0.063	0.059
Cs	133	0.029	0.059	0.053	0.055	0.057	0.053
Ba	137	0.044	0.084	0.051	0.058	0.079	0.065
La	139	0.006	0.011	0.007	0.004	0.006	0.004

Ce	140	0.004	0.009	0.006	0.004	0.005	0.004
Pr	141	0.004	0.008	0.005	0.002	0.004	0.003
Nd	146	0.024	0.049	0.023	0.012	0.023	0.010
Sm	147	0.025	0.053	0.032	0.015	0.028	0.013
Eu	153	0.007	0.014	0.008	0.006	0.009	0.008
Gd	155	0.034	0.065	0.043	0.038	0.049	0.033
Tb	159	0.004	0.009	0.005	0.004	0.004	0.004
Dy	163	0.018	0.035	0.020	0.012	0.015	0.006
Ho	165	0.005	0.010	0.005	0.003	0.004	0.003
Er	166	0.013	0.027	0.014	0.007	0.014	0.006
Tm	169	0.004	0.010	0.004	0.004	0.005	0.004
Yb	172	0.019	0.038	0.025	0.013	0.023	0.014
Lu	175	0.005	0.009	0.006	0.004	0.006	0.004
Hf	178	0.013	0.029	0.013	0.006	0.010	0.007
Ta	181	0.005	0.011	0.006	0.003	0.003	0.002
W	182	0.013	0.030	0.018	0.010	0.014	0.007
Re	185	0.008	0.018	0.011	0.008	0.011	0.008
Pt	195	0.019	0.041	0.024	0.014	0.023	0.011
Au	197	0.014	0.026	0.014	0.011	0.013	0.010
Tl	205	0.010	0.020	0.015	0.012	0.013	0.011
Pb	206	0.019	0.040	0.026	0.020	0.022	0.018
Bi	209	0.016	0.028	0.023	0.022	0.021	0.017
Th	232	0.005	0.011	0.007	0.003	0.004	0.003
U	238	0.003	0.007	0.003	0.002	0.004	0.001

VITA AUCTORIS

Name: Mohamed Shaheen

Place of Birth: Egypt

Year of Birth: 1973

Education: B. Sc. Physics, El-Minoufia University, Egypt, 1995

M. Sc. Physics, Tanta University Egypt, 2001

Ph. D. Environmental Science, University of Windsor, Ontario, Canada, 2010.